Electronic Thesis and Dissertation Repository

8-4-2017 12:00 AM

A Diffusion Tensor Imaging Study of Motor Fibre Path Integrity and Overt Responsiveness in Disorders of Consciousness

Clara A. Stafford, *The University of Western Ontario*

Supervisor: Dr. Adrian Owen, *The University of Western Ontario*
A thesis submitted in partial fulfillment of the requirements for the Master of Science degree in Psychology
© Clara A. Stafford 2017

Abstract

This study investigated the relationship between motor thalamo-cortico-cerebellar fibre path integrity and overt responsiveness in patients with disorders of consciousness (DOC). Additionally, we investigated the potential of imaging these motor tracts at ultra-high fields. Study I and II aimed to map the white matter connections of motor execution fibres in DOC patients. Our results showed significant reductions in motor fibre path integrity across DOC diagnostic categories. Study III and IV aimed to develop a 7T MRI Diffusion Tensor Imaging (DTI) sequence. We optimized this sequence to image motor fibre paths in DOC patients. We concluded that, in healthy controls, probabilistic tractography of these tracts at ultra-high fields was superior to tractography at lower magnetic fields. Further investigation is needed to determine the advantages of imaging these motor tracts at ultra-high fields in patients with disorders of consciousness.

Keywords

Acknowledgments

I would like to thank my supervisor, Dr. Adrian Owen, for his expertise, guidance and the many opportunities he has afforded me to share my research abroad and learn from the scientific community outside Western University. I would also like to thank my co-supervisor, Dr. Davinia Fernández-Espejo, for her unwavering support, patience for my constant questions and encouragement throughout my degree. She is a brilliant scientist who listened to my ideas (regardless of how good they were), pushed me to think critically and fueled my passion for science. Without Dr. Owen and Dr. Fernández-Espejo, I would not have enjoyed sharing the work I have accomplished and I am eternally grateful for their trust, candor and knowledge.

I would also like to thank Dawn Pavich and Haitao Yang. Without their help, I would not have had access to the technical tools required to complete my research. Acquiring and processing my thesis data would have been much more difficult and time consuming if not for their dedication and resourcefulness. I am also grateful to Joe Gati and Trevor Szekeres from Robarts Research Institute, who helped in the development of the diffusion tensor imaging sequences used in my thesis as well as acquired the structural images for my study. No matter the start time or length of my scanning sessions, Joe and Trevor were always positive, accommodating, and ever so patient with me when I was still learning about MR imaging and pestered them with questions and concerns. Without them, I would not have a thesis to share and I will be eternally grateful for all I have learned from their expertise.

Finally, I would like to thank my family: my mother Lynn Mailloux, my sister Ella Stafford and my step-father Jean-Guy Simonato. This degree belongs to them, as I would not be completing my master's without their support. From the start, they believed I could accomplish anything I set my mind to, and each in their own way raised my ambitions beyond my imagination. I would not be the scientist I am today if they had not ignited my dedication and aspirations. Special thanks to Kabir Daljeet for his emotional support throughout this process, and for always making me laugh when I needed it the most.

Table of Contents

List of Tables

List of Figures

List of Appendices

Chapter 1

1. Introduction

1.1 Consciousness

Consciousness is a multifaceted concept that scientists and philosophers alike have tried to disentangle and define for years. In the scientific literature, it is defined by two main pillars: arousal and awareness (Laureys, Owen & Schiff, 2004). Arousal is defined as the level of wakefulness, usually indicated by eye opening and sleep-wake patterns. Sleeping is a state of low arousal (closed eyes) whilst being awake is a state of high arousal. Arousal is supported by the brainstem and reticular activating system (Laureys, Boly, Moonen & Maquet, 2009). Awareness is defined as being cognizant of one's self, and having the ability to respond to one's environment (Laureys et al., 2004). The exact cortical systems supporting awareness are still unknown, however it has been suggested that this pillar of consciousness depends on the integrity of the cortex and its subcortical projections (Laureys, 2009). Multiple theories suggest that thalamocortical (Laureys et al., 2000; Schiff, 2008; Fernández-Espejo et al., 2012) and fronto-parietal mechanisms (Noirhomme et al. 2010; Jin & Chung 2012; Fernández-Espejo et al. 2012) generate the conscious experience.

1.2 Disorders of consciousness

In most states, individuals show equal levels of arousal and awareness. For example, in healthy individuals, the relationship between these two components is positively correlated across sleep stages (dream activity during REM-sleep being the exception) from deep sleep to conscious wakefulness. Comatose patients are an extreme version of this linear and positive relationship: they are unaware because they cannot be awakened. The logic then follows that one must be awake to be aware (Laureys, 2005). In a few rare cases, however, wakefulness and arousal can be dissociated. This disconnection appears in the form of prolonged disorders of consciousness (PDOC), a spectrum of disorders including the vegetative state (VS) and the minimally conscious state (MCS), where either one or both pillars are impaired (see Figure 1). These impairments are usually

caused by acute traumatic (e.g. motor vehicle accident) or non-traumatic brain injuries (e.g. stroke, cardiac arrest) and in rarer cases by degenerative brain disorders or congenital malformations of the nervous system (Multi-Society Task Force on PVS, 1994).
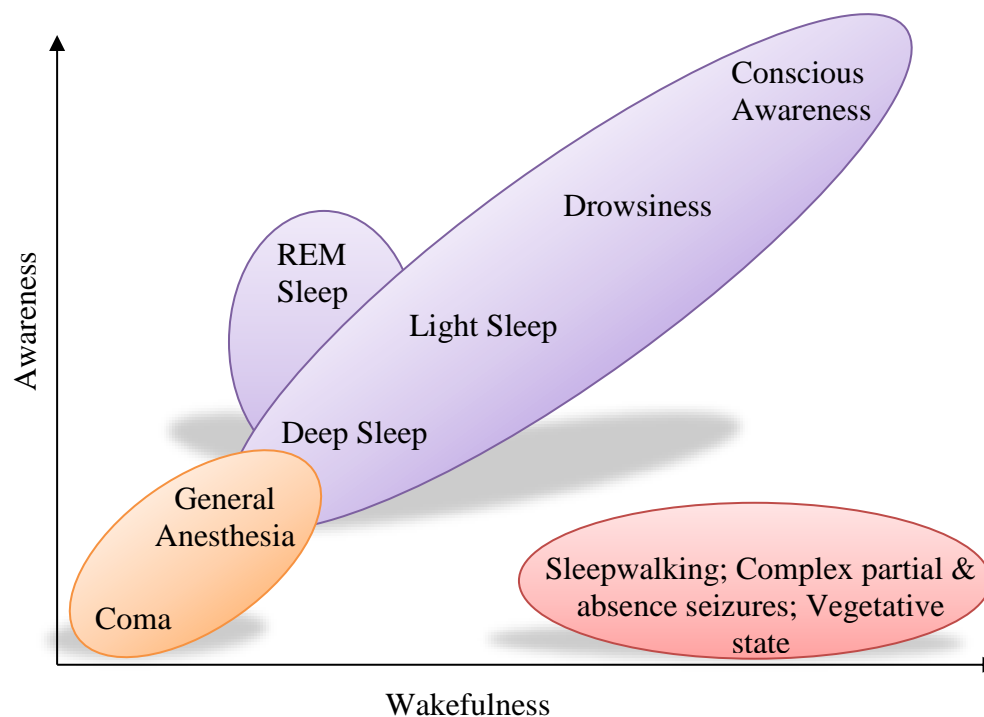
Figure 1: Adapted from Laureys (2005). Figure illustrating the linear and positive relationship between awareness and arousal during sleep stages (purple) with extremes cases of coma illustrated in orange and dissociated states of consciousness in red.

1.2.1 Coma

The comatose state is characterized by an absence of arousal and an absence of awareness. These patients lie with their eyes closed and show no volitional or reflexive behaviours, even after deep noxious stimuli (Posner, Saper, Schiff, & Plum, 2007). To be diagnosed as comatose, patients must be in this state for at least 60 minutes. Coma is typically a time-limited condition: after two to four weeks, patients either slowly recover arousal and awareness, progress into the vegetative state or are diagnosed as brain dead. In some cases, some patients do not recover arousal or awareness but also do not show signs of brain death, as they fall into a state of chronic coma. This, however, is an extremely rare condition (Di Perri et al., 2014; Monti, 2012; Schnakers, Majerus, & Laureys, 2004). Positron emission tomography (PET) scans reveal that global grey

matter glucose metoblism is reduced by 50-70% in coma patients who suffered a traumatic or ischemic brain injury. In patients who suffered anoxic injuries, their global glucose metabolism can be reduced up to 75% of the normal range. (Laureys et al., 2004; Schnakers et al., 2004; Laureys et al., 2009).

1.2.2 The vegetative state

The vegetative state, also sometimes referred to as "unresponsive wakefulness state" (UWS), was first described by Jennett and Plum in 1972. This state is characterized by a normal circadian rhythm and the presence of sleep-wake cycles indicated by spontaneous periods of eye-opening and closing. Behaviourally, these patients show reflexive trunk and limb movements and may respond to noxious stimuli with flexor withdrawal or grimacing (Jennett & Plum, 1972; Jennett, 2002) however they show no sustained signs of awareness. In other words, none of their behaviours are volitional or consistently generated by/directed towards their environment. The VS is declared as permanent contingent on two factors: i) the type of acute injury sustained and ii) the length of the VS. For individuals who sustained a traumatic brain injury (TBI), the VS is declared permanent after 12 months. For non-traumatic brain injuries (anoxic or hypoxic), the VS is declared permanent after 3 months (Multi-Society Task Force on PVS, 1994; Giacino, 2004). PET scans of VS patients reveal a reduction of approximately 40% of global cortical metabolism. Although this metabolic reduction is similar to the reduction seen in coma patients, VS patients show close to normal metabolic function in the brainstem, which explains their preserved basic nervous functions (i.e. sleep-wake cycles, thermoregulation, respiration) (Laureys, Faymonville, & Maquet, 2002; Laureys, 2009; Monti, 2012).

1.2.3 The minimally conscious state

The minimally conscious state is characterized again by normal levels of arousal but contrary to the VS, MCS patients show reproducible signs of awareness. Behaviourally this is usually presented in the form of visual pursuit, low-level responses with gestures and verbalizations or even simple command-following (Giacino et al., 2002; Schnakers et al., 2004; Monti, 2012). When assessing MCS patients, it is important to note that

although they are able to demonstrate reproducible signs of awareness, these behaviours fluctuate greatly and are often followed by prolonged periods of unresponsiveness. The criteria for an MCS diagnosis requires that these behaviours be contingent on environmental triggers, for example crying in response to a noxious stimulus or object reaching (Giacino et al., 2002; Schnakers, Giacino, & Laureys, 2010). One of the earliest signs of progression into the MCS and recovery of consciousness is visual pursuit (Giacino & Kalmar, 2005; Vanhaudenhuyse et al., 2007). PET scans of MCS patients show a reduction of cortical metabolism of 20-40% (Schnakers et al., 2004). Despite prognosis being more favourable for MCS patients, some of these patients can remain in the minimally conscious state for prolonged periods of time, without fully recovering (Giacino & Kalmar, 1997; Schnakers & Majerus, 2012).

1.3 Diagnosing disorders of consciousness

Determining if patients with disorders of consciousness are awake is quite simple. VS and MCS patients have preserved reticular activating systems and thus display behavioural sleep-wake patterns through periods of eye-opening and closing. A valid assumption would be that if one's eyes are open, they are awake. Another way of detecting arousal in these patients is with electroencephalography (EEG). Different stages of arousal are marked by different cortical electrical patterns, which can easily be detected using this technique. EEG has been shown to be able to detect sleep-like patterns in these patients (Cologan & Schabus, 2012; de Biase et al., 2014). Across the spectrum, DOC patients show similar levels of arousal but differ on their level of awareness. In other words, patients higher on the DOC spectrum show more signs of awareness through reproducible, volitional behaviours. One way to measure these behaviours, and thus having a measure of the patient's level of awareness, is to *ask* these patients to produce observable responses to certain stimuli.

Command following is considered a reliable measure for differentiating VS and MCS patients because it is expected that a patient who retains awareness has the volition to respond to these commands (such as an MCS patient) whereas a patient who does not respond to command retains no awareness. A patient's level of awareness cannot yet be estimated objectively; clinicians must interpret a panoply of signs and make inferences

about levels of awareness based on the presence or absence of behaviours. Many bedside behavioural systems have been developed to quantify and standardize the assessment of awareness in DOC patients (Majerus, Gill-Thwaites, Andrews & Laureys, 2005; Schnakers et al., 2008). Some scales have been developed to assess consciousness within the first few hours of the injury, whilst others are more sensitive to changes in consciousness over time. One thing they do have in common is that these scales will be composed of subscales, which assess different behaviours from different modalities, ranging from low-level reflexive movements to high-level command following and communication.

 The Coma Recovery Scale – Revised (CRS-R; Giacino, Kalmar & Whyte, 2004) is often considered the gold-standard for behavioural assessments of DOC patients because it does not require formal training from the authors, it is free and it encompasses multiple facets of behaviours for these patients (Giacino & al., 2004). The assessment is comprised of six subscales: Auditory Function Scale, Visual Function Scale, Motor Function Scale, Oromotor/Verbal Function Scale, Communication Scale and the Arousal Scale. In total, there are 23 items to measure these six facets of behavior; these items are organized in a hierarchical manner where the lowest items indicate reflexive movements and high items denote cognitively-mediated behaviours (Kalmar & Giacino, 2005). The total score on the CRS-R dictates diagnosis. However, there are certain items (i.e. behaviours) that determine diagnosis regardless of the patient's performance in other categories. The CRS-R is usually the tool of choice because although it is a bit more time consuming than other assessments, the CRS-R has demonstrated high agreement between raters and in the same rater over time, showing that raters are able to accurately distinguish between VS, MCS and emergence from MCS (EMCS; Giacino et al., 2004; Kalmar & Giacino, 2005). The increased sensitivity of this scale to detecting MCS patients makes it the most efficient behavioural tool to date for differential diagnosis (Kalmar & Giacino, 2005). The CRS-R subscales and items are outlined in Table 1, along with the diagnosis they denote.

Table 1: CRS-R subscales, behavioural items and diagnostic criteria

Scale	Score	Diagnosis
Auditory Function Scale		
Consistent Movement to Command	4	MCS
Reproducible Movement to Command	3	MCS
Localization to Sound	2	VS
Auditory Startle	1	VS
None	0	VS
Visual Function Scale		
Object Recognition	5	MCS
Object Localization: Reaching	4	MCS
Visual Pursuit	3	MCS
Fixation	2	MCS
Visual Startle	1	VS
None	0	VS
Motor Function Scale		
Functional Object Use	6	EMCS
Automatic Motor Response	5	MCS
Object Manipulation	4	MCS
Localization to Noxious Stimulation	3	MCS
Flexion Withdrawal	2	VS
Abnormal Posturing	1	VS
None/Flaccid	0	VS
Oromotor/Verbal Function Scale		
Intelligible Verbalization	3	MCS
Vocalization/Oral Movement	2	VS
Oral Reflexive Movement	1	VS
None	0	VS
Communication Scale		
Functional: Accurate	2	EMCS
Non-Functional: Intentional	1	MCS
None	0	VS
Arousal Scale		
Attention	3	MCS
Eye opening w/o Stimulation	2	VS
Eye opening w/ Stimulation	1	VS
Unarousable	0	VS

Adapted from Giacino et al., 2004; Kalmar & Giacino, 2005. VS = vegetative state; MCS = minimally conscious state; EMCS = Emergence from MCS

1.3.1 Diagnostic challenges in DOC

As previously discussed, differential diagnosis of vegetative state and minimally

conscious state patients depends on accurate assessment of levels of arousal and

awareness. Behavioural scales, like the CRS-R, are the tools of choice for clinicians, however, there are many challenges associated with their sensitivity and specificity. Retrospective studies have identified several cases of misdiagnosed VS patients, after using behavioural tests. In 1993, Childs et al., found that 37% of their DOC sample (18 out of 44 VS patients) were diagnosed as VS after clinical consensus when in fact they were MCS (Childs, Mercer & Childs, 1993). Similar findings were reported by Andrews et al. (1996) where 43% of their patient group (17 out 40 patients) were misdiagnosed with standard behavioural assessments (Andrews et al., 1996). A more recent study, by Schnakers et al. (2009), used the CRS-R as their diagnostic tool and reported a misdiagnosis rate of 41% (18 out of 44 patients).

Often not considered during these assessments are the external factors that may affect these bedside tests. As previously mentioned, patients in the VS often display an array of spontaneous and reflexive movements. The subjective nature of classifying a vocalization or an eyeblink as reflexive or intentional can affect the final diagnosis (Guldenmund et al., 2012). Furthermore, any comorbid impairments resulting from the aetiology of the injury (e.g. blindness/deafness, motor impairments, seizures) can directly affect a patient's performance while under behavioural assessment (Guldenmund et al., 2012). The rapid and unpredictable shifts in patients' levels of arousal and awareness may also mislead the assessment of true levels of awareness. These behavioural assessments only capture a fraction of a patient's day. As such, if the assessment co-occurs with a period of fatigue or low awareness, misinterpretation of the patient's true capabilities can skew the scores (Guldenmund et al., 2012).

These issues of misdiagnosis, and the confounding variables associated with them, have important implications for this clinical population. The final diagnosis will often determine a patient's prognosis, future care and legal rights. Accuracy in differential diagnosis is paramount, particularly for VS patients, as the diagnosis may serve to help inform decisions about the removal of life-sustaining treatments (Fins, 2003).

1.3.2   Covert Awareness

Behavioural assessments of consciousness are useful for differential diagnosis, prognosis and decisions about patient treatment plan. However, an inherent flaw in these tests is that they only tell one side of the consciousness story: the observer's side. To gain a full perspective on the disconnection between arousal and awareness, we also need to tell the experiencer's story. Studies using neuroimaging techniques such as functional magnetic resonance imaging (fMRI) and EEG have contested the assumption that patients who exhibit no overt behavioural signs of command following should be classified as unaware (Fernández-Espejo & Owen, 2013; Owen et al., 2006). A subgroup of patients has been shown to demonstrate no behavioural evidence of consciousness (i.e. are behaviourally indistinguishable from VS patients) however, when they are subject to neuroimaging paradigms, they show signs of retained or residual awareness. These patients are often referred to as 'covertly aware'. (Fernández-Espejo & Owen, 2013). This subgroup of patients was first identified by Owen et al. (2006), when they used fMRI to study a patient behaviourally diagnosed as VS. They used two mental imagery tasks to assess if she had any pockets of preserved awareness. The first task, a motor imagery task, required the patient to imagine herself playing tennis (i.e. moving her arm back and forth as if hitting the ball) and the second task required the patient to perform spatial navigation on command. That is to say, the patient was required to imagine herself walking around her home. These two imagery tasks recruit different areas of the cortex that are distinguishable in fMRI. The motor imagery task recruits mainly the supplementary motor area (SMA), whilst spatial navigation recruits primarily the parahippocampal gyrus and posterior parietal cortex. In both tasks, the behaviourally VS patient produced neural activity that was not significantly different from the activity recorded in healthy controls. These results show that despite showing behavioural signs of unawareness, it is possible for certain patients to have retained the ability to understand spoken commands and to modulate their neural activity in response to these commands (Owen & al., 2006). Since this study, the prevalence rate of covertly aware patients has been estimated at around one in five patients (20%) as more and more studies use mental imagery tasks to detect evidence of residual cognition. (Fernández-Espejo & Owen, 2013; Monti et al., 2010). Similar results have been replicated in a different

neuroimaging modality, EEG. Cruse et al. (2011) assessed 16 VS patients and asked them to imagine moving their right-hand (in a squeezing movement) or to imagine moving their toes (in a wiggling movement). These movements produce discernible patterns of electrical cortical activity in EEG. They found that three of the 16 VS patients (19%) were able to consistently imagine these two behaviours on command across trials.

Motor execution and motor imagery have been well documented in terms of their functional and structural connectivity (Jeannerod, 1995; Roland et al., 1980). Motor execution primarily recruits white matter fibres that connect the ventrolateral nuclei of the thalamus to the primary motor cortex (M1) and motor imagery will primarily recruit white matter fibres that extend from the ventrolateral nuclei of the thalamus to the SMA. Due to the similar functional and structural connectivity of these two processes, they have often been thought to be concurrent. Covertly aware patients however, challenge this assumption and support the idea that these two motor processes are independent. This is the main hypothesis explaining why these patients are able to perform motor imagery tasks but remain behaviourally unresponsive.

A recent study by Fernández-Espejo, Rossit & Owen (2015) sought to elucidate the mechanisms behind this dissociation. They studied two patients with DOCs and described both the functional and structural connectivity of these patients along with their clinical profiles. The patients performed the tennis motor imagery task described above and its motor execution counterpart. Their functional and structural results were compared to a group of healthy controls. When studying the patterns of activity across the thalamus, M1 and SMA, they found increased activation in the thalamus and M1 during motor execution as compared to motor imagery. Specifically, they identified an excitatory coupling between the thalamus and M1, suggesting excitatory signals from the thalamus to M1 are crucial for motor execution. Additionally, when assessing the integrity of these two white matter paths using diffusion tensor imaging (DTI), they found a significant dissociation in these two paths in a patient who could not overtly respond to commands but showed strong evidence of covert awareness. The path between the thalamus and M1 (motor execution) showed significantly more damage than the path between the thalamus and the SMA (motor imagery). In contrast, these two fibre paths were indistinguishable

in a patient who could behaviourally follow commands and communicate with gestures. This study suggests that the connection between the thalamus and M1 is crucial for motor execution and that damage to this specific tract could explain why covertly aware patients cannot overtly respond to commands.

1.4   Diffusion Tensor Imaging in DOC patients

The neuroimaging techniques discussed above such as fMRI and EEG have been useful in characterizing different DOC diagnostic categories based on brain activity during certain tasks and have been especially useful in the discovery of covertly aware patients. However, these tasks rely on patient participation and run the risk of false negatives if the patient cannot perform the scheduled tasks due to exhaustion or a period of unawareness. Task-free imaging techniques such as FDG-PET, resting state fMRI or even structural imaging allow researchers to identify patterns of activity or structure across diagnostic groups that can help to classify a patient's level of awareness. The main advantage of these task-free techniques is their independence from a patient's ability to perform any task and therefore can be conducted regardless of the patient's state of arousal. The structural imaging technique of interest for this study is Diffusion Tensor Imaging (Basser et al., 1994; Basser et al., 1994).

1.4.1   What is Diffusion Tensor Imaging?

This technique is a model of Diffusion Weighted Imaging (DWI; Le Bihan & Breton, 1985; Merboldt, Hanicke & Frahm, 1985; Taylor & Bushell, 1985; Le Bihan et al., 1986), which is a type of Magnetic Resonance Imaging (MRI). DTI characterizes the boundaries of structures and tissue based on the diffusion rate of water molecules (i.e. whether they diffuse isotropically or anisotropically). In the cortex, white matter (WM) has been found to be highly anisotropic, grey matter (GM) is usually expected to be less anisotropic and cerebrospinal fluid is characterized by unrestricted diffusion (isotropic diffusion; (Pierpaoli et al., 1996; Song et al., 2002; Hagmann et al., 2006). DTI models the principal diffusion direction of each voxel in the 3D image by colour-coding the main eigenvector: voxels with a principal eigenvector along the x-axis (left – right) are coloured red, voxels with a principal eigenvector along the y-axis (rostral-caudal) are coloured green and

voxels with a principal eigenvector along the z-axis (superior-inferior) are coloured blue (see Figure 2).
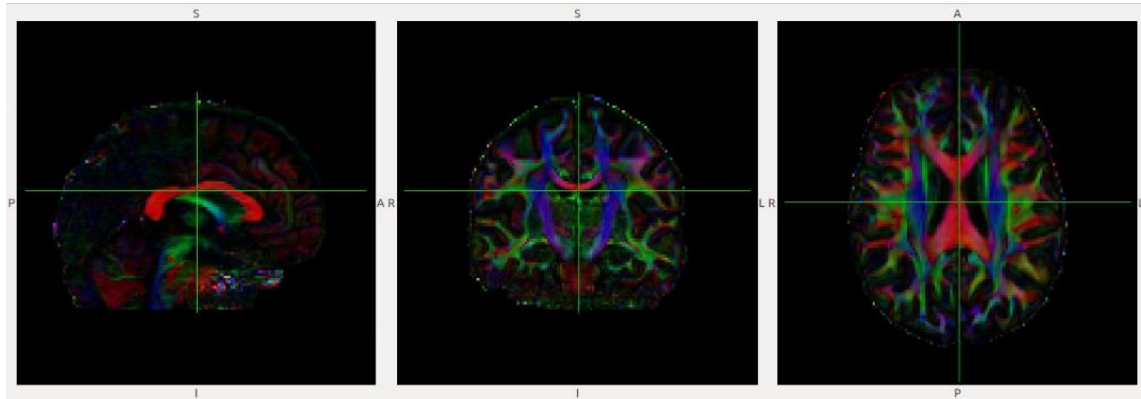
Figure 2: Principal eigenvector colour map (from pilot participant in Study III). Leftmost panel: sagittal view; Middle panel: Coronal view; Rightmost panel: axial view. Red: WM fibre from left-right; Green: WM fibres from rostral-caudal; Blue: WM fibres from superior-inferior.

There are two types of measure one can use to quantitatively describe diffusion in tissue. These measures can quantify diffusion across the cortex or diffusion in specific WM tracts of interests.

Measures of diffusion magnitude. Mean diffusivity, also sometimes referred to as the apparent diffusion coefficient (ADC), is a measure of diffusion magnitude. MD refers to the amount of diffusion in a single voxel and/or all voxels in a tract of interest, and provides information about the molecular diffusion rate. In the context of pathology, when the MD of a WM fibre tract is low, this indicates low diffusivity in the tract of interest which could signify increased cell restriction due to an obstruction such as a solid tumour. Conversely, when the MD or trace of a pathway of interest is high, this means there is high diffusivity in this tract (i.e. increased free diffusion) and this could indicate damaged tissue due to axonal atrophy for example (Soares et al., 2013; Stieltjes et al., 2013).

Measures of diffusion anisotropy. Measures of diffusion anisotropy are used to quantify the shape of diffusion in a voxel and across all voxels in a tract of interest. The most common measure of this kind is fractional anisotropy (FA), because it measures the fraction of the diffusion that is anisotropic in the voxel(s) of interest. In other words, it

measures the magnitude of directionality of anisotropic diffusion. When studying clinical populations, FA is a popular measure to use as it is considered a measure of WM integrity: low FA indicates low anisotropy, hence a damaged fibre tract whereas high FA indicates high anisotropy, illustrating a more intact fibre tract (Alexander et al, 2007; Stieltjes et al., 2013).

1.4.2   Diffusion imaging in the context of severe brain injury

Post-mortem studies conducted on DOC patients' brains have described the neuropathology behind this chronic state of unawareness in some detail. For example, Adams et al. (1999) studied 35 traumatic brain injury patients who, at the time of their death, met diagnostic criteria for the vegetative state. The most common structural abnormalities identified at post-mortem were found to be thalamic damage, diffuse axonal injury (DAI), ischemic damage and brainstem damage. A follow-up study by the same authors, added 14 non-traumatic VS cases. In this aetiological subgroup, diffuse ischemic damage was common to most non-traumatic patients (64%) whilst damage in the thalamus was present in all non-traumatic patients (Adams et al., 2000). Jennett et al. (2001) used a similar methodology in a severely disabled group of patients (due to acute head injury), most of whom met criteria for the minimally conscious state before death. When comparing the post-mortem findings of this MCS group to the VS groups reported by Adams et al. (1999) and Adams et al., (2000), the authors reported that diffuse axonal injury and thalamic damage, the most common abnormalities in VS patients, were not as prominent in the MCS group. Brainstem damage, however, was equally present in both groups. Jennett et al. (2001), along with a review by Graham et al. (2005), concluded that although diffuse axonal injury, global white matter and thalamic damage are common to both VS and MCS patients, it is in fact the magnitude of the damage that distinguishes these two conditions, not the location of the damage.

The main advantage of diffusion tensor imaging, especially for clinical populations like brain injury patients, is that appraisal of the structural damage to cortical tissue can be done *in vivo* rather than post-mortem. To this effect, several DTI studies in DOC patients have confirmed the above findings. Notably, Newcombe et al. (2010) compared patients who were VS with either traumatic or non-traumatic aetiologies to healthy controls. They

reported significant decreases in FA and increases in MD in global brain white matter between these two aetiological groups. They also reported that both patient groups had significantly higher MD in thalamic regions as compared to controls but the aetiological subgroups showed no significant differences in these regions. In a follow-up study, Newcombe et al., 2011 compared the FA and MD parameters in preselected regions of interest (ROIs) and demonstrated similar results: patients in the VS had lower FA and MD in all regions of interest compared to other brain injury groups (Newcombe et al., 2011).

Although both studies support the notion that DTI can be used as a measure to characterize and differentiate WM organization in VS patients and controls, these two DTI studies did not include the full spectrum of DOC diagnoses. They did not include MCS or EMCS patients and therefore could not investigate these WM changes as potential biomarkers for differential diagnosis. Additionally, because they used global white matter ROIs, they could only characterize WM integrity across the cortex, rather than characterize integrity of specific WM paths. This lack of specificity precludes the possibility of identifying the location of the damage potentially responsible for the chronic state of these patients. It could be argued that any differences observed between patients and controls could be attributed to general damage sustained after the original insult.

Another study performed probabilistic tractography in VS, MCS and EMCS patients and investigated the structural connectivity of the default mode network in comparison to healthy controls (Fernández-Espejo et al., 2012). They noted impairment in cortico-cortical connections as well as in thalamo-cortical connections in DOC patients compared to controls. They also reported a main effect of diagnostic category in both tracts, with a more consistent trend of FA decrease as clinical severity increased in the thalamo-cortical tract. The FA values of these tracts significantly correlated with patient CRS-R scores.

Fernández-Espejo et al. (2011) investigated more precise regions of interest than Newcombe et al. (2010, 2011): subcortical white matter, thalamic nuclei and the brainstem to try and differentiate VS and MCS patients. They compared histograms of

MD peak height in DOC patients and controls and across diagnostic categories. They identified changes in subcortical WM and thalamic regions which could predict patient diagnosis with 95% accuracy. These results opened the possibility of using DTI as a diagnostic tool when used alongside functional imaging and behavioural assessments. This study also identified potential biomarkers (subcortical and thalamic white matter) that could explain the chronic dissociation between arousal and awareness in these patients.

These studies demonstrate that DTI is capable of measuring and quantifying damage, specifically in WM tracts, displayed in DOC patients when comparing them to controls. As of yet, it is unclear what specialized WM tracts, if any, can explain the chronic state of these patients. However, results from the studies presented above point towards mechanisms found in subcortical and thalamic regions. These imaging studies also demonstrate the potential of DTI, when used alongside behavioural assessments, to help identify structural diagnostic biomarkers which could aid in differential diagnosis.

1.5 Diffusion tensor imaging at ultra-high magnetic field strengths

Theoretically, if DTI metrics such as FA and MD are accurately estimating the true anisotropy and diffusion rate of water molecules in tissue, these measures should not vary when changing the field strength of the MRI scanner (Shaw et al., 2016). However, when increasing the magnetic field strength, such as going from 3T MRI to 7T MRI, several confounding factors are introduced along with the inherent increase in signal-to-noise ratio (SNR). For example, 7T MRI brings an increase in SNR thus allowing for reduced scan times, increased spatial resolution and in the case of DTI, increased diffusion weighting (Polders et al., 2011). This field strength however, will also introduce artifacts such as eddy-current distortions, magnetic susceptibility gradients and inhomogeneities in the static (B0) magnetic field. These artifacts may offset any advantages incurred by the jump in SNR (Choi et al., 2011; Zhan et al., 2013). Many have tried to describe how DTI metrics are affected by the increase in SNR and by the artifacts that accompany imaging at higher magnetic fields.

Polders et al. (2010; 2011) investigated the differences in FA and MD between 1.5T, 3T and 7T magnetic fields across the same participants. They reported an increase in SNR as the magnetic field strength increased as well as a decrease in *uncertainty* of FA and MD calculations as magnetic field strength increased. These decreases in uncertainty, the authors suggest, improve their usability in white matter fibre tracking in single subject and group-level analyses by effectively increasing their reliability. Multiple computer simulation studies have also reported similar results: as the SNR decreases, uncertainty in DTI metrics increases; specifically, they concluded that in acquisition protocols with low SNR and low diffusion weighting (around 1000s/mm^2), FA calculations are overestimated (Pierpaoli et al. 1996; Jones & Basser, 2004). These studies concluded that to estimate the true anisotropy in an ROI or WM path of interest, SNR and diffusion weighting should be increased when possible. Interestingly, a handful of studies have investigated the effects of increased magnetic field strength on FA and have found that raw FA values increased as the field strength increased (Polders et al., 2009; Huisman et al., 2006; Qin et al., 2009). The authors of these studies could not elucidate these contradictive results and stated that more work in healthy individuals, clinical populations and computational models must be conducted to clarify the effects of higher SNR on DTI metrics.

One important detail to note about these studies and simulations is that the measures of SNR, FA, and MD were all calculated using the basic hardware settings and requirements of each MRI scanner. Although multiple ROIs were involved in these estimations, the diffusion acquisition protocols were not optimized to image the preselected ROIs. Therefore, it remains to be determined how increasing the magnetic field strength affects DTI metrics when the acquisition protocol is optimized to image specific a priori ROIs.

1.6 The present study

1.6.1 Rationale

Motor outputs are the most straightforward modality through which patients can follow commands, communicate and show signs of awareness. However, with the discovery of covertly aware patients, a lack of motor responses may not always be an accurate

indication of a patient's true levels of retained consciousness. One hypothesis to explain this dichotomy is that the fibres connecting the thalamus to the primary motor cortex (M1) are disrupted. Recent DTI work has shown that the integrity of this fibre path is compromised in patients who cannot overtly respond to commands (Fernández-Espejo et al., 2015). Previous animal studies have shown that the ventrolateral nucleus of the thalamus primarily projects to the primary motor cortex (Rispal-Padel, Massion & Grangetto, 1973; Rausell & Avendaño, 1985; Zheng et al., 1986) however connections from this specific thalamic nucleus have yet to be tested *in vivo* in DOC patients.

Previous studies have shown that the dorsomedial (DM) nucleus of the thalamus sustains much of the damage in VS patients (Fernández-Espejo et al., 2011; Fernández-Espejo et al., 2010; Maxwell et al., 2006; Maxwell et al., 2004). The authors propose a model to describe the relationship between damage to the dorsomedial thalamic nuclei and disorders of consciousness: downregulation of frontoparietal systems via suppression from the DM nuclei can lead to absence of awareness in the vegetative state. Conversely, metabolism in thalamo-cortical systems is relatively preserved (Fridman & Schiff, 2014; Schiff, 2010). This model, the mesocircuit hypothesis, postulates that when the central thalamus sustains damage, its excitatory connections with frontoparietal systems become inhibitory therefore precluding these mechanisms from supporting forebrain arousal systems (Fridman & Schiff, 2014; Schiff, 2008; Schiff, 2010). Schiff (2008) suggests certain frontoparietal regions are involved in this circuit, including the frontal eye fields (FEF), supplementary motor area (SMA), anterior cingulate cortex (ACC) and posterior parietal cortex (PPC). The central thalamus has been shown to activate during tasks requiring short-term shifts of attention and during tasks requiring high levels of alertness over extended periods of time (Schiff, 2008). It is then easy to see how selective damage to the central thalamus could impair a patient's overall ability for cognitively mediated tasks or, depending on the extent of the damage, how it could affect the length of time a patient can sustain their attention to complete behavioural or neuroimaging tasks.

Lant et al. (2015) investigated the structural integrity of this circuit in DOC patients and healthy controls. They used diffusion tensor imaging to track the cortico-cortical, subcortico-cortical and subcortico-subortical connections in this circuit and the default

mode network. Their cortical ROIs included the precuneus, temporoparietal junction, frontal medial cortex and dorsolateral prefrontal cortex; their subcortical ROIs included the thalamus, globus pallidus, putamen and caudate nucleus. They found that DOC patients showed significantly lower FA in cortico-cortical and subcortico-cortical connections when compared to controls. They reported similar results when comparing these two tracts in clinically conscious (MCS+EMCS) and clinically unconscious patients (VS). Clinically unconscious patients showed significantly lower FA than clinically conscious patients in both paths. None of the groups showed significant differences in the subcortico-subcortical tracts.

It is clear that to truly understand external responsiveness in DOC patients, the integrity of the thalamic motor system and thalamic awareness system must be dissociated within patients. Identifying the specific thalamic nuclei involved in these systems, however, poses a challenge. Most of what we know about thalamic parcellation is based on *ex vivo* studies, including animal studies and post-mortem studies (Lambert et al. 2016). These mainly characterize the chemoarchitecture and cytoarchitecture of the various cellular populations in the thalamus, to delineate specialized nuclei (Lambert, 2016; Morel, 2007). *In vivo*, low resolution (i.e. 1.5T/3T MRI) human resting state and task-dependent fMRI studies have not been able to establish the role of specific thalamic nuclei due to their small size and the poor spatial resolution of lower magnetic fields (Behrens et al., 2003b; Metzger et al., 2013). In these studies, the thalamus as a whole is used as a region of interest, which oversimplifies the specialized role of each nuclei in various facets of behavior. Furthermore, studies using diffusion weighted imaging have been able to parcellate the thalamus based on it cortical connections, however, these studies used a top-down approach to parcellation. That is to say, they placed their seeds in major cortical areas and identified clusters of thalamic voxels based on the cortical area with which they showed the highest connection probability (Behrens et al., 2003b; Johansen-Berg et al., 2005). This approach, although a viable starting point to map thalamic connectivity *in vivo*, provides artificial boundaries between thalamic nuclei as they are based on gross anatomy and do not account for gradual architectural features between the nuclei (Lambert et al., 2016). As such, ultra-high magnetic fields (i.e. 7T MRI) have been proposed as the solution to parcellate this small subcortical region *in vivo* (Lenglet et al.,

2012; Metzger et al., 2013). Indeed, several studies have been able to segment the thalamus, and surrounding regions such as the basal ganglia, using multimodal imaging at ultra-high fields (Calamante et al., 2012; Calamante et al., 2013; Lenglet et al., 2012; Xiao et al., 2016). In the context of disorders of consciousness, multimodal imaging at ultra-high fields in these patients would allow for the thalamic nuclei involved in the mesocircuit and motor execution loops, thus allowing the dissociation of these two systems within patients.

1.6.2   Objectives and Hypotheses

Study I. Using DTI, we aimed to determine if the disruption in the fibres between the thalamus and M1 reported by Fernández-Espejo et al. (2015) could be replicated in a larger sample of DOC patients and we sought to identify if any trends in damage to this tract correlate with patient diagnosis. This would help determine if damage to this particular path explains overt behavioural performance in a specific diagnostic group or if the damage explains motoric output performance across all diagnoses. We hypothesized that as clinical severity increased, so would the impairment in the thalamus-M1 fibre paths. We expected a direct relationship between overt signs of consciousness and impairment to the thalamus-M1 fibre paths. This would imply that all patients across the board are more conscious than they appear from behavioural assessments, and differentiating covertly aware patients from true VS patients is not possible based on observations from this VL-M1 fibre alone.

Study II. We wanted to investigate if impairment in motor execution in these patients is due to selective damage to the thalamus-M1 path, or if damage to other motor paths could be responsible for a lack of overt responsiveness during assessments. The motor paths of interest in this study were: the connections between the thalamus and M1, M1 and the cerebellum and the thalamus and the cerebellum. Similar to Study I, we expected diagnostic categories to differ in the magnitude of abnormality to the motor tracts of interest not in the location. Additionally, we hypothesized that regardless of diagnosis, our sample of DOC patients would not show impairment in the fibres connecting the thalamus and cerebellum as DOC patients show damage primarily in supratentorial regions (Laureys et al., 2004; Thonnard et al., 2014). In accordance with previous

conclusions by Graham et al. (2005), we expected diagnostic categories to differ in the magnitude of their impairment to these tracts, not in the location of the impairment.

Study III. We sought to develop 7T DTI acquisition sequences with a variety of acquisition parameters, and compare their success at reconstructing the motor fibre paths from Studies I and II. Three DTI acquisition sequences were compared, differing in terms of their gradient sampling directions and phase encoding directions. We hypothesized that acquisition sequences with more diffusion gradient sampling directions would be more successful at probabilistic tractography than the sequences with less sampling directions. Additionally, we hypothesized that acquisition sequences using two bipolar phase encoding directions would require less target masks to help the reconstruction of tractography streamlines.

Study IV. In this study, we compared the reconstructions of motor paths at 7T and 3T in a group of healthy controls. We used the optimized 7T from Study III and its 3T counterpart, for both qualitative and quantitative comparison. Given the current state of the literature and what we know about the benefits and pitfalls of imaging at ultra-high fields, we cannot not predict the directionality of the DTI results from the optimized 7T sequence when compared to its 3T counterpart.

Chapter 2

2. Generic Methods

All studies in this thesis used the regions of interest and exclusion and termination masks described below.

2.1.1 DTI Data Analysis

Data preprocessing and analysis was performed using the FSL Diffusion Toolbox (http://fsl.fmrib.ox.ac.uk/fsl/fslwiki/), following a similar pipeline as Fernandez-Espejo et al. (2012), Fernandez-Espejo et al. (2015) and Lant et al. (2015). There are four main steps to preprocessing DTI data: eddy-current correction, brain extraction tool (BET), dtifit and finally BEDPOSTX. Eddy-current corrections (Andersson & Sotiropoulos, 2016) is used to correct subject movements and correct distortions induced by eddy currents. The BET (Smith, 2002) is used to strip non-brain tissue from a whole-head image. Dtifit is then run to fit the diffusion model (dictated by the protocol parameters) to each voxel. The main output from this step generates the fractional anisotropy (FA) map and the maps for the three eigenvectors (V1, V2 and V3 maps) which are used to analyze the diffusion data. The final step in diffusion data preprocessing is Bayesian Estimation of Diffusion Parameters using Sampling Techniques (BEDPOSTX; Behrens et al., 2003b; Behrens et al., 2007). BEDPOSTX uses Monte Carlo Markov Chain sampling to build a posterior distribution on diffusion parameters at each voxel. That is to say, BEDPOSTX uses MCMC to build a distribution by calculating every possible orientation of the principal eigenvector in a given voxel. Additionally, this feature determines the number of crossing fibres per voxel. BEDPOSTX creates all the files necessary to run probabilistic tractography.

2.1.2 Mask Generation

Primary motor cortex masks. The primary motor cortex masks (M1) were first created in the standard template MNI152 2mm brain in FSL. The center voxel for the left hemisphere mask was placed at x y z coordinates -27, -13, 64 and the center voxel for the right hemisphere mask was placed at coordinates 27, -13, 64, as previously reported in

Fernández-Espejo et al. (2015). Around these center voxels, spheres with a radius of 6mm were created (Figure 3, panel A). Participant b=0 images were registered to the MNI152 2mm template image using FSL's FLIRT (Jenkinson & Smith, 2001; Jenkinson et al., 2002). The resulting transformation matrix was inversed, and applied to each standard mask to unwarp them into each participant's native diffusion space (Figure 3,
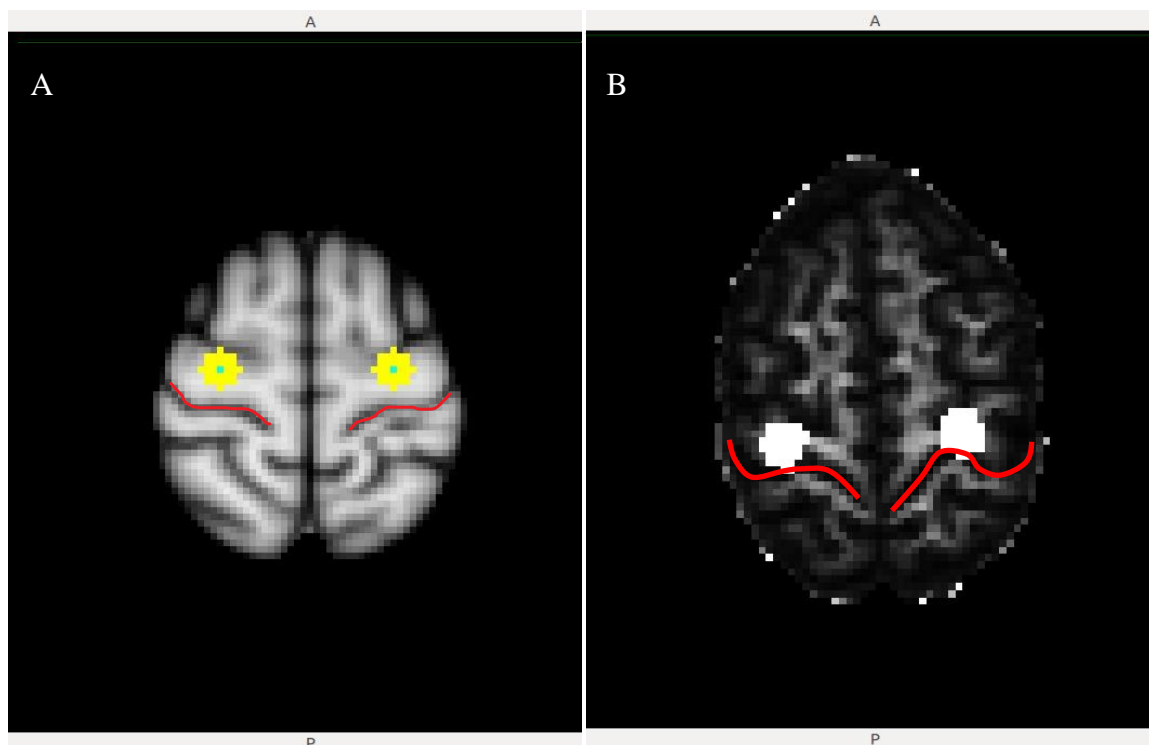
Figure 3: Axial view of cortical center voxels (blue) and spherical primary motor cortex masks (yellow) in standard MNI152 space (Panel A); Axial view of unwarped primary motor cortex masks in native space of a healthy control (Panel B). Central sulci are outlined in red.

panel B).

Thalamic masks. The most dorsal edge of the anterior commissure was visually identified on the axial plane of each participant's dataset (Figure 4, panel A). The center voxels of the masks were created three slices dorsal to the anterior commissure in the left and right ventrolateral nuclei (VL) of the thalamus (Figure 4, panel B). The anterior commissure was chosen as a reference landmark to help identify the ventrolateral nucleus based on the stereotactic atlas of the human thalamus by Morel (2007). These center coordinates were used to generate spherical masks, which had a radius of 4mm and were created in native space for each participant. We can confirm the position of the ventrolateral thalamic masks by looking at the principal eigenvector colour map (V1

map). In the V1 colour map, two main thalamic nuclei can be differentiated: the ventrolateral nuclei and the dorsomedial nuclei. The ventrolateral nuclei appear in purple (as in Figure 4, Panel B) as their M1 projections fall on the z-axis and the dorsomedial
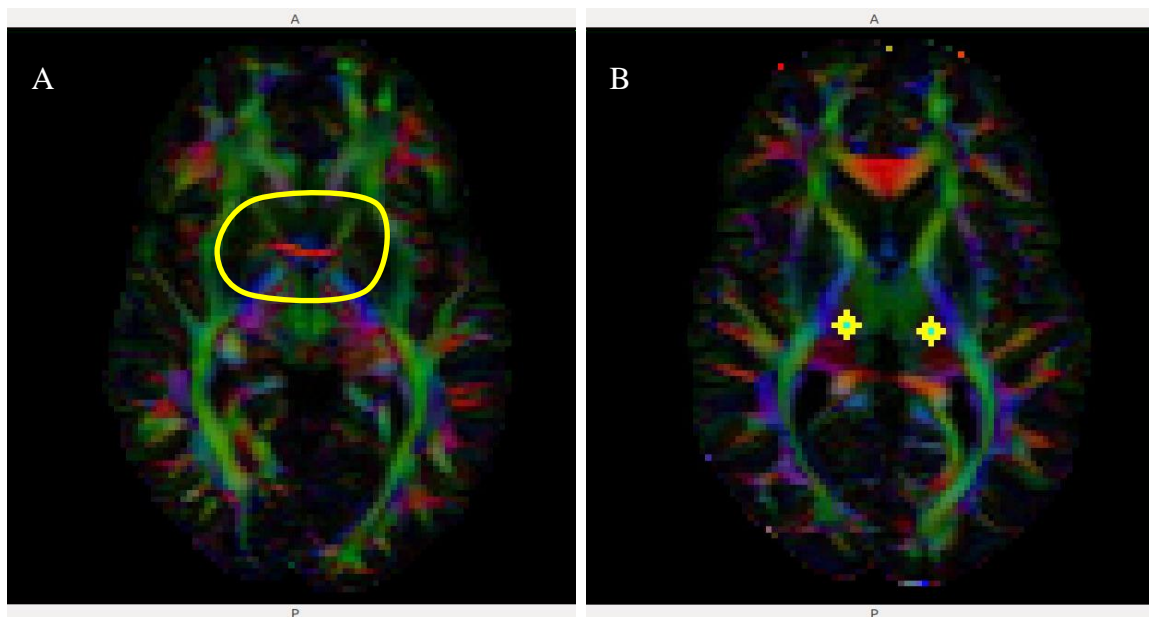
Figure 4: Axial view of anterior commissure circled in Panel A; axial view of thalamic center voxels (blue) and ventrolateral thalamic nuclei masks (yellow) placed dorsal to the anterior commissure (Panel B).

nuclei appear in green as their projections to the frontal lobe fall on the y-axis.

Cerebellar masks. The cerebellar masks were generated using the SUIT atlas template of the human cerebellum and brainstem (Diedrichsen, 2006). The preprocessed masks of the left and right dentate nucleus (DN) from the SUIT atlas were used as a visual reference. The center voxels were placed in the participants' native space region corresponding to the section when Vermis X start to protrude into the 4th ventricle (Figure 5, Panel B). Spherical masks with a radius of 6mm were generated.

Exclusion and Termination masks. An exclusion mask discards any pathway that enters the mask. A termination mask terminates a pathway once it enters the mask. A termination mask was used to help guide the reconstruction of the pathway between the ventrolateral nuclei and the primary motor cortices (ipsilateral connections). In Study I and Study II, a mask was created along the entire hemispheric fissure, to separate both hemispheres. This was done to prevent the reconstruction from crossing into the
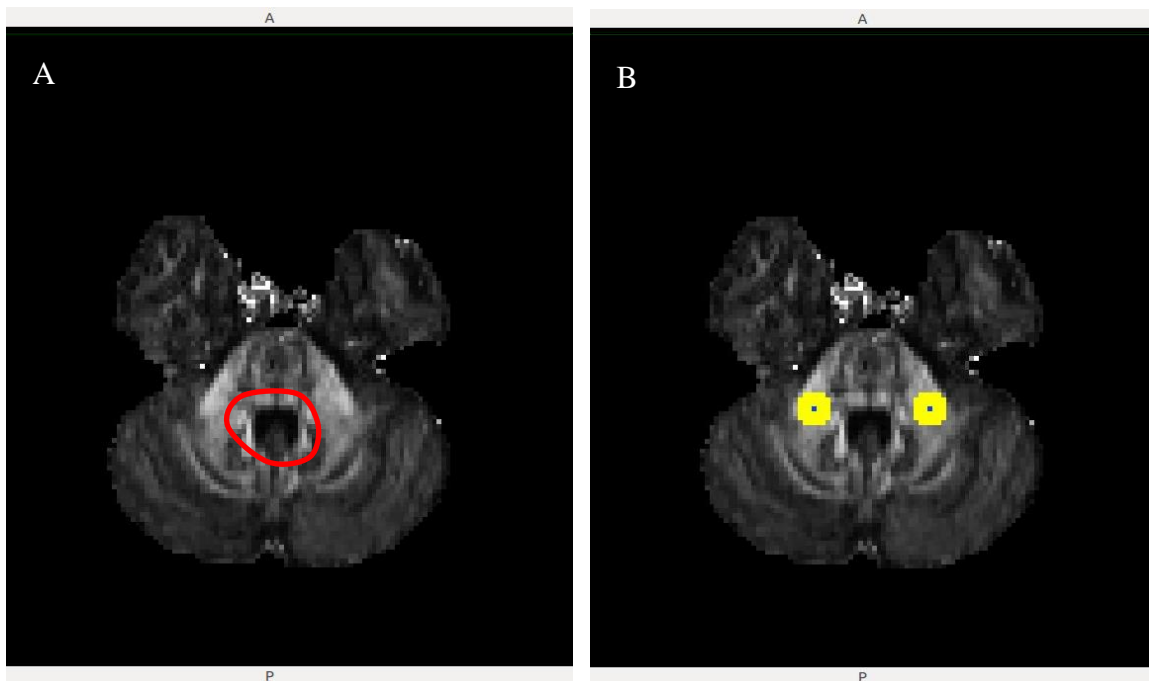
Figure 5: Axial view of Vermis X of the cerebellum protruding into the fourth ventricle circled in red in Panel A; axial view of cerebellar center voxels (blue) and cerebellar dentate nuclei masks (yellow; Panel B).

contralateral hemisphere (henceforth called *hemispheric mask*). A second mask was created on the slice right after the most ventral part of the ventrolateral nuclei masks. This was done to prevent probtrackX from reconstructing a pathway that traveled into the brain stem (henceforth called *brainstem mask*). The hemispheric and brainstem masks were combined to create one mask using fslmaths and this so-called combination mask was used as a termination mask in the reconstruction of the VL-M1 tracts. Furthermore, superior cerebellar peduncle mask spanning over four slices were created in each hemisphere. These were used as exclusion masks when reconstructing VL-DN tracts. These exclusions masks would exclude any fibres crossing into the opposing cerebellar hemisphere. Additionally, we used a termination mask immediately above the most dorsal slice of the thalamic masks – this stopped probtrackX from reconstructing fibres that entered cortical areas. Finally, when tracking M1-DN tracts, an exclusion mask was used to accurately reconstruct the pathway. Finally, a supratentorial mask was created along the hemispheric fissure, extending from the tentorium to the top of the cortex. This would then allow fibres from crossing into the opposing hemisphere through the middle cerebellar peduncles, the anatomically correct crossing point, rather than through the corpus callosum. This supratentorial mask was combined into one mask with the superior

cerebellar peduncle masks described above. All cortical masks, exclusion masks and termination masks were binarized using fslmaths before tractography. Probabilistic tractography can only be run from voxels with a non-zero value. Binarizing the masks used in this study ensures that all voxels in these masks have a value of one and that voxels not included in the masks have a value of zero.

In DOC patients, cortical areas are mostly preserved whilst subcortical areas sustain substantial damage and atrophy. It is often difficult to visually identify subcortical areas in patients, therefore unwarping masks from standard space becomes an unreliable practice. However, this is not a problem with healthy participants, accordingly, it is theoretically possible to unwarp subcortical and cerebellar masks into native space. That being said, to remain consistent across all participants, only the cortical masks were generated in MNI152 standard space and the thalamic and cerebellar masks were manually created in native diffusion space.

2.1.3   Probabilistic Fibre Tracking

Fibre tracking was estimated in native diffusion space for each participant between pairs of regions of interest (ROIs) using probtrackX (Behrens, 2003a; Behrens, 2007). probtrackX repeatedly samples from the distributions built up from BEDPOSTX. At each sample, pobtrackX calculates a streamline (i.e. path) between the seed voxels and all other regions/voxels in the brain. After a large number of samples, it can calculate a dominant streamline stemming from the seed voxels, as well as the probability of each brain voxel belonging to this streamline. Each voxel will receive a value, represented by the number of probtrackX samples that have passed through the voxel. Most brain voxels will have a value of zero (i.e. zero probability of belonging to the dominant streamline). The higher the value in a voxel, the more samples have passed through, implying high connectivity between the voxel and seed voxels. In Study I, the seeds include the ventrolateral thalamic nuclei (VL), the primary motor cortices (M1) while in Studies II, III and IV, the seeds include the VL, M1 and the dentate cerebellar nuclei (DN) Tracking was done in both directions between each ROI and the two probability paths resulting from each tracking pair were averaged and then thresholded. In Study I and II, the fibres connecting the ventrolateral thalamic nuclei and the primary motor cortices and the fibres

connecting the primary motor cortices to the dentate nuclei, were thesholded to removed pathways that had a probability distribution of less than 2%. For the fibres connecting the ventrolateral thalamic nuclei and the dentate nuclei, pathways with a probability distribution of less than 5% were removed. In Study III and IV, all reconstructed streamlines were thresholded at 2%. There is currently no convention about a precise thresholding percentage, however, thresholds between 2-5% have previously proven successful in both healthy and pathological populations (Behrens et al., 2007; Fernández-Espejo et al., 2012; Kinoshita et al., 2015; Sala-Llonch et al., 2010). See Table 2 for tracking pairs. The fibres between VL and M1, VL and DN, M1 and DN will henceforth be referred to as *VL-M1 tracts*, *VL-DN tracts* and *M1-DN tracts* respectively. The resulting fibre tracts were visually inspected for correspondence with known anatomy and to ensure our approach did not remove anatomically viable fibres. We used the White Matter Atlas by Hermoye et al. (http://www.dtiatlas.org/) as a visual reference.

Table 2: Description of pairs of tractography ROIs

Pairs	ROIs[a]	Connection
1	Left VL - Left M1	Ipsilateral
	Right VL - Right M1	Ipsilateral
2	Left VL - Right DN	Contralateral
	Right VL - Left DN	Contralateral
3	Left M1- Right DN	Contralateral
	Right M1 - Left DN	Contralateral

[a] VL = ventrolateral nuclei of the thalamus; M1 = primary motor cortices; DN = dentate nuclei of the cerebellum

Chapter 3

3. Study I – Investigating the relationship between overt behavioural responses and fibre integrity of VL-M1 tracts in patients with disorders of consciousness.

Many animal studies using single-cell recordings, horseradish peroxide and fluorescent tracers have demonstrated that the ventrolateral nucleus of the thalamus projects to the primary motor cortex (Brodmann area 4; Rispal-Padel et al., 1973; Rausell & Avendaño, 1985; Zheng et al., 1986). Lesion studies in the monkey found that when the ventrolateral thalamus was lesioned, cerebellar syndromes occurred, including ataxia and dysmetria (Bornshlegl & Asanuma, 1987). In humans, several diffusion tensor imaging studies have tried to reconstruct the fibres connecting the thalamus to the primary motor cortex, *in vivo*, in the hope of identifying specific thalamic nuclei contributing to human motor control. Behrens et al. (2003b) and Johansen-Berg et al. (2005) both conducted probabilistic tractography between cortical and sub-cortical regions: they placed their seed regions in various major cortical areas and segmented the thalamus based on clusters of voxels which had the highest connection probability with these cortical areas. They reliably segmented the thalamus into several nuclei, reporting that the ventrolateral nucleus of this structure had the highest connection probability with the primary motor cortex. Furthermore, Jakab et al. (2014) used the entire thalamus as a seed, and launched probabilistic tractography to the rest of the cortex. They identified that the ventrolateral nucleus of the thalamus projected to the primary motor cortex.

In this study, we wanted to reconstruct the white matter fibres connecting the thalamus to the primary motor cortex in patients with disorders of consciousness and healthy controls. Specifically, we identified the ventrolateral nucleus of the thalamus using diffusion fractional anisotropy and primary eigenvector maps (see Chapter 2, section 2.1.2) and conducted probabilistic tractography between this seed and the primary motor cortex.

3.1 Materials and Methods

3.1.1 Participants

Patients. A convenience sample of 17 patients who had suffered traumatic brain injury or anoxic brain injury was recruited at the University of Western Ontario (UWO) between 2012 and 2015 as part of a broader research programme. The Western University Health Sciences Research Ethics Board provided ethical approval for the study (Appendix C). The inclusion criteria for this study required patients to be diagnosed with a disorder of consciousness (i.e. VS, MCS or EMCS) therefore two patients were excluded due to their diagnosis of locked-in syndrome (LIS). An additional exclusion criterion was lack of eligibility for the MRI environment. The final sample consisted of eight males and seven females. Ages ranged from 19 to 57 years of age ($M = 37.33$, $SD = 12.25$). Eight patients were VS, five were MCS and two were EMCS. A summary of diagnoses, aetiologies and CRS-R scores and demographic information of the final sample can be found in Table 3. The functional datasets for this patient cohort have previously been reported (Beukema et al., 2016; Fernández-Espejo et al., 2015; Fiacconi and Owen, 2016; Gibson et al., 2014; Gibson et al., 2016; Lant et al., 2015; Naci et al., 2013), only the structural diffusion tensor imaging datasets will be reported in the present study.

Controls. In addition, a cohort of 30 right-handed healthy controls, with no history of psychiatric or neurological disorders, was recruited at UWO between 2011 and 2014 for various research purposes. The UWO Health Sciences Research Ethics Board provided ethical approval for the study. Of these 30 healthy controls, 15 were chosen to match to the patient sample in terms of sex, imaging sequence and scanner system (see MRI acquisition below). The ages of the control group ranged from 18 to 29 years ($M = 24.73$, $SD = 2.69$). For both the patients and healthy controls, functional and structural datasets were collected at the time of scanning.

Table 3: Patient demographic and clinical information

Patient ID	Age	Sex	Diagnosis (CRS-R)	Aetiology[a]	TPI[b] (years)
VS1	38	M	VS (7)	TBI	12
VS2	27	M	VS (8)	TBI	7
VS3	44	F	VS (7)	TBI	20
VS4	57	M	VS (6)	Anoxic	3
VS5	20	F	VS (8)	Other	6
VS6	19	M	VS (7)	Anoxic	2 months
VS7	51	F	VS (5)	Anoxic	1
VS8	52	F	VS (6)	Anoxic	6
MCS1	33	M	MCS (10)	Anoxic	15
MCS2	46	F	MCS (10)	Anoxic	19
MCS3	27	M	MCS (13)	Anoxic	3
MCS4	25	F	MCS (9)	TBI	6
MCS5	40	M	MCS (8)	TBI	3
EMCS1	49	F	EMCS (22)	TBI	12
EMCS2	32	M	EMCS (23)	TBI	4
Mean	37.33				7.81
SD	12.25				6.32

[a] TBI = traumatic brain injury; [b] TPI = time post-ictus

3.1.2   MRI Acquisition

The participant datasets were obtained at the Centre for Functional and Metabolic Mapping (CFMM), at Robarts Research Institute (London, Canada). Between October and December 2013, the CFMM upgraded their 3T Magnetom Trio system (Siemens, Erlangen, Germany) to a 3T Magnetom Prisma system (Siemens, Erlangen, Germany). This upgrade occurred during participant recruitment, as such, some participants were scanned on the first system whilst others were scanned on the second system. Furthermore, two different DTI protocols were used across participants due to the upgrade. The first sequence developed for the Magnetom Trio system included 64 non-collinear directions with a b-value = 700 s/mm^2 (TR = 8700ms, TE = 77ms, voxel size = 2x2x2, no gap, 77 slices). After the upgrade to the Magnetom Prisma system, a matching protocol was created, where the images included 64 non-collinear directions with a b-value = 700 s/mm^2 (TR = 9600ms, TE = 77ms, voxel size = 2x2x2, no gap, 77 slices). A second protocol was designed for the Prisma system, in which the images included 137 non-collinear directions with a b-value = 1500 s/mm^2 (TR = 1980ms, TE = 71ms, voxel size = 2x2x2, no gap, 64 slices, multiband acceleration factor = 4).

Fourteen participants (seven patients, seven healthy controls) were scanned with the Trio system, 16 participants (eight patients, eight healthy controls) were scanned with the Prisma system. Finally, 18 participants (nine patients, nine healthy controls) were scanned with the 64 directions protocol and 12 participants (six patients and six healthy controls) were scanned with the 137 directions protocol.

3.1.3   Statistical Analyses

We calculated the fractional anisotropy (FA) values of each tract in each participant using the FSLUTILS program, fslmaths (http://fsl.fmrib.ox.ac.uk/fsl/fslwiki/Fslutils). Considering we were unable to reconstruct the VL-M1 tracts of interest in three of the 15 DOC patients (MCS1, VS5, VS8), we excluded them from all analyses reported below. We used IBM SPSS Statistics for Windows, Version 23 to run all statistical analyses. To investigate group level difference in fibre tract FA values, we performed repeated measures Analysis of CoVariance (ANCOVA) on lateralized paths. The within-subject factor had two levels, one for each hemisphere. Group (HC/DOC) was used as the between-subject factor when comparing these groups. Linear correlations between the dependent variables and age, sequence, scanner and global FA value were performed to determine which of these variables should be included as non-interest covariates. We tested these variables for covariance to control for the effects of different DTI sequences (64 directions or 137 directions), different scanner (Trio or Magnetom), the natural ageing of the brain and widespread damage sustained after severe brain injury on any differences in VL-M1 tract FA we observed in the data. Only age and global FA values showed significant effects and therefore were included in repeated measures ANCOVA.

A similar approach was used for DOC comparisons. A 2-level within-subject factor was used, one level for each hemisphere. Diagnosis (VS/MCS/EMCS) and clinical level of consciousness (clinically conscious/clinically unconscious) served as between-subject factors. Linear correlations between the dependent variables and age, time post-ictus, aetiology and global FA value were performed to determine which of these variables should be included as covariates. None of these variables showed significant correlations with the dependent variables therefore no covariates were included in repeated measures

ANCOVAs involving DOC patients exclusively. Post-hoc independent samples t-tests were performed when within subject contrasts were significant.

To investigate the relationship between a patient's CRS-R score and their fibre tract FA value, we performed Spearman's rank-order correlations between patient CRS-R scores and each dependent variable. We chose Spearman's rank-order correlation because CRS-R scores are ordinal variables.

3.2   Results

3.2.1   Normality testing

Considering that we would be performing parametric tests for group level comparisons, we tested for homogeneity of variance between groups on each fibre tract as well as normality of fibre tract distribution. Both the left and right fibre tracts violated the homogeneity of variance assumptions between groups. Both healthy control tracts were normally distributed whilst only the right hemisphere fibre tract (right VL to right M1) was normally distributed in patients. The left hemisphere fibre tract (left VL to left M1) in patients was not normally distributed. ANCOVA has been shown to be robust when treating data that deviates from normality or homoscedasticity (Box & Andersen, 1955; Lindman, 1974). As for global FA values, this measure was normally distributed in both the patients and healthy controls and did not violate Levene's test of homogeneity of variance.

3.2.2   Difference between DOC patients and healthy controls

Age and Global FA correlated with the dependent variables so these variables were included as covariates. Repeated measures ANCOVA revealed that DOC patients did not have significantly lower VL-M1 tract FA values than healthy controls ($F_{1,23} = 2.769$, $p = .110$, Partial $\eta^2 = .107$, Observed power: .358). No significant effect of hemisphere or age and global FA was detected. See Figure 6.
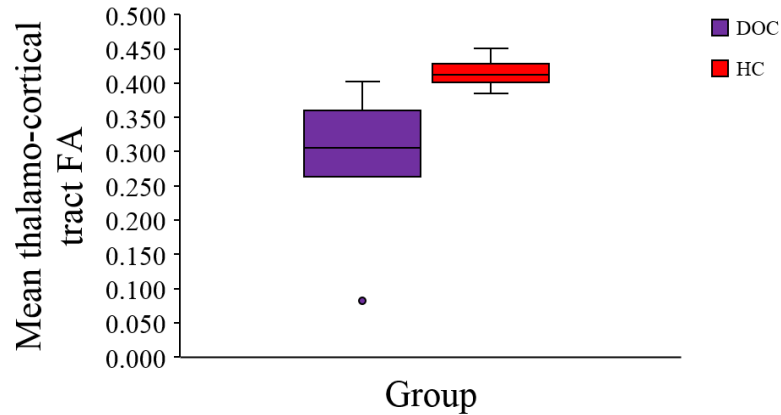
Figure 6: Graphic representation of medians, maximum, minimums and quartiles (25th & 75th) of DOC patients and healthy controls.

3.2.3   Differences within DOC patients

A repeated measures ANCOVA was performed within the patient group, to assess if there were any significant differences between VS, MCS and EMCS FA values. Diagnosis (VS/MCS/EMCS) was the between-subject factor. No covariates were included in this analysis. The effect of diagnosis trended towards significance ($F_{1,9} = 3.494$, $p = .075$, Partial $\eta^2 = .437$, Observed power: .502). Additionally, no significant effects of hemisphere, age or global FA were observed. See Figure 7.
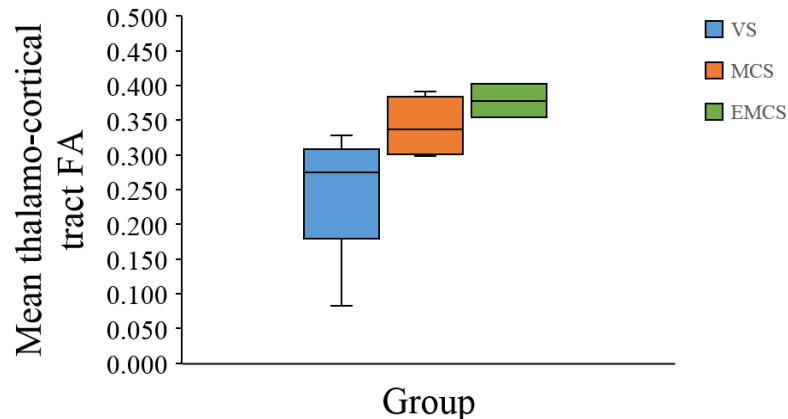
Figure 7: Graphic representation of medians, maximums, minimums and quartiles (25th & 75th) of VS, MCS and EMCS patients.

3.2.4 Difference between clinically conscious and clinically unconscious patients

Due to the low and uneven number of patients in each diagnostic category, we separated patient into two larger groups, based on their capabilities to respond behaviourally. All VS patients were put into one group, henceforth called *clinically unconscious* ($n = 6$), and MCS and EMCS were put together in a second group, henceforth referred to as *clinically conscious* ($n = 6$). Clinical level of consciousness was used as the between-subject factor. Repeated measures ANCOVA revealed that clinically unconscious patients had significantly lower FA values than clinically conscious patients ($F_{1,10} = 7.086$, $p = .024$, Partial $\eta^2 = .415$, Observed power: .671). No significant effects of hemisphere, age or global FA were observed. Additionally, there were no significant differences in time-post ictus ($t_{10} = .115$, $p = .911$) or age ($t_{10} = -.396$, $p = .701$) between clinically conscious and clinically unconscious patients. See Figure 8.
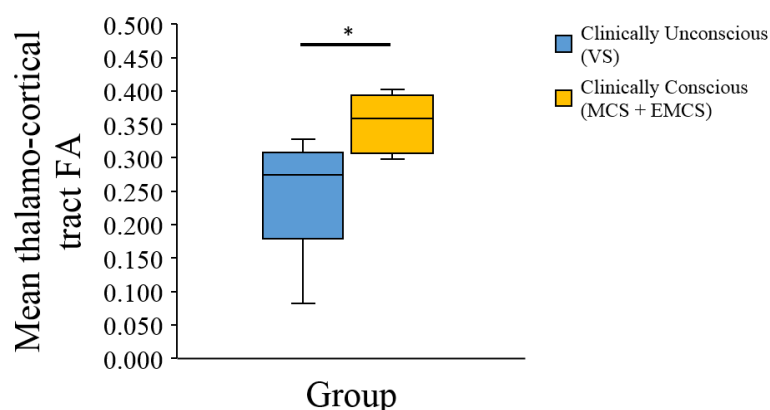
Figure 8: Graphic representation of medians, maximums, minimums and quartiles (25th & 75th) of clinically conscious and clinically unconscious patients.

3.2.5 Differences between clinically conscious patients and healthy controls

Age and Global FA were included as covariates in the following analyses. When comparing clinically conscious (MCS + EMCS) patients to healthy controls, a repeated measures ANCOVA showed that clinically conscious patients had significantly lower FA values than healthy controls ($F_{1,17} = 5.231$, $p = .035$, Partial $\eta^2 = .235$, Observed power:

.578). Furthermore, no significant effects of hemisphere, age or global FA were observed. See Figure 9.
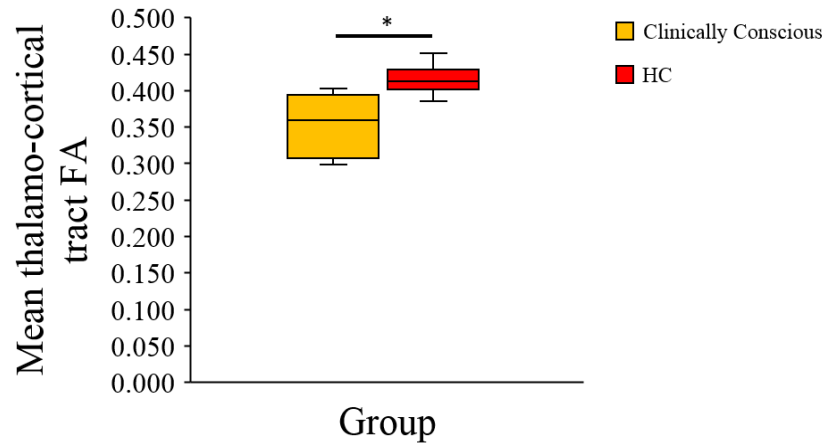
Figure 9: Graphic representation of medians, maximums, minimums and quartiles (25th & 75th) of clinically conscious patients and healthy controls.

3.2.6 Differences between clinically unconscious patients and healthy controls

Age and Global FA were again included in this analysis. After a repeated measures ANCOVA, clinically unconscious patients were revealed to have significantly lower FA values than healthy controls ($F_{1,17} = 7.126$, $p = .016$, Partial $\eta^2 = .295$, Observed power: .711). There were no significant effects of hemisphere, age or global FA. See Figure 10.
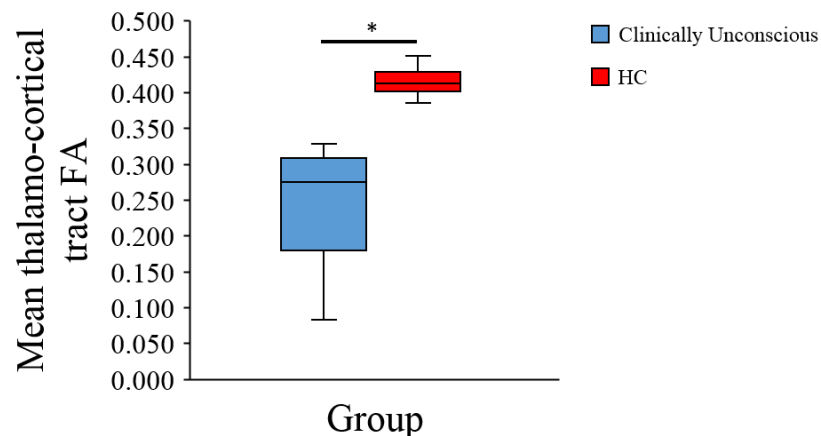
Figure 10: Graphic representation of medians, maximums, minimums and quartiles (25th & 75th) of clinically unconscious patients and healthy controls.

3.2.7 Differences between behaviourally responsive and non-responsive patients

Behaviourally responsive patients were defined as patients who scored a 3 or above on the CRS-R motor subscale (scored above "Reproducible Movement to Command"). These patients showed overt motoric output in response to command. In the following analysis, three patients were behaviourally responsive and nine were behaviourally non-responsive. No covariates were included in this analysis. Repeated measures ANCOVA revealed no significant differences in either fibre tract FA values between behaviourally responsive and non-responsive patients ($F_{1,10} = 1.769$, $p = .213$, Partial $\eta^2 = .150$, Observed power: .226). See Figure 11.
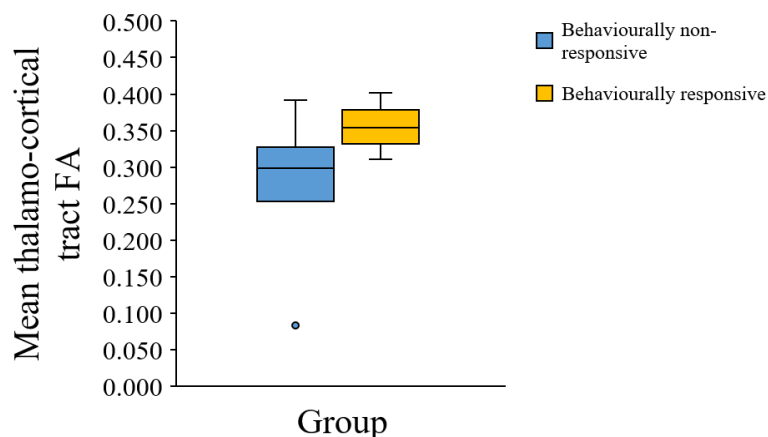
Figure 11: Graphic representation of medians, maximums, minimums and quartiles (25th & 75th) of behaviourally non-responsive and behaviourally responsive patients.

3.2.8 Correlation between fibre tract FA values and CRS-R scores

CRS-R scores were significantly correlated with the left (rho = .815, $p = .001$) and right (rho = .670, $p = .017$) fibre tract. See Figure 12 and 13 for the correlations between CRS-R scores and the dependent variables.
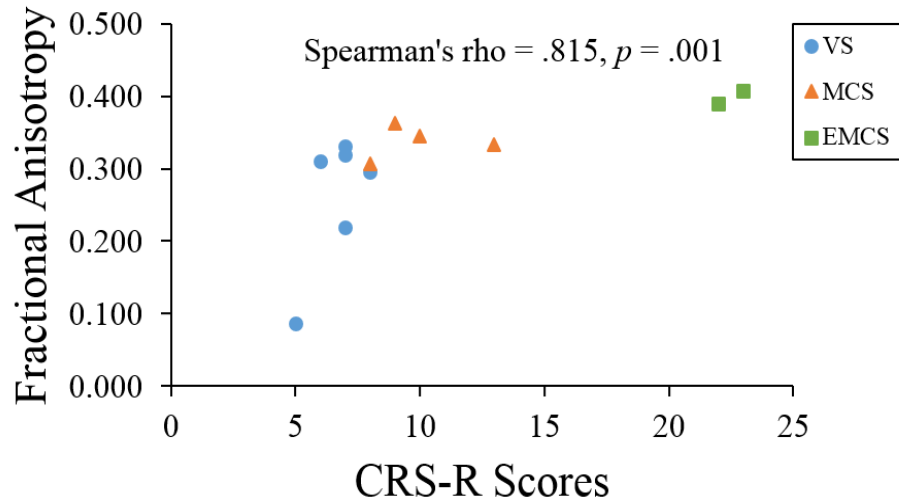
Figure 12: Spearman correlation between the left VL-M1 tract fractional anisotropy values and CRS-R scores in 12 DOC patients.
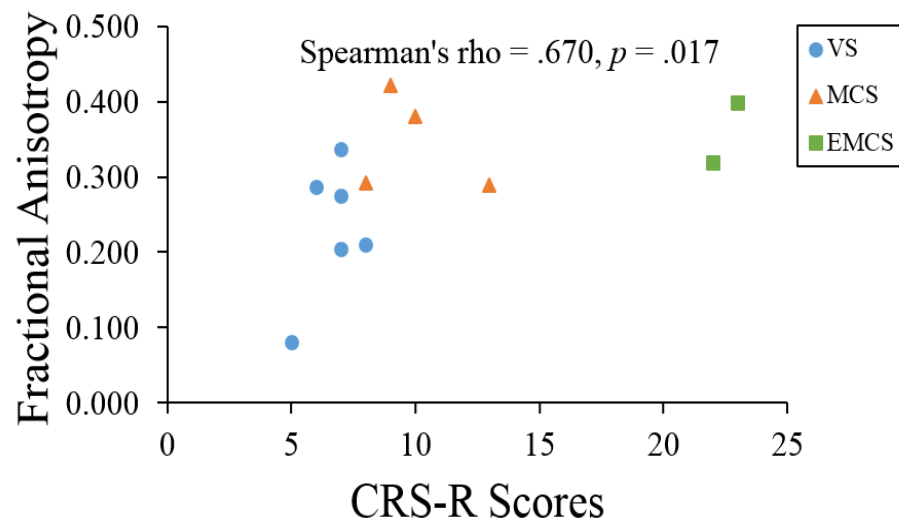
Figure 13: Spearman correlation between the right VL-M1 tract fractional anisotropy values and CRS-R scores in 12 DOC patients.

3.3 Discussion

In this study, we assessed the integrity of white matter fibres between the ventrolateral thalamic nuclei and primary motor cortices in 12 DOC patients *in vivo*. Confirming previous work (Fernández-Espejo et al., 2015), significant abnormalities were observed in the integrity of VL-M1 fibres, when comparing DOC subgroups to healthy controls. Both clinically conscious (VS) and clinically unconscious (MCS+EMCS) DOC patients

showed significant impairment when compared to healthy controls and clinically unconscious patients showed significant impairment when compared to clinically conscious patients. In accordance with previous conclusions posited by Graham et al. (2005), clinically unconscious and clinically conscious patients differed in the magnitude of the abnormalities This is also evidenced by the positive correlation between patient VL-M1 tract FA values and CRS-R scores. This suggests that the integrity of this tract influences performance on the CRS-R. Furthermore, when comparing behaviourally responsive patients to patients who showed no evidence of overt responsiveness, we found no significant differences in VL-M1 FA values between these two groups. This, however, we explain largely in part to low power of the analysis as the groups were unequal in size ($n = 3$ and $n = 9$ respectively) and metrics from the unresponsive groups could easily mask any detectable differences from the small responsive group.

Curiously, when comparing the DOC group as a whole (VS+MCS+EMCS) to the healthy control group, no significant differences were observed. This does not converge with our reported results of each clinical subgroup, where both clinically conscious and clinically unconscious patients showed significant reduction in FA compared to controls. Upon further inspection of the data, there seems to be a single data point in the DOC group that strongly deviates from the mean (Patient left VL-M1 FA, .085 vs DOC group left VL-M1 mean [SD] FA .308 [.085]; Patient right VL-M1 FA, .080 vs DOC group right VL-M1 mean [SD] FA, .291 [.094]). When this data point is removed, the analysis involving all DOC patients compared to controls then becomes significant. Furthermore, the analysis involving the comparison across diagnostic groups (VS/MCS/EMCS) also becomes significant when this data point is excluded. More investigation into the non-normality of this data point must be conducted to further assess its effect on group level analyses and the results reported above.

We reconstructed the fibres carrying ascending information to the cortex (Parent & Hazrati, 1995). Structural impairment of this pathway would perturb communication between the thalamus and the primary motor cortex, thereby hindering patients' abilities to volitionally generate motoric output to respond to command. The 12 patients described above showed significantly lower FA values in this specific tract beyond global white

matter damage, as evidenced by the lack of significant effect of global white matter damage in all analyses reported. Participant age also showed no effect in the repeated measures ANCOVA, which suggests that natural aging of the brain is not driving the significant reduction in FA seen in DOC patients compared to controls. At first glance, these results seem to support the specificity of this VL-M1 tract in explaining the lack of overt responsiveness in these patients. However, the mechanisms supporting this selective damage have yet to be described therefore our results should be interpreted with care.

Chapter 4

4. Study II – Investigating the relationship between overt behavioural responses and motor loop fibre integrity in patients with disorders of consciousness.

To expand on the results from Study I and to further our understanding of the neural underpinnings of motor execution in our patient group, we decided to conduct a follow-up study. Using the same sample of DOC patients as above, we not only reconstructed the tract from the ventrolateral thalamus to M1 but also a closed motor loop: from M1 to the ventrolateral thalamus to the dentate nucleus (DN) in the cerebellum. The dentate nucleus projects to M1 (Allen & Tsukahara, 1974; Hoover & Strick, 1999) via the thalamus (Shinoda et al., 1985; Dum & Strick, 2003; Evrard & Craig, 2008). Specifically, the cerebellum processes behaviourally relevant information received from the primary motor cortex via the corticopontocerebellar tract (the feedforward open loop), before sending the information back out to M1via the ventrolateral thalamus (the feedback open loop). The feedback connection between the cerebellum and M1 has been shown to be involved in adaptive motor learning, and to adapt movements to changes in the environment (Glickstein, 2000). The exact location where pontocerebellar fibres terminate in the cerebellum is still unknown (Glickstein, 2007) which is why we chose the dentate nucleus as an ROI in both VL-DN and M1-DN fibres, to reconstruct a closed cortico-cerebellar motor loop.

In this study, a total of nine DOC patients and five healthy controls were excluded from the original sample. These patients and controls had been scanned with the 64-direction protocol described in Study I and this acquisition protocol was unable to reconstruct two of our three tracts of interest. Therefore, we focused our analyses on the remaining six DOC patients from the sample used in Study I, who had all been scanned with the previously described 137-directions acquisition protocol and with whom we were able to reconstruct all three motor tracts for this study. We included in the study 15 healthy controls who had also been scanned with the 137-directions protocol. In this focused group of DOC patients, we wish to examine if localized impairment to the motor VL-M1 tract explains DOC patients' lack of overt responsiveness or if impairment to other

components of the motor loop contribute to this lack of overt volitional behaviours. As a result of the small sample size in this study, we will focus on describing the clinical profile in concordance with their individual diffusion results, rather than performing group-level analyses.

4.1 Materials and Methods

4.1.1 Participants

Patients. The same convenience sample of 15 DOC patients from Study I was used in this follow-up study. The Western University Health Sciences Research Ethics Board provided ethical approval for the study (Appendix C). After data preprocessing and probabilistic tractography, nine patients were excluded from this study (see DTI Analyses). Therefore, the final sample for this study consisted of six patients, four of whom were female. Ages ranged from 25 to 52 years of age ($M = 40.67$, $SD = 12.14$). Three patients were VS, two were MCS and one was EMCS. A summary of diagnoses, aetiologies and CRS-R scores and demographic information of the final sample can be found in Table 4.

Controls. For this follow-up study, 15 controls were chosen to match the patient sample in terms of imaging sequence (see DTI Analyses). The ages of this control group ranged from 18 to 29 years ($M = 23.80$, $SD = 3.34$) and this sample was composed of seven males and eight females.

4.1.2 Clinical Descriptions

Patient VS2 was a male who, seven years before the MRI session, at the age of 20, suffered a severe closed head injury in a motor vehicle accident. The patient's Glasgow Coma Scale (GCS) score at the scene and from the ER were not available in the medical records provided to the UWO research team. A CT scan during his admission revealed bilateral intracerebral bleeds as well as left temporal and ventricular hemorrhage. The scan also showed a lacunar infarct in the right lentiform nuclei with ischemic changes in the deep white matter of the right occipitoparietal region. The patient also exhibited frequent focal seizures on admission. On admission to our study, VS2's medical

diagnosis indicated a prolonged period of decreased levels of consciousness. Over a five-day period in 2014, a total of five behavioural assessments by the Owen research team were conducted at the University of Western Ontario using the Coma Recovery Scale – Revised (CRS-R). In all of them the patient showed responses consistent with a diagnosis of VS. See Table 5 for details. This patient was unable to overtly respond to commands nor did they show evidence of covert command following.

Patient VS7 was a female who suffered a myocardial infarction at the age of 50, one year before admission to this study. Acute records including the patient's GCS score at the scene and from the ER, as well as CT scan upon admission were not available to the UWO research team. The medical diagnosis upon admission was that of the persistent vegetative state. According to records kept by the patient's kin reporting their impressions throughout their relative's hospitalization, it was noted that the attending physicians deemed all movements as reflexive (no intentional movements). During her five day stay at the University of Western Ontario, she was assessed five times using the CRS-R. In all of them the patient showed responses consistent with a diagnosis of VS. See Table 5 for behavioural features. This patient did not show evidence of behavioural command following or covert command following.

Table 4: Patient demographic and clinical information

Control ID	Age	Sex	Diagnosis (CRS-R)	Aetiology[a]	TPI[b] (years)
VS2	27	M	VS (8)	TBI	7
VS7	51	F	VS (5)	Anoxic	1
VS8	52	F	VS (6)	Anoxic	6
MCS4	25	F	MCS (9)	TBI	6
MCS5	40	M	MCS (8)	TBI	3
EMCS1	49	F	EMCS (22)	TBI	12
Mean	40.67				5.83
SD	12.14				3.76

[a] TBI = traumatic brain injury; [b] TPI = time post-ictus

Patient VS8 was a female who suffered from hypoxic ischemic encephalopathy at the age of 45, seven years before her MRI. The acute records provided to our research team did not include details about GCS score at the scene and from the ER or CT scan findings. However, their hospital admission diagnosis indicated that she was deeply comatose, responded momentarily to deep painful stimuli and presented decorticate

posture. Over a four-day period at the University of Western Ontario, she was behaviourally assessed four times using the CRS-R. In all of them, the patient showed responses consistent with a diagnosis of VS. See Table 5 for behavioural features. This patient showed no evidence for behavioural or covert command following.

Patient MCS4 was a female who suffered a closed head motor vehicle accident six years before the MRI scan at the age of 20. The acute records did not include details about patient's GCS score at the scene and from the ER. A CT scan during her admission revealed a bilateral basal ganglia subarachnoid hemorrhage, intraventicular hemorrhage, a right caudate infarct, a right frontal hemorrhage, a small right parietal subdural hematoma and a left sacral fracture. At admission to our study, her medical records indicated severe cognitive impairments and severe motor/coordination impairments that would be consistent with a minimally conscious state. Over a five-day period at the University of Western Ontario, the patient was behaviourally assessed five times using the CRS-R and the above diagnosis was confirmed. The patient showed consistent visual pursuit and was thus diagnosed as MCS. See Table 5 for behavioural features. Patient MCS4 showed no evidence of behavioural command following nor did they show evidence of motor imagery; however, they did show consistent evidence of spatial navigation.

Patient MCS5 was a male who suffered a closed head injury in a motor vehicle accident 3 years before his MRI scan, at the age of 36 years old. The patient's GCS score at the scene was 5 and was 3-5 in the ER, indicating consistent comatose state across both assessments. There is no information about his CT scan upon admission however it was reported that at the scene he was bleeding from his left ear canal, suffered a basal skull fracture and multiple facial bone fractures. On admission to our study, medical records show that his medical diagnosis was persistent vegetative state. However, over the five-day period of tests at the University of Western Ontario, he was behaviourally assessed five times using the CRS-R and showed reproducible evidence of visual pursuit, which is consistent with a diagnosis of MCS. See Table 5 for behavioural features. Patient MCS5 showed no evidence of behavioural or covert command following.

Table 5: Patient behavioural features from the CRS-R

	Patient ID					
	VS2	VS7	VS8	MCS4	MCS5	EMCS1
Auditory Function Scale						
4-Consistent movement to command*	0	0	0	0	0	4
3-Reproducible movement to command*	0	0	0	0	0	0
2-Localization to sound	2	0	0	2	0	0
1-Auditory startle	0	1	1	0	1	0
0-None	0	0	0	0	0	0
Visual Function Scale						
5-Object Recognition*	0	0	0	0	0	5
4-Object localization: Reaching*	0	0	0	0	0	0
3-Visual pursuit*	0	0	0	3	3	0
2-Fixation*	0	0	0	0	0	0
1-Visual startle	1	1	0	0	0	0
0-None	0	0	0	0	0	0
Motor Function Scale						
6-Funtional object use*	0	0	0	0	0	6
5-Automatic motor response*	0	0	0	0	0	0
4-Object manipulation*	0	0	0	0	0	0
3-Localizatoin to noxious stimulation*	0	0	0	0	0	0
2-Flexion withdrawal	2	0	2	0	0	0
1-Abnormal posturing	0	1	0	1	1	0
0-None/Flaccid	0	0	0	0	0	0
Oromotor/Verbal Function Scale						
3-Intelligible verbalization*	0	0	0	0	0	0
2-Vocalization/oral movement	0	0	0	0	0	2
1-Oral reflexive movement	1	1	1	1	1	0
0-None	0	0	0	0	0	0
Communication Scale						
2-Functional: Accurate[+]	NA	0	0	0	0	2
1-Non-functional: Intentional*	NA	0	0	0	0	0
0-None	NA	0	0	0	0	0
Arousal Scale						
3-Attention	0	0	0	0	0	3
2-Eye opening w/o stimulation	2	0	2	2	2	0
1-Eye opening w/ stimulation	0	1	0	0	0	0
0-Unarousable	0	0	0	0	0	0
TOTAL CRS-R SCORE	8	5	6	9	8	22

[+] Denotes emergence from MCS; * Denotes MCS; NA: Could not be evaluated/observed

Finally, **patient EMCS1** was female who, 13 years before her MRI scan, at the age of 36, suffered a closed head injury in a motor vehicle accident. The patient's GCS at the scene

was 3. Her GCS score in the ER was not recorded. There is no information about her admission CT scan although it was noted that the patient presented with global cerebral dysfunction, infrequent epileptic seizures and multiple contractures. Their medical records show that on admission to our study, EMCS1 was diagnosed as persistent vegetative/minimally responsive states. During the week of the patient's scan, she was only assessed on two occasions, with the use of the CRS-R. On one day, she was diagnosed as EMCS because she showed evidence of functional object use with their right upper limb however on the second assessment day, she was diagnosed as MCS because she showed evidence of object manipulation instead. This patient visited the University of Western Ontario on two occasions prior to her scans, where she was assessed with the CRS-R: once three months prior and a second time two months before her scans. Both assessments showed diagnoses of EMCS, again because she reliably demonstrated functional object use. See Table 5 for behavioural features. As described above, patient EMCS1 showed consistent evidence of behavioural command following and she also showed consistent evidence of spatial navigation. She did not, however, show evidence for motor imagery.

4.1.3 MRI Acquisition

The participant datasets were obtained at the Centre for Functional and Metabolic Mapping (CFMM), at Robarts Research Institute (London, Canada). The DTI protocol used for this study was designed for the 3T Magnetom Prisma system, in which the images included 137 non-collinear directions with a b-value = 1500 s/mm^2 (TR = 1980ms, TE = 71ms, voxel size = 2x2x2, no gap, 64 slices, multiband acceleration factor = 4). In total, 21 participants (six patients and 15 healthy controls) were scanned with the 137 directions protocol for this study.

4.1.4 Statistical Analyses

Single case-control statistical analyses were conducted using the BTD_Cov.exe program that accompanies the paper from Crawford, Garthwaite & Ryan (2011). This program compares a patient's score to the score of the control group sample, in the presence of covariates. Linear correlations between the six dependent variables and age and global

FA values were performed, to determine which of these variables should be included as non-interest covariates. Age showed significant effects for both VL-M1 and M1-DN tracts. We excluded global FA as a variable in the following analyses because we are studying more fibres of interest. Global FA in not needed to control for the specificity of any impairment observed as we can test for impairment specificity by observing any differential effects at each fibre. Additionally, BTD_Cov.exe provides a point estimate (as well as the 95% confidence intervals) of the abnormality of the patient's score. In other words, it provides an estimate of the percentage of the control population that would obtain a score lower than the patient's (Crawford, Garthwaite & Ryan, 2011). Finally, this program also provides an interval estimate of the effect size (ES) of the difference between the case and control group. See Table 6 for fibre tract FA values for each patient and healthy control group means and standard deviations. We hypothesized that all the patients' tracts would have lower FA values than the healthy control group's mean FA and thus we established significance at one-tail $\alpha = .05$.

To investigate the relationship between a patient's CRS-R score and their fibre tract FA value, we performed Spearman's rank-order correlations between CRS-R scores and each dependent variable.

Table 6: Healthy controls' fibre tracts FA means and standard deviations and individual patient's fibre tract FA values

Group		LVL-LM1	RVL-RM1	LM1-RDN	RM1-LDN	LVL-RDN	RVL-LDN
				Fibre tracts			
Healthy controls	Mean	.398	.402	.416	.406	.352	.305
	SD	.024	.021	.021	.025	.029	.030
DOC patients	VS2	.296	.210	.294	.276	.353	.368
	VS7	.085	.080	.260	.267	.290	.337
	VS8	.000	.000	.000	.000	.242	.252
	MCS4	.361	.422	.378	.417	.437	.406
	MCS5	.305	.291	.332	.287	.365	.265
	EMCS1	.389	.320	.390	.277	.437	.317

4.2 Results

We reconstructed all three tracts in five of the six patients and all 15 healthy participants. In patient VS8, we could only reconstruct the VL-DN tract and therefore they could not be included in four of the six analyzes described below. As in Study I, we used mean FA as a measure of the structural integrity of each tract. We hypothesized that all the patients' tracts would have lower FA values than the healthy control group's mean FA and thus we established significance at one-tail $\alpha = .05$.

4.2.1 Differences between VS patients and healthy controls

Patient VS2 showed FA values that were significantly different from the healthy group, bilaterally, on the VL-M1 tract, the M1-DN tract and showed lateralized significant differences in the right VL-DN tract. The FA value of this patient's VL-DN tract was significantly *higher* compared to the control group. The left VL-DN tract did not differ from the healthy control group

Patient VS7 showed significantly reduced FA bilaterally in the VL-M1 tract and M1-DN tract. They also showed significantly lower FA in the left VL-DN tract. The right VL-DN tract did not differ from the healthy control group.

In patient VS8, we were unable to reconstruct the VL-M1 and M1-DN tracts; we were only able to reconstruct the VL-DN tract, which we include in the following analyses. Patient VS8 showed reduced FA in the left hemisphere of the VL-DN tract and showed a trend toward significant FA reduction in the right hemisphere of this tract. See Table 7.

4.2.2 Differences between MCS/EMCS patients and healthy controls

Patient MCS4 showed no significant reduction in FA values in either VL-M1 tracts or M1-DN tracts. Their left M1-DN tract however, trended towards significance. Additionally, patient MCS4 showed no significant reduction in FA values in the bilateral VL-DN tracts – they showed significantly *higher* FA values in both tracts compared to the healthy control group.

Table 7: P-values, point estimates and effect sizes of patient FA values

Patient	Fibre tract	*P*-value	Point estimate	Effect size (UCI-LCI)
VS2	Left VL-M1	0.00126	0.1257	-4.124 (-2.289 - -5.629)
	Right VL-M1	0.00000	0.0001	-9.229 (-5.437 - -12.330)
	Left M1-DN	0.00007	0.0066	-5.915 (-3.410 - -7.963)
	Right M1-DN	0.00021	0.0209	-5.190 (-2.959 - -7.014)
	Left VL-DN	0.48190	51.8102	0.048 (0.554 - -0.048)
	Right VL-DN	0.03045	96.9551	2.105 (3.014 - 1.169)
VS7	Fibre tract	*P*-value	Point estimate	Effect size (UCI-LCI)
	Left VL-M1	0.00019	0.0186	-11.905 (-5.234 - -17.468)
	Right VL-M1	0.00002	0.0016	-15.277 (-7.550 - -21.650)
	Left M1-DN	0.02805	2.8048	-5.250 (-0.263 - -9.676)
	Right M1-DN	0.04163	0.0833	-4.697 (0.184 - -9.070)
	Left VL-DN	0.03049	3.0486	-2.104 (-1.171 - -3.014)
	Right VL-DN	0.15803	84.1970	1.074 (1.701 - 0.419)
VS8	Fibre tract	*P*-value	Point estimate	Effect size (UCI-LCI)
	Left VL-M1	NA	NA	NA
	Right VL-M1	NA	NA	NA
	Left M1-DN	NA	NA	NA
	Right M1-DN	NA	NA	NA
	Left VL-DN	0.00133	0.1333	-3.761 (-2.285 - -5.218)
	Right VL-DN	0.05083	5.0828	-1.810 (-0.963 - -2.631)
MCS4	Fibre tract	*P*-value	Point estimate	Effect size (UCI-LCI)
	Left VL-M1	0.09776	9.7762	-1.470 (-0.639 - -2.164)
	Right VL-M1	0.19774	80.2256	0.946 (1.541 - 0.259)
	Left M1-DN	0.05931	5.9315	-1.800 (-0.867 - -2.571)
	Right M1-DN	0.32813	67.1869	0.490 (1.035 - -0.103)
	Left VL-DN	0.00660	0.0132	2.931 (4.105 - 1.732)
	Right VL-DN	0.00273	99.7273	3.391 (4.720 - 2.040)
MCS5	Fibre tract	*P*-value	Point estimate	Effect size (UCI-LCI)
	Left VL-M1	0.04482	4.4818	-3.158 (-0.154 - -5.828)
	Right VL-M1	0.00474	0.4742	-5.241 (-1.756 - -8.202)
	Left M1-DN	0.07172	7.1721	-2.681 (0.234 - -5.307)
	Right M1-DN	0.01380	1.3801	-4.273 (-1.027 - -7.079)
	Left VL-DN	0.32739	67.2609	0.472 (0.998 - -0.071)
	Right VL-DN	0.10758	10.7575	-1.341 (-0.623 - -2.033)
EMCS1	Fibre tract	*P*-value	Point estimate	Effect size (UCI-LCI)
	Left VL-M1	0.37681	62.3189	0.752 (4.709 - -3.280)
	Right VL-M1	0.06461	6.4609	-3.814 (0.615 - -7.825)
	Left M1-DN	0.31098	68.9024	1.186 (5.132 - -2.884)
	Right M1-DN	0.04375	4.3745	-4.350 (0.175 - -8.405)
	Left VL-DN	0.00652	99.3484	2.937 (4.113 - 1.736)
	Right VL-DN	0.34981	65.0191	0.407 (0.927 - -0.128)

Patient MCS5 demonstrated bilateral FA reductions on both VL-M1 tracts and the right M1-DN tract. They showed no significant differences in the left M1-DN tract or either VL-DN tracts.

Finally, patient EMCS1 showed a trend towards a significant FA reduction in the right VL-M1 tract, and a significant FA reduction in the right M1-DN tract. She showed no significant FA reduction in either the left VL-M1 or M1-DN tracts. Additionally, this patient showed no significant reduction in FA values in the left VL-DN tract – she showed significantly *higher* FA values compared to the healthy control in the left VL-DN tract. See Table 7.
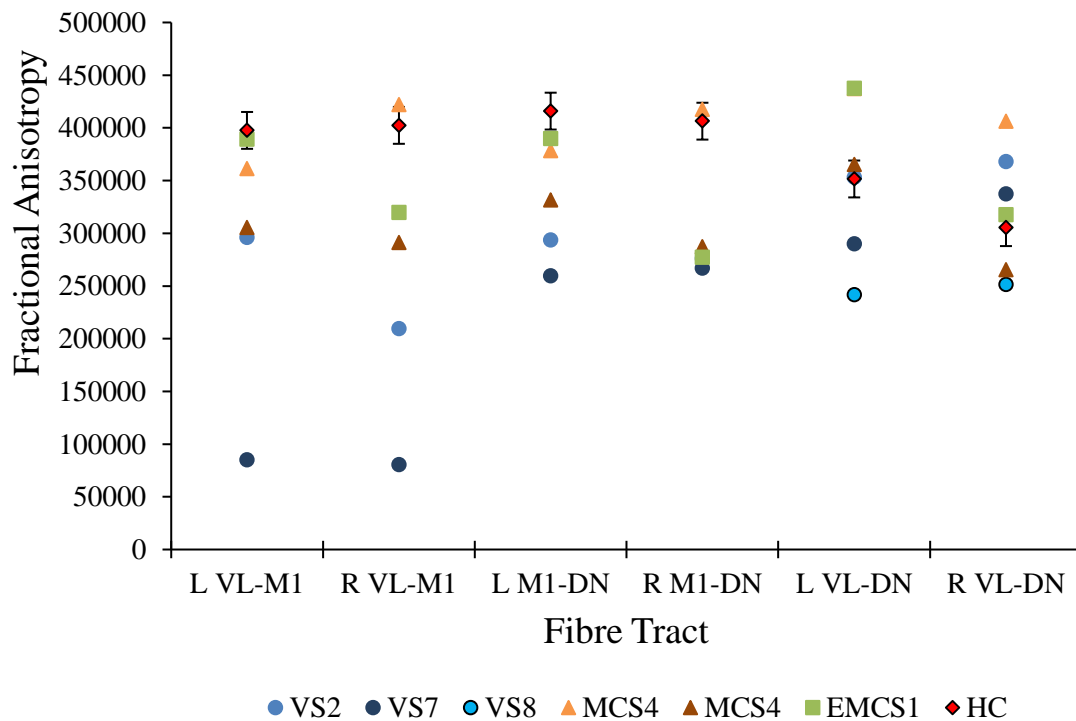
Figure 14: Raw fractional anisotropy score of each DOC patient and controls for each motor fibre path.

4.2.3   Correlation between fibre tract FA values and CRS-R scores

CRS-R scores were significantly correlated with the left hemisphere FA values of each tract of interest: left VL-M1 fibre tract (rho = .975, p = .005), left M1-DN fibre tract (rho = .975, p - .005) and left VL-DN fibre tract (rho = .928, p = .008). CRS-R scores were

not significantly correlated with any of the right hemisphere fibre tract FA values (see Figure 15).
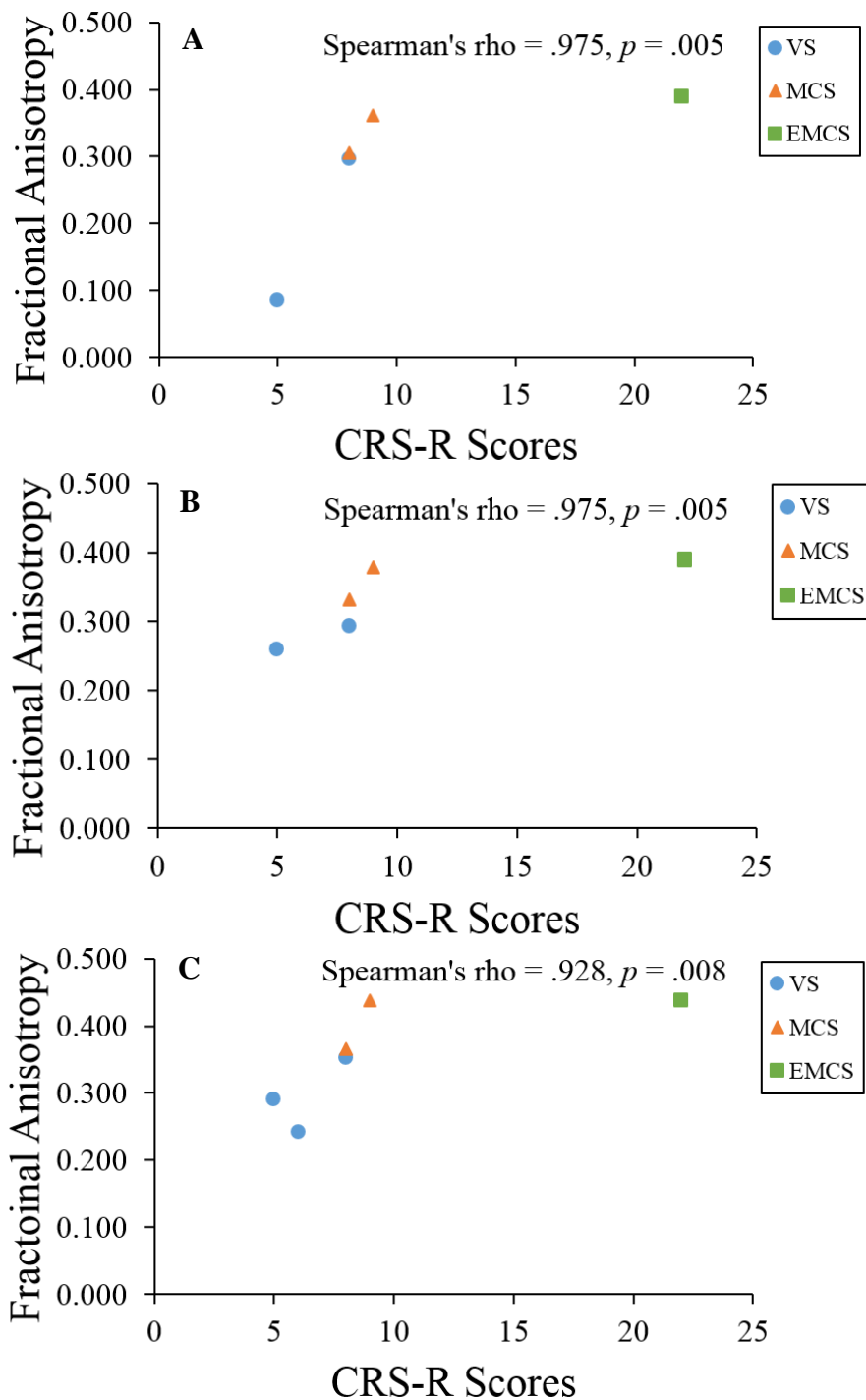
Figure 15: Significant spearman correlations of CRS-R scores and fibre tract FA values for DOC patients. Panel A: left VL-M1 tract, $n = 5$; B: left M1-DN tract, $n = 5$; Panel C: left VL-DN tract, $n = 6$.

4.3 Discussion

In Study II, we reconstructed a closed motor cortico-cerebellar loop: we reconstructed efferent connections from the primary motor cortices to the cerebellum, efferent connections from the dentate nucleus of the cerebellum to the ventrolateral thalamus and as in Study I, afferent information to the primary motor cortex from the ventrolateral thalamus. We assessed the integrity of each of these loop segments in each DOC patient compared to a group of healthy controls using single-case comparison methodology. None of the patients in this study showed evidence of covert awareness in any fMRI or EEG task.

In patient VS2, bilateral VL-M1 and M1-DN tracts showed significant impairments compared to controls. VL-DN tracts were intact in this patient. When described alongside their clinical profile, the structural impairment supports their overt capabilities: this patient showed consistent evidence of localization to sound. Their selective damage to VL-M1 and M1-DN would prevent them producing volitional, cognitively-mediated output in response to command. However, as they showed low level responses in a different modality, it may be reasonable to speculate that their intact VL-DN tracts support this ability, considering the cerebellum's implication in orienting movements to changes in the environment (Tseng et al., 2007; Galea et al., 2011). When testing for localization to sound, CRS-R guidelines require the examiner to stand behind the patient, out of view and present an auditory stimulus (voice or noise) for five seconds on each side. For a patient to successfully complete this task, they must orient their head or eye in the direction of stimulus presentation on two trials (in the same direction), and scoring *is not* dependent on degree or duration of the head/eye movement (Giacino & Kalmar, 2004). The patient is not overtly asked to orient their head/eyes in the direction of the stimulus. Their response is not goal-directed, it is reactionary. Acoustic processing (verbal and non-verbal sounds) has been found to involve the primary auditory cortices and surrounding lateral superior temporal cortices (Formisano et al., 2003; Wessinger et al., 2001; Zatorre & Belin, 2001). More complex auditory processing, such as lexico-semantic processing, is supported by the anterior, middle, inferior and medial temporal areas in addition to inferior parietal and anterior inferior prefrontal regions (Binder et al.,

2000; Longoni et al., 2005; Majerus et al., 2002; Martin, 1996). As such, the sound of paper rustling or a click is a much simpler stimulus to respond to, as opposed to generating movement in response to an auditory command. It has previously been shown that both VS and MCS respond similarly in response to auditory stimuli. Both diagnostic groups showed increased activation in auditory cortices, in addition to transverse temporal gyri and superior temporal gyrus. VS patients however, showed a much weaker activation in these areas compared to MCS patients (Boly et al., 2004). Furthermore, MCS patients demonstrated preserved functional connectivity between secondary auditory cortices, posterior temporal and prefrontal areas. The authors suggest that this preserved connection between auditory cortices and higher association areas allows MCS patients to process more complex auditory stimuli and to reliably demonstrate signs of command following. In the case of VS2, higher association motor areas like M1 may therefore not be required to generate movement in response to acoustic noise the environment. Higher association areas may only be recruited when processing stimuli requiring a cognitively-mediated response. We could therefore hypothesize that intact VL-M1 and/or M1-DN tracts are not essential to orient simple movements to low-level stimuli. It should be noted that localization to sound and auditory startle are two separate items. Auditory startle is a loud, unexpected stimulus used to elicit a reflexive response. Localization to sound is designed to assess if the patient can appraise that there is a change in their acoustic environment.

Similar results were found in patients VS7 and VS8. Structurally, both patients showed bilateral impairment in the VL-M1 and VL-DN tracts. However, they showed lateralized impairments in the VL-DN tracts. Behaviourally, these two patients differed from patient VS2 in that they could not localize to sound. This further supports the idea that connections between the cerebellum and thalamus could support low-level movements, as simple as a glance, in response to stimuli that do not require cognitive mediation.

Both MCS4 and MCS5 were diagnosed as MCS based on their ability for visual pursuit. Interestingly, they showed significant structural differences: MCS4 showed no significant impairment in any of the three tracts of interest, with the left M1-DN tract trending

towards significance while MCS5 showed significant impairment in bilateral VL-M1 tracts and the right M1-DN tract.

One explanation for MCS4's intact motor tracts but lack of other signs of awareness could be related to their subcategorization within the MCS population. MCS patients can be divided into two groups: MCS+ and MCS-. MCS+ patient usually show more complex signs of return to consciousness, such as object reaching or intelligible verbalizations. (Bruno et al., 2011; Bruno et al., 2012). It is possible that MCS4 is MCS- and does not possess a level of awareness that would allow her to perform complex behaviours beyond visual pursuit which suggests that the CRS-R is capturing the real of awareness of this patient. Another characteristic of the MCS- subgroup is their consistent difficulty to focus their attention and maintain vigilance (Thonnard et al., 2014). This could point to impairment in the mesocircuit, as discussed in Chapter 1. With an intact cortico-cerebellar motor loop, they may have the physical ability to generate overt responses but are unable to sustain sufficient levels of arousal to complete the tasks. It has previously been shown that a return of sustained arousal is most often followed by a return of motor functions (Schiff, 2010). This would call for further investigation of mesocircuit and cortico-subcortico-cerebellar paths within individual DOC patients to dissociate the involvement motor impairments from depressed arousal in patient overt responsiveness. However, the fact that MCS4's cortico-cerebellar loop was intact would contradict the notion that they are MCS-, as preserved brain networks are characteristic of MCS+ patients (Bruno et al., 2011; Bruno et al., 2012). Another, simpler, explanation for an intact cortico-cerebellar loop but simultaneous lack of complex behaviours would be the fluctuating vigilance in MCS patients (whether MCS+ or MCS-). The visual function scale is the second scale to be assessed during administration of the Coma Recovery Scale-Revised. It is possible that after successfully completing visual pursuit, MCS4 was overcome by fatigue after the effort. As discussed in Chapter 1, many external factors can affect a patient's performance on behavioural scales. Exhaustion is one of these exogenous variables, and may have precluded MCS4 from completing the rest of the assessment, despite possessing enough awareness and the physical ability to do so.

A simple explanation for MCS5's clinical presentation would be supporting Graham et al. (2005)'s idea of magnitude, not location. Although MCS5 sustained damage similar to VS2, they did not sustain *as much* damage as VS2 and thus the residual motor capabilities allow MCS5 to demonstrate visual pursuit. We could speculate that MCS5 is truly and MCS- patient and does not possess the capabilities to perform complex behaviours beyond visual pursuit.

Patient EMCS1, interestingly, displayed selective, lateralized damage to the right M1-DN tract and the impairment in their right VL-M1 tract trended towards significance. They did not show damage in either VL-DN tract. Behaviourally, EMCS1 was capable of: consistent movement to command, functional object use, and functional communication. Specifically, this patient was capable of these behaviours only with the right side of their body. That is to say, that their entire left M1-DN motor loop was intact, allowing for these overt responses, whilst their right VL-M1 and M1-DN tracts were significantly impaired, seemingly precluding the left side of their body from overt responsiveness. In this patient, their structural damage and behavioural profile provides further evidence for the hypothesis that in some patients, impairment of motor tracts may be affecting their overt capabilities to respond.

Interestingly, we found lateralization effects in the relationship between impairment to the motor tracts studied above and CRS-R scores. Only the left hemisphere tracts significantly correlated with CRS-S scores, while none of the right hemisphere tracts showed significant effects. This confirms previous results by Lutkenhoff et al. (2015), who found increased left-lateralized damage to the thalamus in non-traumatic brain injury DOC patients. Although the functional significance of this lateralization has yet to be examined, the authors do stress the dependence of clinical behavioural assessments on residual language processing in these patients and highlight the need to develop non-language based tasks when evaluating awareness.

 A future direction for this study would be the description of the basal ganglia's role in motor execution. The cortico-cerebellar loop described above works in conjunction with a smaller motor loop, involving the basal ganglia (Parent & Hazrati, 1995; Hoover &

Strick, 1999). The basal ganglia comprise the striatum, pallidum substantia nigra and subthalamic nucleus. This cluster of regions receive input from the primary motor cortex and feeds back into M1 through the ventrolateral thalamus, thus creating the cortico-basal ganglia-thalamo-cortical loop (Hoover & Strick, 1999). These two motor loops operate alongside each other in coordinating goal-directed behavior. The role of the cerebellum in motor control has been well established (Britsch et al., 1996; Lotze et al., 1999; Nair et al. 2003) but the exact role of the basal ganglia in motor control is still unclear (Parent & Hazrati, 1995). One of its proposed functions is the selection and triggering of coordinated voluntary movements. Indeed, patients with damage to one or all basal ganglia structures have shown hyperkinetic disorders, including chorea, ballism and tics or hypokinetic disorders such as akinesia, bradykinesia and rigidity (Albin, Young & Penney, 1989). In the above study, we did not reconstruct the cortico basal ganglia-thalamo-cortical loop. Therefore, the involvement of the cerebellum in DOC responsiveness proposed earlier must remain speculative. Additional investigation of the implications of both these motor loops in motor control in DOC must be undertaken before robust conclusions can be made about the involvement of motor impairment in overt responsiveness in this clinical population.

Chapter 5

5.   Study III - Assessment of different diffusion tensor acquisition protocols at ultra-high fields

Although understanding the type of information DTI provides and how to interpret this information is important, starting from ground zero and ensuring that the scanner acquisition parameters detect the correct information is vital. If the acquisition protocol cannot correctly model the tissue anisotropy, then any metrics or analyses that follow will be skewed, regardless of the field strength at which they were acquired. There are a handful of parameters that researchers and clinicians need to consider when acquiring diffusion data. These are parameters that researchers and clinicians can control and adjust to optimize the diffusion acquisition depending on the characteristics of the chosen field strength and regions of interest.

The diffusion-weighting factor (b-value). A valuable tool in adjusting a DTI sequence's capabilities at accurately detecting water diffusion is by changing the gradient amplitude, the duration of the sensitizing gradients and the time between the gradient pair. This diffusion weighting factor, or b-value, is measured in units of s/mm2, and can be expressed by the Stejskal-Tanner expression (Basser et al., 1994):

$$b = \gamma^2 G^2 \delta^2 (\Delta - \delta/3)$$

Where γ is the gyromagnetic ratio, G is the strength of the diffusion sensitizing gradients, δ is the duration of the gradient pulses and Δ is the time interval between the gradients. High b-values are achieved by increasing the strength, duration and time interval of the gradients. The higher the b-value, the more the image will be sensitive to diffusion, at the cost of the SNR (Descoteaux, Deriche, Knösche & Anwander, 2009; Figueiredo, Borgonovi & Doring, 2011). It has been noted that most DTI studies use relatively low b-values, ranging from 700-1000 s/mm^2 (Soares et al., 2013). Furthermore, the current clinical standards for diffusion weighted imaging use b-values of around 1000 s/mm^2 (Mukherjee, Chung, Berman, Hess, & Henry, 2008; Stieltjes et al., 2013).

An important factor to consider when determining the diffusion sensitivity of a DTI acquisition is the fibre tract(s)/voxel(s) of interest to be studied. If a path/voxel in a single orientation is to be estimated (e.g. lies primarily on one axis) then b-values of ≤ 1000 s/mm^2 are appropriate as they fit the tensor estimate and increase the SNR of the acquisition. On the contrary, if the path(s) of interest contain voxels with multiple fibre crossings, a high b-value (e.g. 3500 s/mm^2) is appropriate to fit the data (Stieltjes et al., 2013). Although low b-values increase the SNR of the acquisition, the information contained in these smaller measurements is inadequate to correctly estimate and resolve crossing WM fibres.

Gradient sampling (diffusion directions). DWI treats each voxel as a perfect sphere. The minimum number of directions in which to apply excitation gradient to cover the entire surface of the sphere and collect diffusion information is six: anterior, posterior, superior, inferior, left and right. Measuring these six independent directions acquires enough information to determine the principal eigenvectors and eigenvalues. However, increasing the number of unique gradient directions (i.e. increasing the number of diffusion samples) leads to a more unbiased estimate of the tensor matrix, hence a more accurate reconstruction of fibre orientation. In 2004, Jones demonstrated that 30 unique diffusion directions are needed for a statistically rotationally-invariant reconstruction. In other words, when applying the gradient in 30 unique directions, the variance in the tensor parameters became independent of the orientation of the WM fibres. Conversely, when different tensor models are used, such as spherical deconvolution, up to 45 unique gradient directions can be needed (Tournier, Calamante, Connelly, 2009). Additionally, increasing the gradient diffusion samples increases the signal-to-noise ratio of the data (Ni, Kavcic, Zhu, Ekholm & Zhong, 2006). The number of directions to create a perfect estimate of the diffusion tensor is still unknown (Jones, Knösche, & Turner, 2013) as factors such as tensor model, and area of interest can affect the number of gradient sampling directions required to fit the tensor estimate accurately. Additionally, when the number of sampling directions increases, so does the diffusion acquisition time (Alexander et al., 2007; Ni et al., 2006) therefore the sampling directions can increase or decrease depending on the population being scanned and how long they can remain in the scanner.

Phase encoding direction(s). Single-shot echo planar imaging is most commonly used in diffusion MR imaging. Although this technique comes with many advantages, notably its rapid image acquisition, this technique can also cause severe distortions. These distortions present themselves in the form of inhomogeneities of the static magnetic (B0) field, the magnetic field that is parallel to the subject when they are in the supine position in the MR scanner. These inhomogeneities result in spatial and intensity distortions in the EPI images (Wu et al., 2008; Holland, Kuperman & Dale, 2010; Chang & Fitzpatrick, 1992, Morgan et al., 2004; Andersson, Skare & Ashburner, 2003) along the phase encoding direction (i.e. along the axis in which the images were acquired). Several methods have been proposed to correct for these distortions, however there is no consensus on the optimal solution. Much like choosing the number of gradient diffusion directions, choosing the inhomogeneity correction method depends on the areas of interest (Wu et al., 2008; Holland et al., 2010).

One approach gaining in popularity because of its ability to increase the SNR of the diffusion data, albeit at the expense of scan time, is the reverse gradient methods proposed by Bowtell et al. (1994) and extended by Andersson et al., (2003). This requires the acquisition of two EPI diffusion images: one along the main phase encoding axis (e.g. right to left, anterior to posterior or superior to inferior) and the second images along the same axis, but in the reversed direction (e.g. left to right, posterior to anterior or inferior to superior). These images are then superimposed to average the reconstructions and to estimate the field map of the undistorted image as they should look like in a homogenous field. This method will essentially double the scan time however it will also increase the SNR and ensure the minimization of EPI distortions.

In this study, we designed three DTI acquisition protocols with a varying number of diffusion gradient sampling directions (65 directions, 137 directions and 139 directions) and phase encoding directions (single encoding direction (AP) or dual encoding directions (AP-PA)). We assessed how well each acquisition protocol performed probabilistic tractography of each fibre tract of the motor cortico-cerebellar loop. We hypothesized that the 137 and 139 directions acquisition protocols would outperform 65 directions based on number of gradient sampling directions and that the 137 and 139

directions acquisition protocols would outperform 65 directions based on their phase encoding directions.

5.1 Materials and Methods

5.1.1 Participants

Two healthy participants were recruited to undergo DTI acquisitions at 3T and at 7T. One subject was male, right-handed and 27 years of age; the second participant was female, left-handed and 23 years of age. The UWO Health Sciences Research Ethics Board provided ethical approval for the study (Appendix D and E). Anatomical T1, susceptibility weighted and FLAIR structural images were also acquired during these scans.

5.1.2 MRI Acquisitions

Pilot datasets were obtained at the Centre for Functional and Metabolic Mapping (CFMM) at Roberts Research Institute (London, Ontario). Three DTI protocols were acquired in each scanner, adding to a total of six DTI protocols used in the study. Three protocols were designed for the Siemens Magnetom Prisma 3T MRI system. The first of these protocols included 65 non-collinear directions with a b-value = 1000 s/mm^2 (TR = 7500ms, TE = 55ms, voxel size = 1.5x1.5x1.5mm, no gap, 84 slices), the second protocol included 137 non-collinear directions, with a b-value = 1000 s/mm^2 (TR = 4080ms, TE = 62.30ms, voxel size = 1.5x1.5x1.5. no gap, 84 slices, multiband acceleration factor = 2, PA-AP) and finally the third 3T DTI protocol included 139 non-collinear directions with a b-value = 2000s/mm^2 (2 shells, TR = 4370ms, TE = 69.40ms, voxel size = 1.5x1.5x1.5, no gap, 84 slices, multiband acceleration factor = 2, PA-AP) (Appendix A). The other three DTI protocols were designed for the Siemens Magnetom 7T MRI system and similar in their parameters to the 3T protocols for a more accurate comparison. The first of the 7T protocols included 65 non-collinear directions, with a b-value = 1000s/mm^2, (TR = 6000ms, TE = 49.2, voxel size = 1.5x1.5x1.5, no gap, 84 slices) and was approximately nine minutes long, the second protocol included 137 non-collinear directions with b-value = 1000s/mm^2 (TR = 4000ms, TE = 53.4ms, voxel size = 1.5x1.5x1.5, no gap, 84 slices, multiband acceleration factor = 2, AP-PA) and took 11

minutes to acquire images per phase encoding direction (approximately 22 minutes total) and the last 7T DTI protocol included 139 non-collinear with a b-value of 2000s/mm^2 (2 shells, TR = 4000ms, TE = 60.2ms, voxel size = 1.5x1.5x1.5, no gap, 84 slices, multiband acceleration factor = 2) and was approximately 12 minutes long in each phase encoding direction (approximately 24 minutes total; Appendix B).

5.2 Results

No quantitative measures were estimated at this point. Visual inspection of the streamlines from all three protocols was used to assess the results. We did not want to bias our estimation of the success probabilistic tractography of each protocol by comparing DTI metrics (FA and MD), therefore, we picked the optimized protocol solely based on the reconstructed streamlines. Criteria for a successful reconstruction included: the success of the streamline of reaching both target masks, little to no streamline deviation into neuroanatomically incorrect regions, and finally the necessity of exclusion or termination masks to aid in reconstructing an accurate streamline. We used the White Matter Atlas by Hermoye et al. (http://www.dtiatlas.org/) as a visual reference to ensure that the streamlines were anatomically sound. Since this study sought to optimize DTI parameters at 7T, only the streamlines from this magnetic field will be reported below. 3T streamlines of the optimized protocol will be reported in Chapter 6.

5.2.1 VL-M1 streamlines

Fibres between the thalamus and primary motor cortices belong to the cortico-spinal tract. As such, the fibres connecting the ventrolateral thalamic nuclei and M1 pass through the posterior limb of the internal capsule, ascend into the superior thalamic radiations followed by the superior region of the corona radiata and terminate in the motor cortices, anterior to the central sulci. The neuroanatomical accuracy did not differ between streamlines. Furthermore, all three reconstructions required termination masks directly under the thalamic ROI mask, to prevent probtrackX from including voxels

outside the ROIs of interest which could skew any quantitative metrics. They did not differ in the amount of "help" required to reconstruct an accurate path.
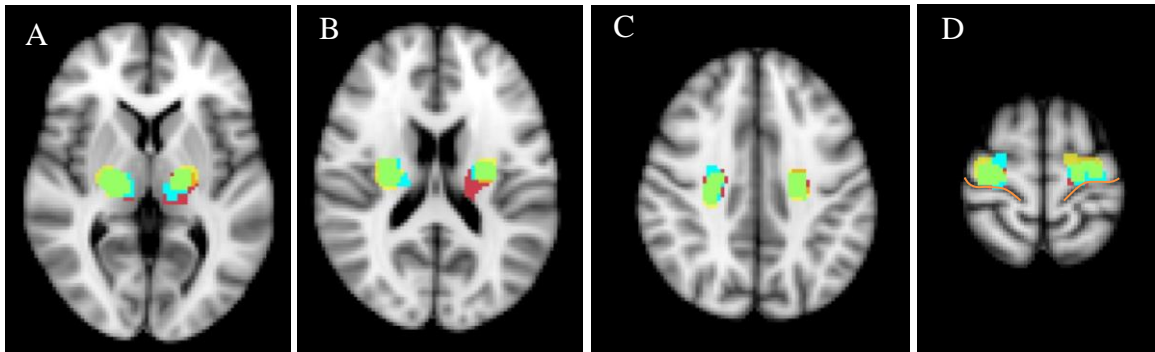
Figure 16: Anatomical accuracy of three 7T VL-M1 streamlines. 65 directions protocol in yellow, 137 directions protocol in light blue and 139 directions protocol in burgundy. Panel A: internal capsule (z = 38); Panel B: anterior thalamic radiations (z = 45); Panel C: corona radiata (z = 55); Panel D: primary motor cortices (z = 69) with central sulci in orange.
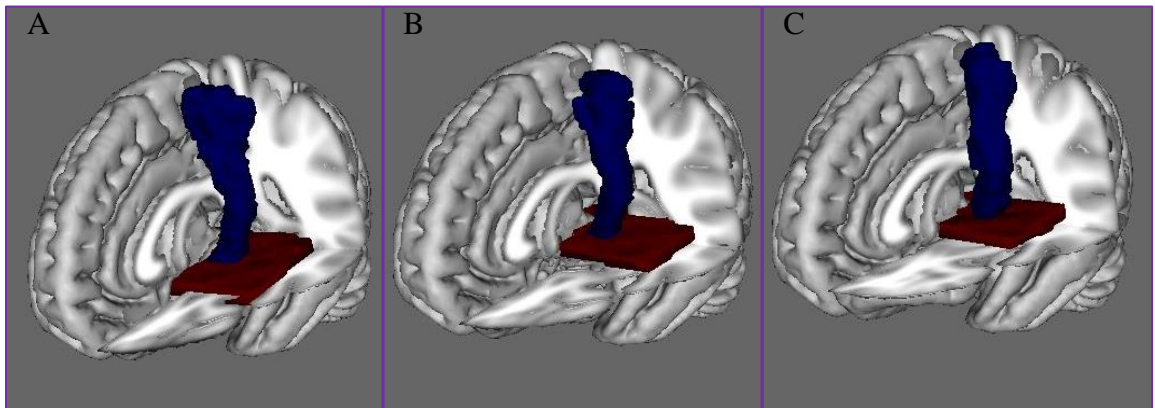
Figure 17: VL-M1 streamline reconstructions in MNI152 standard space, anterior view. Panel A: 65 directions protocol; Panel B: 137 directions protocol; Panel C: 139 directions protocol. Streamlines in blue, target masks in red.

5.2.2 M1-DN streamlines

We reconstructed fibres between the primary motor cortices and the dentate nuclei as part of the corticopontocerebellar tract, which is made up of two smaller tracts: corticoponto fibres and pontocerebellar fibres. The fibres from the primary motor cortices descend into the pontine nuclei through by way of the corona radiata and internal capsule (corticponto fibres). Then, the fibres cross at the middle cerebellar peduncles into the contralateral cerebellar hemisphere and terminate in the dentate nuclei. In terms of reconstructing

corticoponto fibres, both the 65 directions and 137 directions protocols accurately reconstructed M1 to pons fibres by passing through the corona radiata followed by the internal capsule. The 139 directions protocol did not perform as well: when descending into the corona radiata, the streamline in the left hemisphere reconstructed voxels passing through the corpus callosum thus prematurely crossing in to the opposite hemisphere. A supratentorial termination mask across the hemispheric fissure was required for this protocol. In terms of pontocerebellar fibres, both the 137 directions and 139 directions protocols performed equally well, by crossing at the middle cerebellar peduncles and terminating in the contralateral dentate nuclei. The 65 directions protocol successfully resolved this crossing at the middle cerebellar peduncles, however in the left hemisphere path, it also reconstructed ascending voxels from the contralateral cerebellum, traveling up the cortex. No exclusion nor termination mask could be placed in an anatomically sound region to prevent the streamline from reconstructing these "stray" voxels. We therefore judged the 137 directions as the best protocol for the M1-DN streamline as it accurately reconstructed fibres from the corticoponto and pontocerebellar tracts with aid from exclusion or termination.
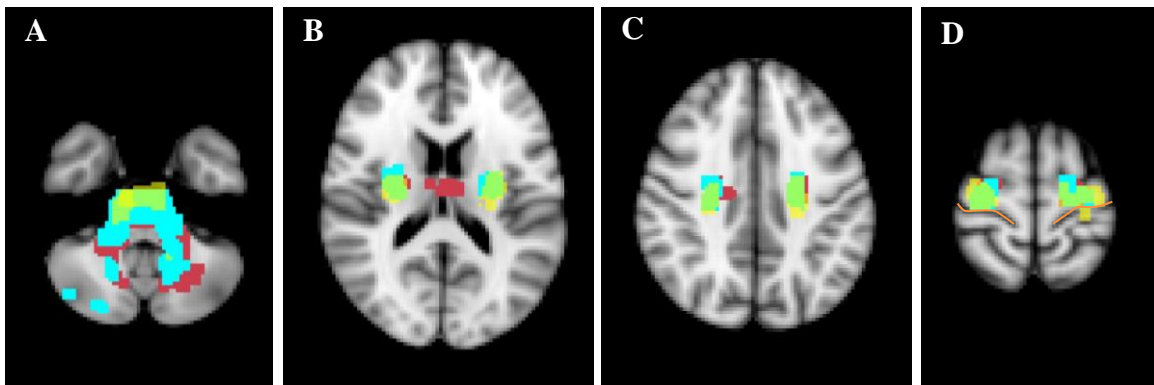
Figure 18: Anatomical accuracy of three 7T M1-DN streamlines. 65 directions protocol in yellow, 137 directions protocol in light blue and 139 directions protocol in burgundy. Panel A: dentate nuclei (z = 16); Panel B: where 139 directions crosses through corpus callosum (z = 44); Panel C: corona radiata (z = 55); Panel D: primary motor cortices (z = 69) with central sulci in orange.
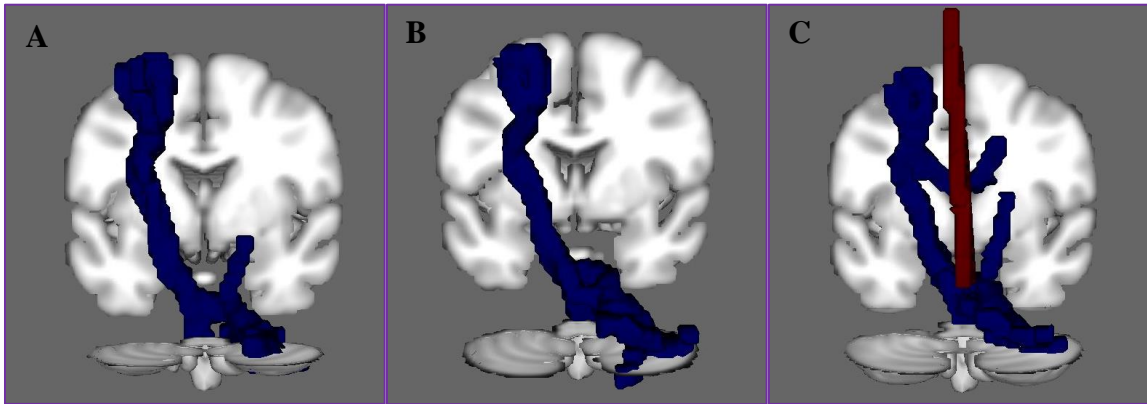
Figure 19: M1-DN streamline reconstructions in MNI152 standard space, posterior view. Panel A: 65 directions protocol; Panel B: 137 directions protocol; Panel C: 139 directions protocol. Streamlines in blue, target mask in red.

5.2.3   VL-DN streamlines

Fibres between the ventrolateral nuclei and dentate nuclei descend from the thalamus, into the decussation of the cerebellar peduncle, cross into the contralateral hemisphere and terminate in the dentate nuclei by way of the superior cerebellar peduncle. Both the 137 directions and 139 directions protocols performed equally: streamlines in both hemispheres required exclusion masks in the superior cerebellar peduncle that were ipsilateral the thalamic nuclei and contralateral to the dentate nuclei. That is to say, when tracking fibres between the left ventrolateral thalamic nucleus and right dentate nucleus, the superior cerebellar peduncle was placed in the left hemi sphere, and vice versa. Superior cerebellar peduncle exclusion masks were also placed in the 65 directions
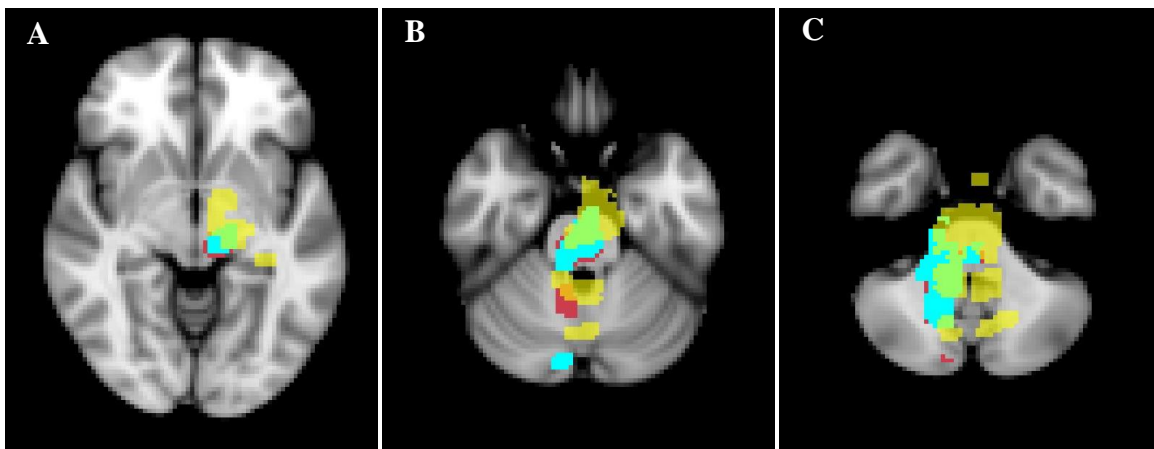
Figure 20: Anatomical accuracy of three 7T VL-DN streamlines. 65 directions protocol in yellow, 137 directions protocol in light blue and 139 directions protocol in burgundy. Panel A: ventrolateral thalamic nucleus (z = 33); Panel B: crossing into superior cerebellar peduncle (z = 22); Panel C: dentate nucleus.

streamlines however, they did not aid in the reconstruction and neuroanatomically incorrect voxels were reconstructed in the opposite cerebellar hemisphere.
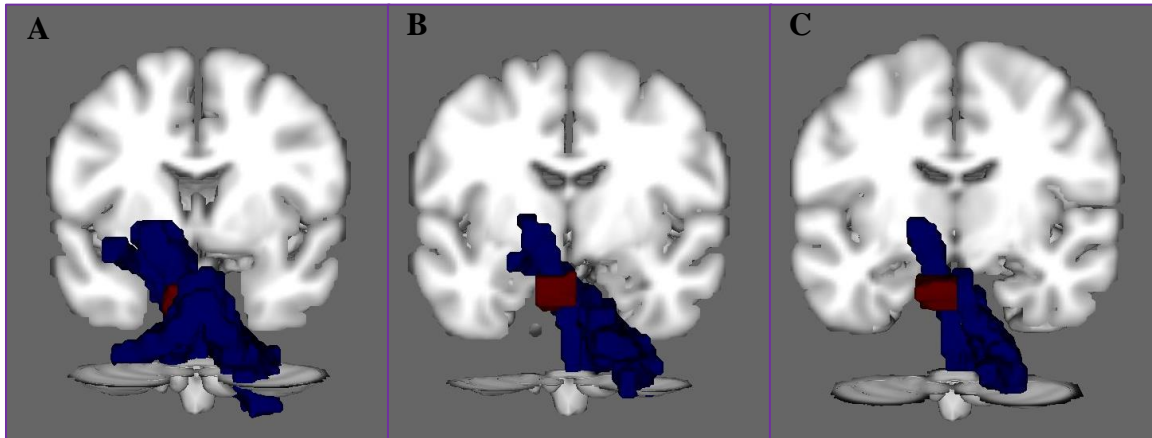
Figure 21: VL-DN 7T streamline reconstructions in MNI152 standard space, posterior view. Panel A: 65 directions protocol; Panel B: 137 directions protocol; Panel C: 139 directions protocol. Streamlines in blue, target mask in red.

5.3 Discussion

In Study III, we visually assessed and compared the probabilistic tractography results of three diffusion tensor imaging sequences, at 7T MRI. Specifically, we reconstructed fibres from the primary motor cortex to dentate nucleus of the cerebellum, the dentate nucleus to the ventrolateral nucleus and finally fibres from the ventrolateral nucleus to the primary motor cortex.

We confirmed our hypotheses for this study. The more information gained about the diffusion profile, the more accurate and less uncertain the probabilistic streamline reconstructions. We hypothesized that the 137 directions and 139 directions protocol would outperform the 65 directions protocol based on the number of gradient sampling directions and artifact correction with a dual phase encoding scheme. This was true for two of the three tracts of interest. For longer and more complex tracts such as the VL-DN and M1-DN tracts, the streamlines from the 65 directions protocol underperformed compared to the two other protocols.

Using Monte Carlo simulations, Jones (2004) determined that at least 20 unique gradient sampling directions are required for a robust and rotationally invariant estimation of anisotropy, while at least 30 unique directions are required for a robust estimation of the

diffusion tensor model. One could argue that sampling at 65, 137 or 139 directions would therefore not yield superior estimates of diffusion anisotropy or orientation if 30 sampling directions are enough for robust estimates. Increasing the number of sampling directions also increases acquisition time, making protocols with many diffusion encoding directions difficult for use in clinical settings. On the other hand, increasing the number of diffusion gradient sampling directions increases the signal-to-noise ratio (SNR) of the DTI acquisitions (Alexander et al., 2007; Ni et al., 2006). DTI acquisitions with insufficient SNR will bias the estimated diffusion tensor parameters (Jones & Basser, 2004). Weak diffusions signals tend to be overestimated at low SNR which results in the underestimation of diffusion metrics (e.g. primary eigenvectors and mean diffusivity) and an underestimation of anisotropy measures (e.g. fractional anisotropy) (Mukherjee et al., 2008). In this study, we can visually observe the effects of increased SNR (i.e. increased sampling directions) on the streamline reconstructions of each protocol: as sampling directions increase, the streamline becomes more "narrow". This is not an indication of a more accurate reconstruction but rather an indication that the uncertainty of the reconstructed streamline based on principal diffusion direction is low (Behrens et al., 2003b). This could help explain why the 65 directions protocol underperformed compared to the two other acquisitions: there was high uncertainty in the reconstructed streamlines of this protocol, so much so that even termination and exclusion masks could not help guide accurate reconstruction. Our results thus provide some evidence that more gradient sampling directions reduce the uncertainty of connections based on principal diffusion direction. The effects of SNR on estimation of DTI metrics have been well documented (Anderson, 2001; Pierpaoli & Basser, 1996; Bastin et al., 1998; Armitage & Bastin, 2001; Farrell et al., 2007). Although our results suggest that more gradient sampling directions, and *de facto* higher SNR, visually yield more accurate streamline reconstructions, quantitative analyses need to be conducted to determine the effect of the parameters on DTI metrics.

Chapter 6

6. Study IV – Comparison of DTI streamlines and metrics at 3T and 7T MRI

In this study, we validated the 7T DTI acquisition sequence from Study III in a larger healthy control group. We compared qualitative and quantitative results of this 7T acquisition to DTI from a similar 3T acquisition sequence. Our seeds of interest in this study include the ventrolateral nuclei (VL), primary motor cortices (M1) and dentate nuclei of the cerebellum (DN). This sequence was designed to aid in the parcellation of thalamic nuclei, to better understand their fibre paths connections to rest of the cortex *in vivo*. As discussed, previous DTI studies have preliminarily confirmed results from animal studies, concluding that the ventrolateral nucleus of the thalamus in primarily involved in motor performance due to its connection to the primary motor cortices and cerebellum. These human studies however, lacked specificity in their seeds or termination regions of their tractography streamlines. They either oversimplified thalamic connections by using the entire thalamus as a seed (rather than a specific nucleus) or used a top-down approach and seeded the cortex with the thalamus as the general termination region. This lack of specificity is in part due to the fact that thalamic nuclei have not been reliably parcellated at low magnetic fields (1.5T/3T) because of the low spatial resolution and the size of the thalamus (Behrens et al., 2003; Metzger et al., 2013). The goal of this study is to assess if imaging at ultra-high fields can aid in the identification of specific thalamic nuclei and in the reconstructions of fibre projections, as compared to imaging at low magnetic fields.

6.1 Materials and Methods

6.1.1 Participants

A group of 10 right-handed healthy controls were recruited for this study. The ages of this control group ranged from 22 to 29 years ($M = 24.70$, $SD = 2.36$) and this sample was composed of six males and four females. The UWO Health Sciences Research Ethics Board provided ethical approval for the study (Appendix D and E). Anatomical T1,

susceptibility weighted and FLAIR structural images were also acquired during these scans.

6.1.2 MRI Acquisitions

Datasets of all participants were obtained at the Centre for Functional and Metabolic Mapping (CFMM) at Roberts Research Institute (London, Ontario). Participants were scanned once at 3T MRI then at 7T MRI on a separate day. The 137 directions protocol from Study III was acquired in each scanner, adding to a total of two DTI acquisitions per participant: 3T protocol included 137 non-collinear directions, with a b-value = 1000 s/mm^2 (TR = 4080ms, TE = 62.30ms, voxel size = 1.5x1.5x1.5. no gap, 84 slices, multiband acceleration factor = 2, PA-AP) and the 7T protocol included 137 non-collinear directions with b-value = 1000s/mm^2 (TR = 4000ms, TE = 53.4ms, voxel size = 1.5x1.5x1.5, no gap, 84 slices, multiband acceleration factor = 2, AP-PA).

6.1.3 Statistical Analyses

We could reconstruct all three bilateral tracts of interest in all participants. Probabilistic tractography was visually assessed as described in Chapter 5 section 5.2. Fractional anisotropy, mean diffusivity and volume were calculated for each tracts and global fractional anisotropy was calculated for each participant in both scanners using the FSLUTILS program, fslmaths (http://fsl.fmrib.ox.ac.uk/fsl/fslwiki/Fslutils). Using a paired sample t-test, we compared the metrics of each tract across scanners. To follow-up on fractional anisotropy comparisons, we used FMRIB's Automated Segmentation Tool (Fast; Zhang et al., 2001) to acquire white matter masks from each participant's anatomical T1 image. We multiplied this segmented white matter map by the fractional anisotropy mask and calculated whole brain fractional anisotropy. We then proceeded to average FA *ratios* for paired comparisons. That is to say, for each tract, we divided the raw FA values by global white matter and averaged these ratios across participants. We compared these new average tract FA values between scanners.

We also calculated the amount of overlap between 3T and 7T ROI placement and streamline location by warping the masks and fibre paths into T1 anatomical space. To do so, we registered the 7T T1 anatomical images to the 3T T1 anatomical images in every

participant, using FMRIBS's Linear Image Registration Tool (FLIRT; Jenkinson & Smith, 2001; Jenkinson et al., 2002). Then, we registered every participant's b=0 image to the 3T-7T coregistered T1 image and used the resulting transformation matrix to warp each ROI ask from diffusion space into T1 anatomical. We followed up on these analyses by using the same procedure to transform ROI masks and path streamlines into MNI standard space. We registered participants' b=0 to the MNI152 2mm brain template and used the resulting transformation matrix to warp ROI masks and fibre streamlines to MNI space. We used IBM SPSS Statistics for Windows, Version 23 to run all statistical analyses.

6.2   Results

6.2.1   Probabilistic tractography of motor tracts of interest

3T Probabilistic Tractography. In 100% of participants (10/10 participants), a brainstem termination mask placed below the thalamic masks was necessary for an accurate reconstruction of ipsilateral VL-M1 fibres. For accurate M1-DN streamline reconstructions, 70% of participants (7/10 participants) required a mask to aid reconstructing this contralateral fibre tract. Four of these participants required a supratentorial exclusion mask along the hemispheric fissure to prevent the reconstructed fibre path from prematurely crossing into the opposite hemisphere through the corpus callosum. Two participants required a superior cerebellar peduncle exclusion mask as their streamline was crossing into the contralateral hemisphere through the superior peduncle instead of the middle cerebellar peduncle, which is the anatomically correct trajectory. One participant required a hemispheric supratentorial exclusion mask along with a superior cerebellar peduncle exclusion mask (only in the right hemisphere) to arrive at an anatomically correct streamline. When reconstructing the fibre tracts between the thalamic and dentate nuclei ROIs, 100% of participants required a superior cerebellar peduncle exclusion mask that was ipsilateral to the thalamic ROI and contralateral to the dentate ROI. When calculating streamlines between the left ventrolateral thalamic nucleus and right dentate nucleus, the superior cerebellar peduncle was placed in the left hemisphere.

7T Probabilistic Tractography. The fibre path between the ventrolateral thalami and M1 performed similarly to tracking at 3T: 100% of participants required a brainstem termination mask below the thalamic ROIs. When tracking fibres between the primary motor cortices and the dentate nuclei, pilot results from Study III replicated in 60% of participants (6/10 participants). These participants did not require any mask to aid in the reconstruction of this streamline. In the remaining four participants, some help was needed when tracking this path. Three of these participants required a hemispheric supratentorial exclusion mask as voxels were crossing into the opposite hemisphere via the corpus callosum. In the last subject, adjustment was needed in only one hemisphere: a superior cerebellar peduncle exclusion mask was necessary in the right hemisphere to correctly resolve crossing at the anatomically correct middle cerebellar peduncle. Fibre tracking from the ventrolateral thalami to the dentate nuclei also performed like 3T streamlines. All participants required a superior cerebellar peduncle exclusion masks to accurately reconstruct this path.

6.2.2   Differences in fractional anisotropy

Paired t-test comparisons of average raw FA values revealed significant differences at every comparison. 3T Global FA was significantly lower than 7T Global FA, $t(9) = -15.025$, $p < .001$. Both left ($t(9) = -6.234$, $p < .001$) and right ($t(9) = -3.537$, $p = .006$) VL-M1 tract FA values were significantly lower at 3T than 7T. Similar results were observed for M1-DN tracts: left 3T tract had significantly lower FA values than 7T tracts ($t(9) = -14.300$, $p < .001$) and right 3T tracts also showed significantly lower FA values than their 7T counterparts ($t(9) = -6.702$, $p < .001$). VL-DN tracts showed similar results: both hemispheres showed significantly reduced FA values at 3T compared to 7T (Left: $t(9) = -6.100$, $p < .001$; Right: $t(9) = -5.673$, $p < .001$). See Table 8.

Table 8: Paired sample t-tests of mean fibre tract and global FA between scanners (raw scores)

Pair	Fibre tract	Mean FA	SD	t	df	*p*-value
1	3T Global FA	0.394	0.006	-15.025	9	.000*
	7T Global FA	0.414	0.008			
2	3T LVL-LM1	0.441	0.02	-6.234	9	.000*
	7T LVL-LM1	0.485	0.023			
3	3T RVL-RM1	0.432	0.024	-3.537	9	.006*
	7T RVL-RM1	0.471	0.029			
4	3T LM1-RDN	0.470	0.017	-14.300	9	.000*
	7T LM1-RDN	0.545	0.015			
5	3T RM1-LDN	0.477	0.023	-6.702	9	.000*
	7T RM1-LDN	0.539	0.019			
6	3T LVL-RDN	0.420	0.034	-6.100	9	.000*
	7T LVL-RDN	0.518	0.033			
7	3T RVL-LDN	0.411	0.034	-5.673	9	.000*
	7T RVL-LDN	0.499	0.045			

*p < .05

Paired t-test comparisons of average FA ratio values (Tract FA/WM FA) revealed similar results. Both left ($t(9) = -4.755$, $p = .001$) and right ($t(9) = -3.025$, $p = .014$) VL-M1 tract FA ratios were significantly lower at 3T than 7T. Similar results were observed for M1-DN tracts: left 3T tract had significantly lower FA values than 7T tracts ($t(9) = -8.310$, $p < .001$) and right 3T tracts also showed significantly lower FA values than their 7T counterparts ($t(9) = -6.091$, $p < .001$). Both VL-DN tracts showed significantly reduced
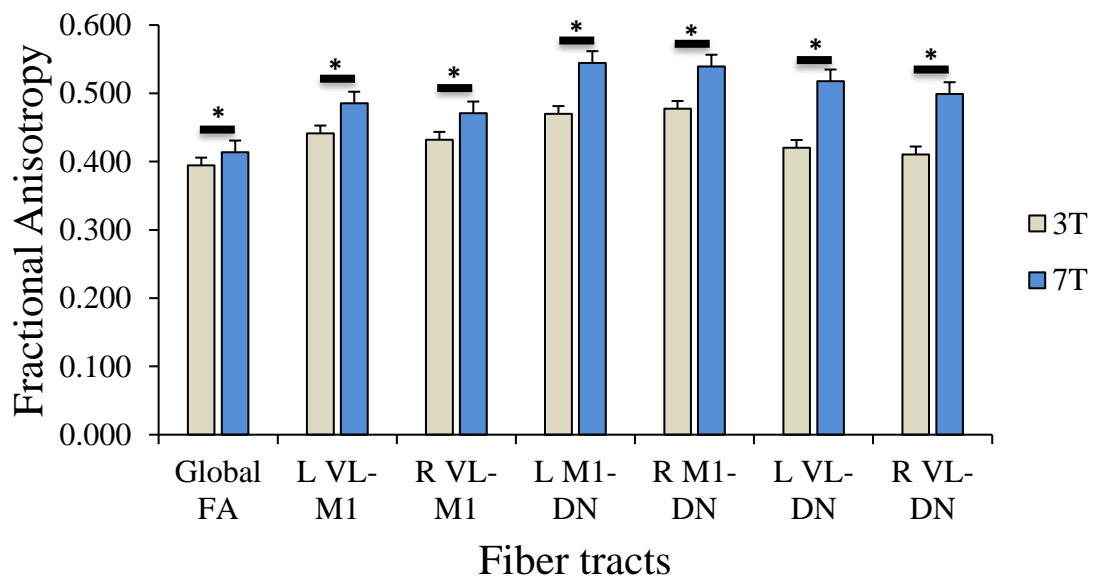
Figure 22: Average fibre tract FA value at 3T and 7T. **p < .05.*

FA values at 3T compared to 7T (Left: $t(9)$ = -5.637, p <.001; Right: $t(9)$ = -5.149, p < .001). See Table 9.

Table 9: Paired sample t-tests of mean fibre tract and global FA between scanners (ratios)

Pair	Fibre tract	Mean FA ratio	SD	t	df	*p*-value
1	3T Global FA	.276	.009978763	-2.124	9	0.063
	7T Global FA	.282	.008399647			
2	3T LVL-LM1	1.602	.063269949	-4.755	9	.001*
	7T LVL-LM1	1.722	.065766496			
3	3T RVL-RM1	1.568	.066984481	-3.025	9	0.014*
	7T RVL-RM1	1.671	.08790794			
4	3T LM1-RDN	1.708	.098102257	-8.310	9	< .001*
	7T LM1-RDN	1.934	0.066948044			
5	3T RM1-LDN	1.734	0.104389032	-6.091	9	< .001*
	7T RM1-LDN	1.915	0.076900765			
6	3T LVL-RDN	1.527	0.134713547	-5.637	9	< .001*
	7T LVL-RDN	1.837	0.097920299			
7	3T RVL-LDN	1.492	0.138181509	-5.149	9	.001*
	7T RVL-LDN	1.772	0.16541819			

*p < .05
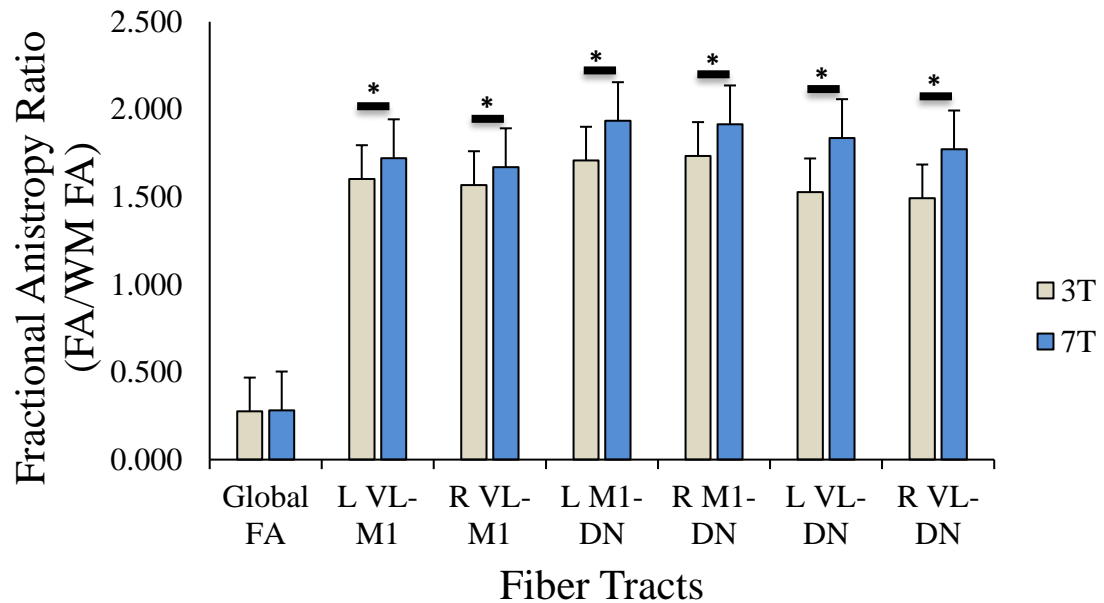
Figure 23: Average fibre tract FA ratio at 3T and 7T. *p < .05.

6.2.3   Differences in mean diffusivity

Paired t-test comparisons of average mean diffusivity (MD) values revealed non-significant differences at every comparison. The MD of 3T fibre tracts and the MD of 7T fibre tracts were not significantly different from each other. See Table 10.

Table 10: Paired sample t-tests of mean fibre tract MD between scanners

Pair	Fibre tract	Mean MD	SD	t	df	*p*-value
1	3T LVL-LM1	0.000699	0.000011	1.811	9	0.104
	7T LVL-LM1	0.000694	0.000016			
2	3T RVL-RM1	0.000711	0.000009	2.100	9	0.065
	7T RVL-RM1	0.000697	0.000022			
3	3T LM1-RDN	0.000713	0.000017	0.291	9	0.778
	7T LM1-RDN	0.000710	0.000033			
4	3T RM1-LDN	0.000706	0.000019	-0.024	9	0.981
	7T RM1-LDN	0.000707	0.000019			
5	3T LVL-RDN	0.000722	0.000028	0.567	9	0.584
	7T LVL-RDN	0.000714	0.000039			
6	3T RVL-LDN	0.000729	0.034000	-0.149	9	0.885
	7T RVL-LDN	0.000731	0.045000			

*p < .05
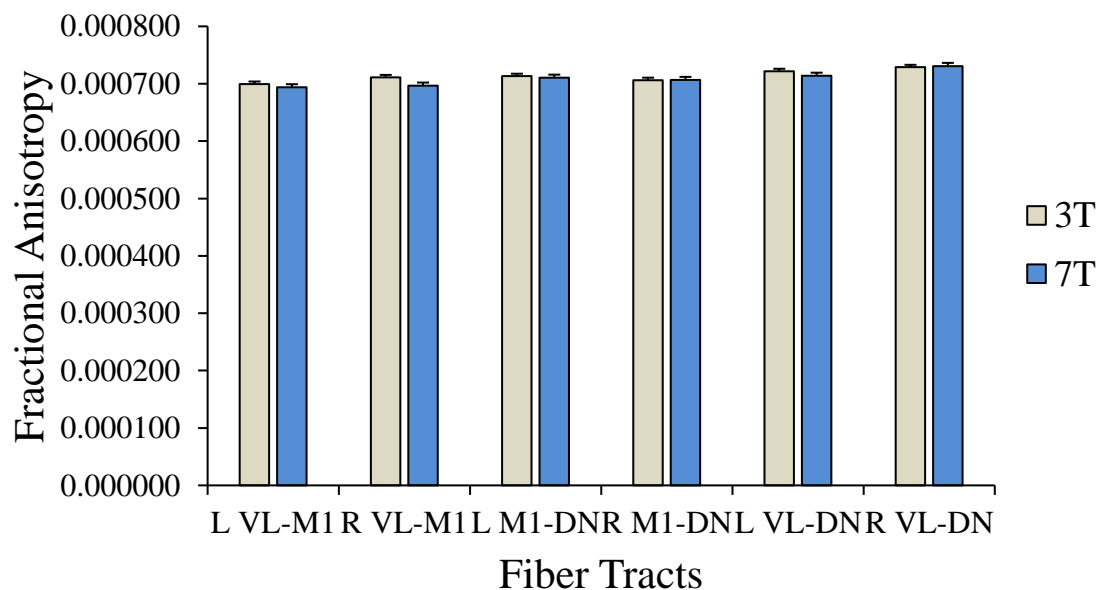
Figure 24: Average fibre tract MD value at 3T and 7T. **p < .05.*

6.2.4 Differences in volume

Only two paired between scanner comparisons of tract volume were significant. The mean right M1-DN tract volume was significantly lower at 3T compared to 7T $t(9) = -3.714$, $p = .005$. Opposite results were observed in the left VL-DN tract: mean tract volume at 3T was significantly higher than mean tract volume at 7T, $t(9) = 3.371$ $p = .008$. See Table 11.

Table 11: Paired sample t-tests of mean fibre tract volumes between scanners

Pair	Fibre tract	Mean volume	SD	t	df	p-value
1	3T LVL-LM1	2916.980	463.061	-.003	9	.998
	7T LVL-LM1	2917.662	519.706			
2	3T RVL-RM1	2967.073	321.774	.607	9	.559
	7T RVL-RM1	2856.664	482.185			
3	3T LM1-RDN	6022.747	1025.578	-1.479	9	.173
	7T LM1-RDN	6511.409	694.984			
4	3T RM1-LDN	5864.314	1038.388	-3.714	9	.005*
	7T RM1-LDN	6844.981	638.883			
5	3T LVL-RDN	6265.175	2800.13	3.371	9	.008*
	7T LVL-RDN	3291.145	958.579			
6	3T RVL-LDN	5088.359	2405.269	-0.436	9	.673
	7T RVL-LDN	5736.842	2960.889			

*$p < .05$
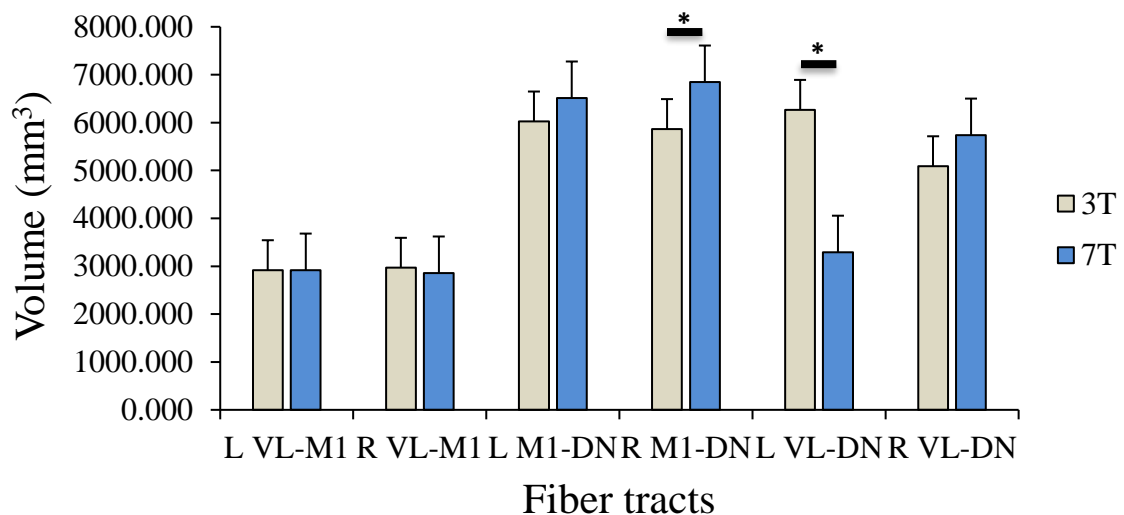
Figure 25: Average fibre tract volume at 3T and 7T, *$p < .05$.

6.2.5   Percentage overlap in ROI placement

When comparing the percentage of overlap in ROI placement across scanners in T1 anatomical space, little overlap was observed in thalamic and cerebellar ROIs. Between 3T and 7T ventrolateral thalamic nuclei ROIs, there was a 10.55% and 15.35% overlap for the left and right hemispheres respectively. Between the dentate nuclei ROIs, overlap
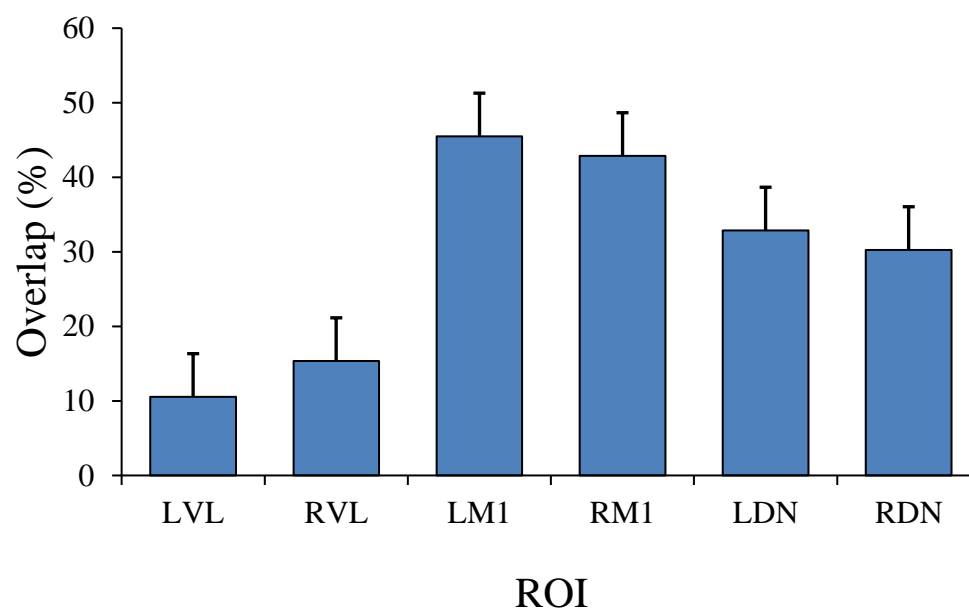
Figure 26: Average ROI overlap (%) across scanners in T1 anatomical space. VL: ventrolateral nuclei; M1: primary motor cortices; DN: dentate nuclei.

more than doubled: there was a 32.87% overlap in the left hemisphere and 30.30% overlap in the right hemisphere. Cortical M1 ROIs displayed the highest amount of overlap. Between the left 3T and 7T ROIs, we found a 45.49% overlap and a 42.87% overlap between the right 3T and 7T ROIs (See Figure 26). We performed the same analyses but this time in standard space (MNI152). The trend in results was similar for this analysis. Thalamic and cerebellar ROIs had lower percent overlap than cortical M1 masks. Specifically, left and right thalamic ROIs had overlaps of 9.09% and 12.10% respectively while left and right dentate nuclei ROIs overlapped across scanners by 18.29% and 21.06% respectively (See Figure 27).
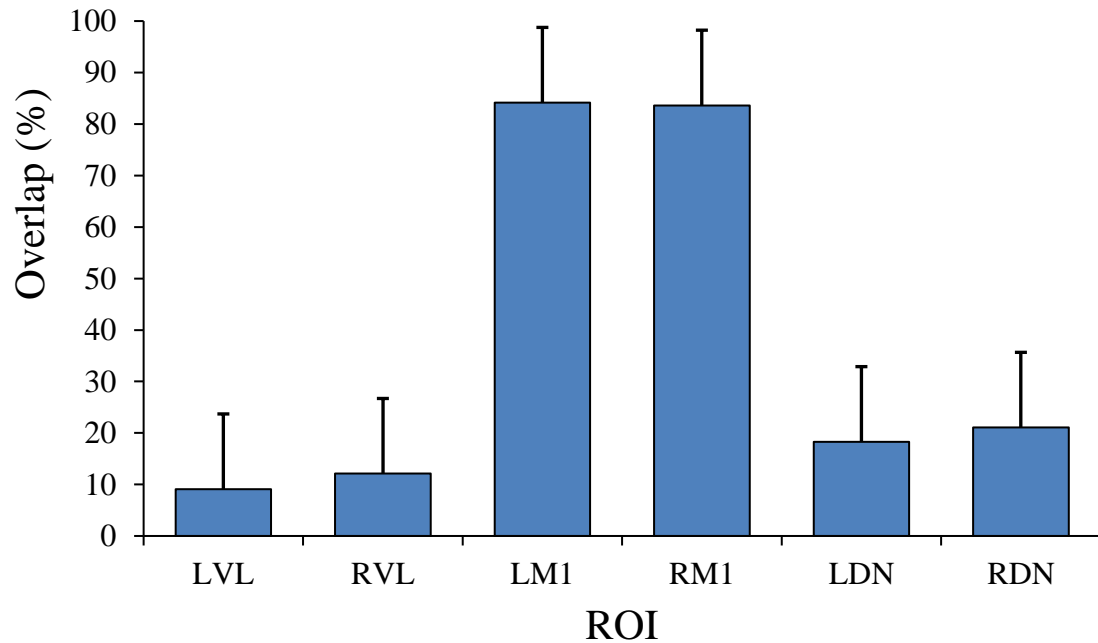
Figure 27: Average ROI overlap (%) across scanners in MNI152 standard space. VL: ventrolateral nuclei; M1: primary motor cortices; DN: dentate nuclei.

6.2.6   Percentage overlap in reconstructed fibre tracts

When comparing the percentage of overlap in streamline location across scanners in T1 anatomical space, the path with the highest average overlap between participants was the right VL-M1 tracts (34.15%). The left VL-M1 tracts averaged 29.25% overlap. Between
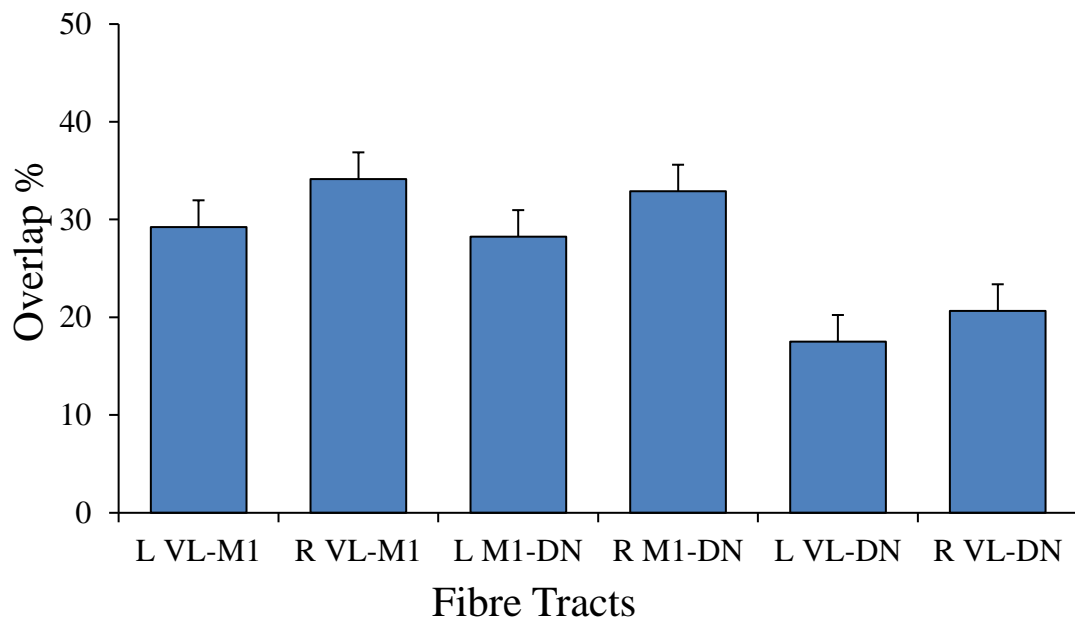
Figure 28: Average streamline overlap (%) across scanners in T1 anatomical space. VL: ventrolateral nuclei; M1: primary motor cortices; DN: dentate nuclei.

3T and 7T M1-DN streamlines, there was a 28.24% and 32.88% overlap for the left and right hemispheres respectively. Between the VL-DN paths, there was a 17.51% overlap in the left hemisphere and 20.66% overlap in the right hemisphere (See Figure 28). We performed the same analyses but this time in standard space (MNI152). The trend in results was similar for this analysis. VL-M1 tracts showed the highest amount of overlap with 42.10% and 42.67% for the left and right hemispheres respectively. The left and right M1-DN tracts had overlaps of 32.70% and 34.45% respectively while left and right VL-DN fibre paths overlapped across scanners by 22.12% and 24.17% respectively (See Figure 29).
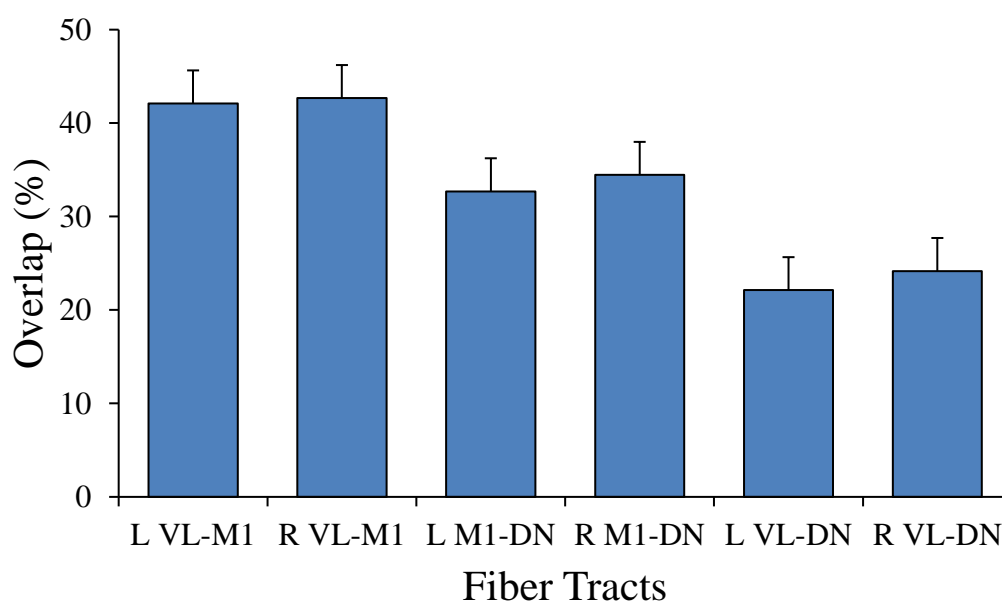
Figure 29: Average streamline overlap (%) across scanners in MNI152 standard space. VL: ventrolateral nuclei; M1: primary motor cortices; DN: dentate nuclei.

6.3 Discussion

In Study IV, in 100% of participants, both the VL-M1 and VL-DN streamlines were reconstructed with the help of exclusion and terminations masks at 3T and 7T. For the M1-DN streamline, 70% of participants at 3T required at least one exclusion or termination mask, while at 7T this was true for only 40% of participants. In 30% of participants at 3T and 60% of participants at 7T, this M1-DN streamline did not require any aid from target masks to accurately reconstruct the fibre path. These probabilistic tractography results provide superficial evidence that the 7T sequence used in this study is adequate for imaging these motor tracts and can better resolve crossing fibres near the

cerebellum compared to its 3T counterpart. It is possible that ultra-high fields more easily reconstructed the M1-DN streamlines because of the increased SNR, leading to a more accurate tensor estimate and subsequently less uncertainty of the fibre pathway (Mukherjee et al., 2008). However, only quantitative analyses can elucidate 7T's true gains for this sequence, as visual inspection of probabilistic streamlines is not sufficient.

We found significant differences between 3T and 7T average FA values for each tract and for global FA values. Even when we used a ratio of the raw FA values and global white matter FA, significant differences were observed in every fibre tract, except for global fractional anisotropy. FA values at 7T were consistently significantly higher than FA values at 3T. This seems to contradict previous work (Pierpaoli & Basser, 1996; Pierpaoli et al. 1996; Jones & Basser, 2004) which have found higher FA values at low SNR. This trend is usually interpreted as an overestimation of the anisotropy measures – interestingly a few studies have found higher FA values at higher field strengths, however none could provide a definite explanation for the observations (Huisman et al., 2006; Polder et al., 2009; Qin et al., 2009). Indeed, as Huisman et al. (2006) propose, the fact that our results contradict previous Monte Carlo simulations showing the relationship between FA values and SNR (Pierpaoli & Basser, 1996) leads us to believe that differences in SNR between the 3T and 7T acquisitions are not responsible for the measured differences. However, the noise level modeled in simulation studies is a fixed parameter; conversely in the scanner, exogenous factors such a movement artifacts, eddy-current distortions, chemical shift artifacts and field (B0/B1) inhomogeneities can all affect the true SNR profile of the acquisition (Farrell et al., 2007).

On the one hand, perhaps B0 and B1 inhomogeneity artifacts were so severe at 7T that diffusion signal loss decreased the SNR of the acquisition, therefore increasing FA estimates compared to 3T estimates. Some studies have shown SNR loss of up to 15% at ultra-high fields because of these artifacts (Speck & Zhong, 2009). However, quality control of the diffusion data prior to any tractography or quantitative analyses did not reveal any serious artifacts of this sort. On the other hand, common 3T DTI acquisition parameters include 30 gradient diffusion directions and 2mm^3 isotropic voxels (Mukherjee et al., 2008). In our own 3T acquisition, we increased the gradient sampling

directions to 137 and increased the spatial resolution with smaller voxel sizes ($1.5mm^3$ isotropic voxels) thereby theoretically increasing the SNR and reducing partial volume effects of the acquisitions (Alexander et al., 2007), perhaps then leading to higher SNR than at 7T. This could also explain our contradictory results. An important note to make is that a single measure of raw FA values of a fibre tract is arbitrary and meaningless when observed in isolation – this metric only become meaningful when compared across groups (e.g. clinical populations) or longitudinally to observe microstructural changes of a path over time. Therefore, the fact that our 7T average FA values are significantly higher than 3T average FA values cannot speak to the quality of the DTI sequence in each scanner. A more accurate measure of the scanner's performance of estimating FA is modeling the *uncertainty* of the FA values of each tract (Farrell et al., 2007; Polders et al., 2010; Polders et al., 2011) at different SNR values. By doing this, the effects of SNR on the *precision* of DTI metrics can be evaluated. This is also a major limitation to our study. We did not measure the SNR of each scanner's acquisition, nor did we calculate the uncertainty of our metrics and until these two analyses are performed, we cannot reliably interpret our observations of significant differences in FA values across magnetic fields.

We proceeded to investigate the reliability of ROIs across scanners, to ensure that our seed placement did not affect the tractography results. We calculated the overlap between 3T and 7T masks for each ROI (thalamic, cerebellar and cortical) and as reported, we found very low agreement in ROI placement between 3T and 7T acquisitions. Human error is a simple and easy explanation for these results as thalamic and cerebellar masks were manually created in the native diffusion space of each participant. However, acquisitions at both scanners had the same field of view and number of slices so theoretically the anatomical markers used to create these masks should occur at the same position in each scanner. For thalamic masks, the most dorsal slice of the anterior commissure was identified and center voxels for this ROI were place 3 slices (4.5 mm) dorsal to this landmark. For cerebellar masks, the slice where Vermis X protrudes into the 4th ventricle was used as the landmark at which to place center voxels for this ROI. Upon

further inspection of the data, we noticed that in the 7T acquisitions, the participants'
heads were tilted forward as compared to the 3T acquisitions. This misalignment between
both scanners is what we posit as the cause behind the low overlap between regions of
interest. The forward tilt of the head at 7T would skew the placement of ROIs at that
field, placing them much lower in anatomical space than they appeared in diffusion space
(see Figure 30). These effects could only be observed once both 3T and 7T ROIs had
been warped into native coregistered T1 and standard MNI152 space. Another important
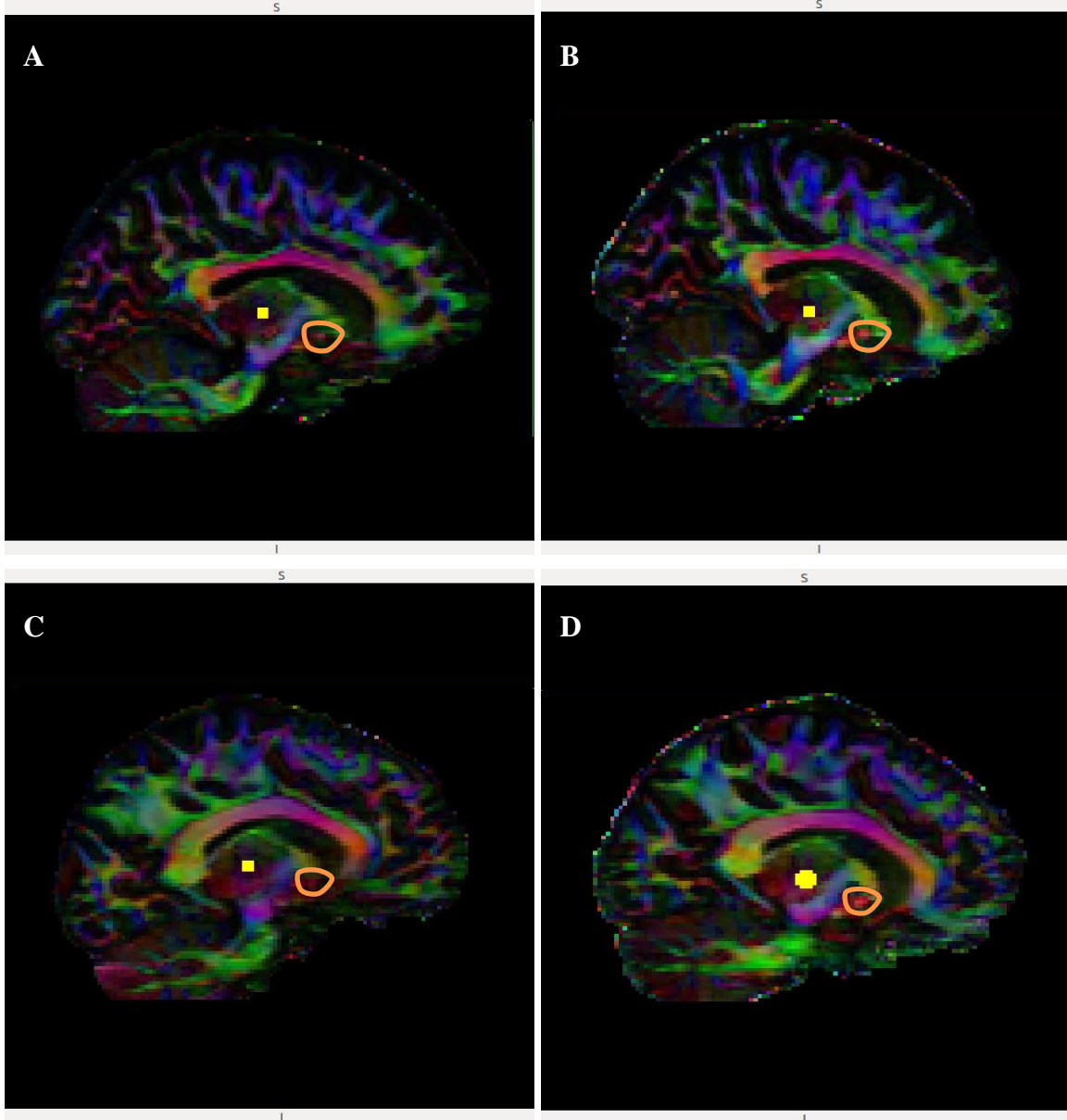
Figure 30: Representation of head tilt at 3T and 7T. HC1 at Panels A and B; HC2 at Panels C and D. Panels A and C
are diffusion space from 3T acquisitions and Panels B and D are diffusion space from 7T acquisitions. The left
ventrolateral thalamic nucleus ROI in yellow and the anterior commissure circle in orange.

detail to note is that 7T ROIs significantly differed to 3T ROIs on the z-axis plane. They did not differ on the x-axis or y-axis planes, thus supporting the head tilt hypothesis. This low agreement could be problematic for our probabilistic tractography results. If the ROIs are significantly different from each other, then perhaps our streamlines are reconstructing different fibre paths across scanners, which could speak to the differences we observed in tractography success. To measure if the difference in ROI placement affected streamline reconstructions, we warped the streamlines into T1 anatomical and MNI152 space to calculate the amount of overlap between 3T and 7T fibre paths. Our results lead us to conclude that the significant differences in ROI placement did in fact lead to significant differences in streamline location, mainly demonstrating differences in the z-axis plane (similar to the ROI overlap results). We reported mediocre agreement between 3T and 7T streamlines.

We further reported comparisons in MD and volume of each fibre tract between scanners. We observed no differences between scanners of average MD values of any of the six tracts of interest. When considered alongside the observed differences in FA values however, this observation is curious. Fractional anisotropy and mean diffusivity have an inverse relationship (Alexander et al., 2007): as FA increases, MD decreases. As such, we would expect this relationship to persist in our own results. We would expect MD to be significantly higher at 3T than at 7T, considering FA at 3T was significantly lower than at 7T. This is, however, was not the case. Mean diffusivity is not affected by incorrect estimation of the principal eigenvector in a given voxel as MD is the mean off all three diffusion directions (Soares et al., 2013). Fractional anisotropy on the other hand, is highly affected by incorrect estimation of the principal diffusion direction (i.e. it is highly affected by unresolved crossing fibres in a voxel). It has been shown that MD is a stable metric across different levels of SNR (Farrell et al., 2007) which leads us to conclude that there is a high level of uncertainty in our estimations of fractional anisotropy at either 3T or 7T (or both) potentially caused by incorrect estimation of principal eigenvectors. This would explain why we observed significant differences in this metric across scanners. These speculations can be addressed only once we model the uncertainty in both FA and MD estimations at different SNR levels. Finally, we only observed significant differences of fibre tract volume between 3T and 7T right M1-DN tracts and left VL-DN tracts. The

volume of fibre paths is calculated by multiplying the voxel volume of the acquisition ($3.375mm^3$ in our case) by the number of voxels included in the streamline. This measure cannot speak to any differences in the microstructure of the fibre paths of interest however in the context of comparison of tractography streamlines, it could be useful. If the volume of tracts (i.e. the number of voxels of each tract) does not differ between scanners, then we could conclude that streamlines of similar sizes are being reconstructed. This would add additional support to the idea that although our ROI placements differed between scanners, the streamlines themselves overlapped adequately and did not significantly differ in terms of their size.

Chapter 7

7.   General Discussion

The overall goals of this thesis were twofold:

1) First, map the white matter connections of motor execution loops in patients with disorders of consciousness.

2) Second, develop a 7T DTI sequence optimized to image these motor tracts in DOC patients, and assess if imaging at ultra-high fields incurs any gains in the identification of the ventrolateral thalamic nuclei and its cortical projections.

The first two studies were designed to further the investigation into the neural underpinnings of motor performance in this patient group and expand results from Fernández-Espejo et al. (2015). Studies I and II showed preliminary evidence of the involvement of impairments to the motor system in overt responsiveness in DOC patients. Our results from these studies suggest that across diagnostic categories, DOC patients demonstrate some level of motor impairment. This impairment is contaminating their performance on behavioural assessments and prevents these patients from overtly demonstrating their true level of awareness. None of the patients described in these two studies demonstrated covert awareness, suggesting that motor function abnormalities are pervasive to all patients in this clinical population, not just those few who have manifested retained awareness with impaired motor execution functions. Based on our results, one could then ask the question: if all DOC patients have impaired motor abilities, are these truly disorders of consciousness or rather disorders of cortical motor systems? At first glance, we could conclude that these patients are in fact all aware of themselves and their surroundings, and simply lack the motor capabilities to interact with their environment.

The involvement of the motor system in DOC, however, is only one piece of the puzzle. As demonstrated by post-mortem studies of this patient group (Adams et al., 1999; Adams et al., 2000; Jennett et al., 2001), widespread damage to the thalamus is the most

common injury in DOC patients. This highlights the need to investigate the thalamus'
role in DOC, specifically investigating the functions of different thalamic nuclei. As
discussed above, parcellation of these subcortical nuclei is not possible at 3T due to the
low spatial resolution and the small size of the regions under investigation (Behrens et al.,
2003; Metzger et al., 2013). Multimodal imaging at ultra-high fields, however, has been
shown to be successful at segmenting the thalamus (Calamante et al., 2011; Lenglet et al.,
2012; Xiao et al., 2016) and opens the possibility to investigate multiple thalamic
mechanisms in DOC patients. Future directions for Studies I and II to complete this
puzzle would be to map out fibres from the dorsomedial nucleus of the thalamus and to
reconstruct its cortical and subcortical connections, in accordance with Schiff's (2008)
mesocircuit hypothesis. This control fibre would help elucidate the role of the motor
system and the role of the arousal system in differentiating a "true" VS from covert
awareness.

Beyond the implications for patients with disorders of consciousness, Studies I and II also
inform current capabilities of acquiring diffusion data 3T and demonstrated the need for
imaging at ultra-high fields in this clinical population. As described in Study II, more
than half our sample of DOC patients and a third of our healthy control group had to be
excluded from the study because we were unable to reconstruct VL-DN and M1-DN
tracts. These excluded participants were scanned with a less informative diffusion
sequence than the patients and controls described in Study II. This demonstrated the
importance of acquisition parameters in diffusion tensor imaging and their impact in
imaging clinical populations. Study III confirmed this conclusion: the less informative of
the three tested protocols did not perform as well as the other two acquisition protocols of
interest. Based on these results, we chose the acquisition protocol that required the least
"help" possible in reconstructing neuroanatomically correct streamlines. In our fourth
study, we proceeded to validate this protocol choice in a group of healthy participants,
where we acquired the 7T acquisition of interest as well as the images from its 3T
counterpart in each participant. We then proceeded to qualitatively and quantitatively
compare the reconstructions of motor tracts across healthy participants. Study IV
demonstrated preliminary evidence that acquisitions at 7T performed better probabilistic
tractography than at 3T. Conversely, there was very low agreement in ROI mask

placement and streamline location across magnetic fields. More studies are needed to determine the cause of this low agreement and how this affects probabilistic tractography and DTI metrics. A main limitation of this study was the lack of investigation into the effects of the SNR of each scanner on DTI metric. Specifically, more studies need to be conducted to model the SNR of each acquisition and to model the SNR's effect on raw fractional anisotropy values as well as the uncertainty of DTI metrics. This will determine if there is any true gain to be had when imaging at ultra-high fields, beyond tractography. This modeling will also help explain the unexpected relationship between FA and MD observed, and will elucidate how well either magnetic field estimated these metrics. The next step with the optimized 7T sequence would be to investigate tractography from different thalamic nuclei, specifically from the mediodorsal nucleus. Successful tractography in healthy controls from this thalamic nucleus would confirm the clinical relevance of this 7T sequence in allowing a double dissociation between motor execution fibres and mesocircuit fibres.

It is important to stress that the analysis pipeline and diffusion protocols designed in this study were designed specifically to be used in a clinical population. This affected how we performed probabilistic tractography, influenced the possible diffusion parameters we could adjust to benefit our sequence and constrained our results from the beginning. Firstly, there are two main techniques in placing ROIs to initiate probabilistic tractography. Manual placement of ROIs, the method used in this thesis, is highly susceptible to human error and bias based on neuroanatomical priors. The second "brute force" method consists of seeding all voxels in the cortex to generate all possible white matter streamlines and manually selecting the tracts of interest (Mukherjee et al., 2008). Although this second technique is considered technically superior, this is not a viable option for the clinical population of interest in this thesis. Due to the global damage sustained by severe brain injury patients, using the brute force method of ROI generation would be unreliable as the white matter tracts in these patients severely deviate from healthy white matter streamlines. Additionally, due to the herniation process that occur in traumatic brain injury patients, manual placement of ROIs has been the most reliable way to ensure that the correct regions are being seeded and included in the streamlines of interest in the patients studied. In clinical populations, accurate estimation of white matter

microstructure is paramount if researchers and clinicians seek to characterize damage or disruption to white matter paths as part of the pathological process (Horsfield & Jones, 2002). It has been established that increasing the number of gradient sampling directions will yield a better estimation of the diffusion tensor (Mukherjee, 2008). Conversely, a better estimation of the tensor leads to less uncertainty in streamline reconstructions (Behrens et al., 2003b) which is beneficial when the goal is to infer the microstructure of specific white matter paths. This, however, will also increase the scanning time which is not always possible when imaging a clinical population, especially patients with disorders of consciousness. We therefore were constrained to optimize parameters to fit a specific timeframe. In the end, the protocol used in Study IV took 22 minutes to run, 11 minutes in each phase encoding direction.

Finally, future studies are needed to validate the optimized 7T sequence in DOC patients. Only then will we be able to determine if this 7T sequence brings any benefit above and beyond the capabilities at 3T MRI when characterizing white matter microstructure in a chronic brain injury patient. This will also demonstrate if this 7T sequence is adequate to parcellate thalamic nuclei to investigate other mechanisms which may be underlying DOC symptomology.

References

Adams, J. H., Jennett, B., McLellan, D. R., Murray, L. S., & Graham, D. I. (1999). The neuropathology of the vegetative state after head injury. *Journal of Clinical Pathology, 52*, 804-806.

Adams, J. H., Graham, D. I., & Jennett, B. (2000). The neuropathology of the vegetative state after an acute brain insult. *Brain, 123*, 1327-1338.

Albin, R. L., Young, A. B., & Penney, J. B. (1989). The functional anatomy of basal ganglia disorders. *Trends in Neuroscience, 12*(10), 366-375.

Alexander, A. L., Lee, J. E., Lazar, M., & Field, A. S. (2007). Diffusion tensor imaging of the brain. *Neurotherapeutics: The Journal of the American Society for Experimental NeuroTherapeutics, 4*(3), 316-329. doi: 10.1016/j.nurt.2007.05.11.

Allen, G. I., & Tsukahara, N. (1974). Cerebrocerebellar communications systems. *Physiological Reviews, 54*, 957-1006.

Anderson, A. W. (2001). Theoretical analysis of the effects of noise on diffusion tensor imaging. *Magnetic Resonance in Medicine, 46*, 1174-1188.

Andersson, J. L. R., Skare, S., & Ashburner, J. (2003). How to correct susceptibility distortions in spin-echo echo-planar images: application to diffusion tensor imaging. *NeuroImage, 20*, 870-888.

Andersson, J. L. R., & Sotiropoulos, S. N. (2016). An integrated approach to correction for off-resonance effects and subject movement in diffusion MR imaging. *NeuroImage, 125*, 1063-1078.

Andrews, K., Murphy, L., Munday, R., & Littlewood, C. (1996). Misdiagnosis of the vegetative state: retrospective study in rehabilitation unit. *BMJ (Clinical Research Ed.), 313*(7048), 13-16. doi: 10.1136/bmj.313.7048.13.

Armitage, P. A., & Bastin, M. E. (2001). Utilizing the diffusion-to-noise ratio to optimize magnetic resonance diffusion tensor acquisition strategies for improving measurements of diffusion anisotropy. *Magnetic Resonance in Medicine, 45*, 1056-1065.

Bastin M. E., Armitage, P. A., & Marshall, I. (1998). A theoretical study of the effect of experimental noise on the measurement of anisotropy in diffusion imaging. *Magnetic Resonance Imaging, 16*, 773-785.

Basser, P., Mattiello, J., Le Bihan, D. (1994). Estimation of the effective self-diffusion tensor from the NMR spin echo. (Series B). *Journal of Magnetic Resonance, 103*, 247-254.

Basser, P., Mattiello, J., & Le Bihan, D. (1994). MR diffusion tensor spectroscopy and imaging. *Biophysical Journal, 66*, 256-267.

Basser, P. J. (1995). Inferring microstructural features and the physiological state of tissues from diffusion-weighted images. *NMR in Biomedicine, 8*, 333-344.

Behrens, T.E.J., Woolrich, M.W., Jenkinson, M., Johansen-Berg, H., Nunes, R.G., Clare, S., Matthews, P.M., Brady, J.M., & Smith, S.M. (2003b). Characterization and propagation of uncertainty in diffusion-weighted MR imaging. *Magnetic Resonance in Medicine*, *50*(5), 1077-1088.

Behrens, T.E.J., Johansen Berg, H., Jbabdi, S., Rushworth, M. F. S., & Woolrich, M. W. (2007). Probabilistic diffusion tractography with multiple fibre orientations: What can we gain? *NeuroImage, 34*(1), 144-155. doi: 10.1016/j.neuroimage.2006.09.018.

Beukema, S., Gonzalez-Lara, L. E., Finoia, P., Kamau, E., Allanson, J., Chennu, S., … Cruse, D. (2016). A hierarchy of event-related potential markers of auditory processing in disorders of consciousness. *NeuroImage: Clinical, 12,* 359-371. doi: 10.1016/j.nicl.2016.08.003.

Binder, J. R., Frost, J. A., Hammeke, T. A., Bellgowan, P. S. F., Springer, J. A., Kaufman, J. N., & Possing, E. T. (2000). Human temporal lobe activation y speech and nonspeech sounds. *Cerebral Cortex, 10*, 512-528.

Birtsch, P. M., Grodd, W., Klose, U., Ackerman, H., & Voigt, K. (1996). Functional MRI of the cerebellum during voluntary hand and foot movement with multislice EPI. *NeuroImage, 3*(3), Supplement 378.

Boly, M., Faymonville, M-E., Peigneux, P., Lambermont, B., Damas, P., Del Fiore, G., …, Laureys, S. (2004). Auditory processing in severely brain injured patients: differences between minimally conscoius state and the persistent vegetative state. *Archives of Neurology, 61*(2), 233-238.

Bornshlegl, M., & Asanuma, H. (1987). Importance of the projection from the sensory to motor cortex for recovery of motor function following partial thalamic lesion in the monkey. *Brain Research, 437*, 121-130.

Box, G. E.P., & Andersen, S. L. (1955). Permutation theory in the derivation of robust criteria and the study of departures from assumption. *Journal of the Royal Statistical Society B (Statistical Methodology), 17*, 1-34.

Bowtell, R., McIntyre, D. J. O., Commandre, M. J., Glover, P. M., Mansfield, P. (1994). Correction of geometric distortion in echo planar images. *Proceedings of the 2nd Meeting of the Society of Magnetic Resonance,* 411.

Bruno, M-A., Majerus, S., Boly, M., Vanhaudenhuyse, A., Schnakers, C., Gosseries, O., …, Laureys, S. (2012). Functional neuroanatomy underlying the clinical subcategorization of minimally conscious state patients. *Journal of Neurology, 259*(6), 1087-1098. doi: 10.1007/s00415-011-6303-7.

Bruno, M-A., Vanhaudenhuyse, A., Thibaut, A., Moonen, G., & Laureys, S. (2011). From unresponsive wakefulness to minimally conscious plus and functional locked-in syndromes: Recent advances in our understanding of disorders of consciousness. *Journal of Neurology, 258*, 1373-1384.

Calamante, F., Oh, S.H., Tournier, J. D., Park, S. Y., Son, Y. D., Chung., J. Y., …, Cho, Z. H. (2013). Super-resolution track-density imaging of thalamic substructures: comparison with high-resolution anatomical magnetic resonance imaging at 7.0T. *Human Brain Mapping, 34*, 2538-2548.

Calamante, F., Tournier, J. D., Kurniawan, N. D., Yang, Z., Gyengesi, E., Galloway, G. I., …, Connelly, A. (2012). Super-resolution track-density imaging studies of mouse brain: comparison to histology. *NeuroImage, 59*(1), 286-296.

Chang, H., & Fitzpatrick, J. (1992). A technique for accurate magnetic resonance imaging in the presence of field inhomogeneities. *IEEE Transactions on Medical Imaging, 11*, 319-329.

Childs, N., Mercer, W., & Childs, H. (1993). Accuracy of diagnosis of persistent vegetative state. *Neurology, 43*(8), 1465-1467.

Choi, S., Cunningham, D. T., Aguila, F., Corrigan, J. D., Bogner, J., Mysiw, J., …, Schmalbrock, P. (2011). DTI at 3T and 7T: systematic comparison of SNR and its influence on quantitative metrics. *Magnetic resonance Imaging, 29*(6)., 739-751. doi: 10.1016/j.mri.2011.02.009.

Cologan, V., & Schabus, M. (2012). Sleep in disorders of consciousness. In C. Schnakers & S. Laureys (Eds.), *Coma and Disorders of Consciousness* (85-95). London: Springer-Verlag.

Crawford, J. R., Garthwaite, P. H., & Ryan, K. (2011). Comparing a single case to a control sample: Testing for neuropsychological deficits and dissociations in the presence of covariates. *Cortex, 47*, 1166-1178.

Cruse, D., Chennu, S., Chatelle, C., Bekinschtein, T. A., Fernández-Espejo, D., Pickard, J. D., …, Owen, A. M. (2011). Bedside detection of awareness in the vegetative state: a cohort study. *The Lancet, 378*(9808), 2088-2094.

De Biase, S., Gigli, G. L., Lorenzut, S., Bianconi, C., Sfreddo, P., Rossato, G., …, Basaldella, F., Fuccaro, M., Corica, A., Tonon, D., Barbone, F., & Valente, M.

(2014). The importance of polysomnography in the evaluation of prolonged disorders of consciousness: sleep recordings more adequately correlate than stimulus-related evoked potentials with patients' clinical status. *Sleep Medicine, 15*(4), 393-400.

Descoteaux, M., Deriche, R., Knösche, T. R., & Anwander, A. (2009). Deterministic and probabilistic tractography based on complex fibre orientation distributions. *IEEE Transactions on Medical Imaging, 28*, 269-286.

Diedrichsen, J. (2006). A spatially unbiased template of the human cerebellum. *Neuroimage, 33*(1), 127-138.

Di Perri, C., Thibaut, A., Heine, L., Soddu, A., Demertzi, A., & Laureys, S. (2014). Measuring consciousness in coma and related states. *World Journal of Radiology, 6*(8), 589-597.

Dum R. P., & Strick, P. L. (2003). An unfolded map of the cerebellar dentate nucleus and its projections to the cerebral cortex. *Journal of Neurophysiology, 89*, 634-639.

Evrard, H. C., & Craig, A. D. (2008). Retrograde analysis of the cerebellar projections to the posteroventral part of the ventral lateral thalamic nucleus in the macaque monkey. *Journal of Comparative Neurology, 508*, 286-314.

Farrell, J. A., Landman, B. A., Jones, C. K., et al. (2007). Effects if signal-to-noise ratio on the accuracy and reproducibility of diffusion tensor imaging-derived fractional anisotropy, mean diffusivity, and principal eigenvector measurements at 1.5T. *Journal of Magnetic Resonance Imaging, 26*, 756-767.

Fernández-Espejo, D., Bekinschtein, T., Monti, M. M., Pickard, J. D., Junque, C., & Coleman, M. R. …, Owen, A. M. (2011). Diffusion weighted imaging distinguishes the vegetative state from the minimally conscious state. *NeuroImage, 54*, 103-112. doi: 10.1016/j.neuroimage.2010.08.035.

Fernández-Espejo, D., Junque, C., Bernabeu, M., Roig-Rovira, T., Vendrell, P., Mercader, J. M. (2010). Reductions of thalamic volume and regional shape changes

in the vegetative and the minimally conscious states. *Journal of Neurotrauma, 27*(7), 1187-1193.

Fernández-Espejo, D., & Owen, A. M. (2013). Detecting awareness after severe brain injury. *Nature Reviews: Neuroscience, 14*, 801-809.

Fernández-Espejo, D., Rossit, S., & Owen, A. M. (2015). A thalamocortical mechanism for the absence of overt motor behaviour in covertly aware patients. *JAMA Neurology, 72*(12), 1442-1450.

Fernández-Espejo, D., Soddu, A., Cruse, D., Palacios, E. M., Junque, C., & Vanhaudenhuyse, A. (2012). A role for the default mode network in the bases of disorders of consciousness. *Annals of Neurology, 72*, 335-343. doi: 10.1002/ana.2363.

Fiacconi, C. M., & Owen, A. M. (2016). Using a facial electromyography to detect preserved emotional processing in disorders of consciousness: A proof-of-principle study. *Clinical Neurophysiology, 127*(9), 3000-3006. doi: 10.1016/j.clinph.2016.06.006.

Figueiredo, E. H., Borgonovi, A. F., & Doring, T. M. (2011). Basic concepts of MR imaging, diffusion MR imaging, and diffusion tensor imaging. *Magnetic Resonance Imaging Clinics of North America, 19*, 1-22.

Fins, J. J. (2003). Constructing an ethical stereotaxy for severe brain injury: balancing risks, benefits and access. *Nature Reviews: Neuroscience, 4*, 323-327.

Formisano, E., Kim, D. S., Di Salle, F., Van de Moortele. P. F., Ugurbil, K., & Goebel, R. (2003). Mirror-symmetric tonotopic maps in human primary auditory cortex. *Neuron, 40*, 859-869.

Fridman, E. A., & Schiff, N. D. (2014). Neuromodulation of the conscious state following severe brain injuries. *Current Opinion in Neurology, 29*, 172-177.

Galea, J. M. Vazquez, A., Pasricha, N., Orban de Xivry, J-J, O., & Celnik, P. (2011). Dissociating the roles of the cerebellum and motor cortex during adaptive learning: the motor cortex retains what the cerebellum learns. *Cerebral Cortez, 21*(8), 1761-1770. doi: 10.1093/cercor/bhq246.

Giacino, J. T., & Kalmar, K. (1997). The vegetative and minimally conscious states: A comparison of clinical features and functional outcome. *Journal of Head Trauma Rehabilitation, 12*(4), 36-51.

Giacino, J. T., Ashwal, S., Childs, N., Cranford, R., Jennett, B., Katz, D. I., …, Kelly, J. P., Rosenberg, J. H., Whyte, J., Zafonte, R. D., & Zasler, N. D. (2002). The minimally conscious state: Definition and diagnostic criteria. *Neurology, 58*, 349-353.

Giacino, J. T. (2004). The vegetative and minimally conscious states: Consensus-based criteria for establishing diagnosis and prognosis. *NeuroRehabilitation, 19*, 293-298.

Giacino, J. T., & Kalmar, K. (2004). *Coma Recovery Scale – Revised: Administration and scoring guidelines*. Retrieved from http://www.coma.ulg.ac.be/images/crs_r.pdf.

Giacino, J. T., & Kalmar, K. (2005). Diagnostic and prognostic guidelines for the vegetative and minimally conscious states. *Neuropsychological Rehabilitation, 15*(3-4), 166-174. doi: 10.1080/09602010443000498.

Giacino, J. T., Kalmar, K., & Whyte, J. (2004). The JFK Coma Recovery Scale-Revised: measurement characteristics and diagnostic utility. *Archives of Physical Medicine and Rehabilitation, 85*, 2020-2029.

Gibson, R. M., Chennu, S., Fernández-Espejo, D., Naci, L., Owen, A. M., & Cruse, D. (2016). Somatosensory attention identifies both overt and covert awareness in disorders of consciousness. *Annals of Neurology*, *80*(3), 412-423. doi: 10.1002/ana.24726.

Gibson, R. M., Fernández-Espejo, D., Gonzalez-Lara, L., Kwan, B. Y., Lee, D. H.,
    Owen, A. M., & Cruse, D. (2014). Multiple tasks and neuroimaging modalities
    increase the likelihood of detecting covert awareness in patients with disorders of
    consciousness. *Frontiers in Human Neuroscience, 8*, 950. doi:
    https://doi.org/103389/fnhum.2014.00950.

Gill-Thwaites, H., & Munday, R. (2004). The sensory modality assessment and
    rehabilitation technique (SMART): a valid and reliable assessment for vegetative
    state and minimally conscious state patients. *Brain Injury, 18*(20), 1255-1269.

Glickstein, M. (2000). How are visual areas of the brain connected to motor areas for the
    sensory guidance of movement? *Trends in Neuroscience, 23*, 613-617.

Glickstein, M. (2007). What does the cerebellum really do? *Current Biology, 17*(19),
    824-826.

Gosseries, O., Vanhaudenhuyse, A., Bruno, M-A., Demertzi, A., Schnakers, C., Boly, M.
    M., Maudoux, A., Moonen, G., & Laureys, S. (2011). Disorders of consciousness:
    Coma, vegetative and minimally conscious states. In D. Cvetkovic and I. Cosic
    (Eds.), *States of Consciousness* (pp. 29-55). Berlin Heidelberg: Springer-Verlag.

Graham, D. I., Adams, J. H., Murray, L. S., & Jennett, B. (2005). Neuropathology of the
    vegetative state after head injury. *Neuropsychological Rehabilitation, 15*, 198-213.

Guldenmund, P., Stender, J., Heine, L., & Laureys, S. (2012). Mindsight: Diagnostics in
    disorders of consciousness. *Critical Care Research and Practice, 2012*, 1-13. doi:
    10.1155/2012/624724.

Hagmann, P., Jonasson, L., Maeder, P., Thiran, J. P., Wedeen, V. J., & Meuli, R. (2006).
    Understanding diffusion MR imaging techniques: from scalar diffusion-weighted
    imaging to diffusion tensor imaging and beyond. *Radiographics,* 26(Suppl. 1),
    S205–S223.

Holland, D., Kuperman, J. M., Dale, A. M. (2010). Efficient correction of inhomogeneous static magnetic distortion in echo planar imaging. *Neuroimage, 50*(1), 175.

Hoover, J. E., & Strick, P. L. (1999). The organization of cerebellar and basal ganglia outputs to primary motor cortex as revealed by retrograde transneuronal transport of herpes simplex virus type 1. *The Journal of Neuroscience, 19*, 1446-1772.

Horsfield, M. A., & Jones, D. K. (2002). Applications of diffusion-weighted and diffusion tensor MRI to white matter diseases – a review. *NMR in Biomedicine, 15*, 570-577.

Huisman, T. A. G. M., Loenneker, T., Barta, G., Bellemann, M. E., Hennig, J., Fisher, J. E., & Il'yasov, K. A. (2006). Quantitative diffusion tensor MR imaging of the brain: field strength related variance of apparent diffusion coefficient (ADC) and fractional anisotropy (FA) scalars. *European Radiology, 16*, 1651-1658.

Jakab, A., Blanc, R., Berényi, E. L., & Székely, G. (2014). Generation of individualized thalamus target maps by using statistical shape models and thalamocortical tractography. *American Journal of Neuroradiology, 36*(5), 2110-2116.

Jeannerod, M. (1995). Mental imagery in the motor context. *Neuropsychologia, 33*(11), 1419-1432.

Jennett, B. (2002). The vegetative state. *Journal of Neurology, Neurosurgery & Psychiatry, 73*(4), 355-357. doi: 10.1136/jnnp.73.4.355.

Jennett, B., & Plum, F. (1972). Persistent vegetative state after brain damage: A syndrome in search of a name. *The Lancet, 299*(7753), 734-737.

Jennett, B., Adams, J. H., Murray, L. S., & Graham, D. I. (2001). Neuropathology in vegetative and severely disabled patients after head injury. *Neurology, 56*, 486-940.

Jenkinson, M., & Smith, S. M. (2001). A global optimisation method for robust affine registration of brain images. *Medical Image Analysis, 5*(2), 143-156.

Jenkinson, M., Bannister, P. R., Brady, J. M., & Smith, S. M. (2002). Improved optimisation for the robust and accurate linear registration and motion correction of brain images. *NeuroImage, 17*(2), 825-841.

Jin, S-H., & Chung, C. K. (2012). Messages from the Brain Connectivity Regarding Neural Correlates of Consciousness. *Experimental Neurobiology, 21*(3), 113.

Johansen-Berg, H., Behrens, T. E., Sillery, E., Ciccarelli, O., Thompson, A. J., Smith, S. M., & Matthews, P. M. (2005). Functional-anatomical validation and individual variation of diffusion tractography-based segmentation of the human thalamus. *Cerebral Cortex, 15*(1), 31-39. doi: 10.1093/cercor/bhh105.

Jones, D. K., Knösche, T. R., & Turner, R. (2013). White matter integrity, fiber count, and other fallacies: The do's and don'ts of diffusion MRI. *Neuroimage, 73*, 239-254. doi: 10.1016/j.neuroimage.2012.06.081.

Jones, D. K. (2004). The effect of gradient sampling schemes on measures derived from diffusion tensor MRI: A Monte Carlo study. *Magnetic Resonance in Medicine, 51*, 807-815.

Jones, D. K., & Basser, P. J. (2004). "Squashing peanuts and smashing pumpkins": How noise distorts diffusion-weighted MR data. *Magnetic Resonance in Medicine, 52*(5), 979-993. doi: 10.1002/mrm.2083.

Kalmar, K., & Giacino, J. T. (2005). The JFK Coma Recovery Scale – Revised. *Neuropsychological Rehabilitation 15*(3-4), 454-460. doi: 10.1080/09602010443000425.

Kinoshita, M., de Champfleur, N. M., Deverdun, J., Moritz0Gasser, S., Herbert, G., Duffau, H. (2015). Role of fronto-striatal tract and frontal aslant tract in movement and speech: an axonal mapping study. *Brain Structure and Function, 220*(6), 3399-3412. doi:10.1007/s00429-014-0863-0.

Lambert, C., Simon, H., Colman, J., & Barrick, T. R. (in press). Defining thalamic nuclei and topographic connectivity gradients in vivo. *NeuroImage*.

Lant, N. D., Gonzalez-Lara, L. E., Owen, A. M., Fernández-Espejo, D. (2015). Relationship between the anterior forebrain mesocircuit and the default mode network in the structural bases of disorders of consciousness. *NeuroImage: Clinical, 10*, 27-35.

Laureys, S., Boly, M., Moonen, G., & Maquet, P. (2009). Coma. *Encyclopedia of Neuroscience, 2*, 1133-1142.

Laureys, S., Faymonville, M-É., Luxen, A., Lamy, M., Franck, G., & Maquet, P. (2000). Restorations of thalamocortical connectivity after recovery from persistent vegetative state. *The Lancet, 355*(9217), 1790-1791. doi: 16/S0140-6736(00)02271-6.

Laureys, S., Faymonvillle, M-É., & Maquet, P. (2002). Quelle conscience durant le coma? *Pour la Science, 302*, 122-128.

Laureys, S., Owen, A. M., & Schiff, N. D. (2004). Brain function in coma, vegetative state, and related disorders. *The Lancet Neurology, 3*(9), 537-546.

Laureys, S. (2005). The neural correlates of (un)awareness: lessons from the vegetative state. *TRENDS in Cognitive Sciences, 9*(12), 556-559.

Le Bihan, D., & Breton, E. (1985). Imagerie de diffusion *in vivo* par résonance magnétique nucléaire. *Comptes-Rendus de l'Académie des Sciences, 93*(5), 27-34.

Le Bihan, D., Breton, E., Lallemand, D., Grenier, P., Cabanis, E., Laval-Jeantet, M. (1986). MR imaging of intravoxel incoherent motions: applications to diffusion and perfusion in neurologic disorders. *Radiology, 161*, 401-407.

Lenglet, C., Abosch, A., Yacoub, E., De Martino, F., Sapiro, G., & Harel, N. (2012). Comprehensive *in vivo* mapping of the human basal ganglia and thalamic

connectome in individuals using 7T MRI. *PLoS ONE, 7*(1), e29153. doi: https;//doi.org/10.137/journal.pone.0029153.

Lindman, H. R. (1974). *Analysis of variance in complex experimental designs.* San Francisco: W.H. Freeman & Co. New Jersey: Erlbaum.

Longoni, F., Grande, M., Hendrich, V., Kastrau, F., & Huber W. (2005). An fMRI study on conceptual, grammatical, and morpho-phonological processing. *Brain and Cognition, 57*, 131-134.

Lotze, M., Montoya, P., Erb, M., Hulsmann, E., Flor, H., Klose, U., …, Grodd, W. (1999). Activation of cortical and cerebellar motor areas during executed and imagined hand movements: An fMRI study. *Journal of Cognitive Neuroscience, 11*(5), 491-501.

Lutkenhoff, E. S., Chiang, J., Tshibanda, L., Kamau, E., Kirsch, M., Pickard, J. D., …, Monti, M. M. (2015). Thalamic and extrathalamic mechanisms of consciousness after severe brain injury. *Annals of Neurology, 78*, 68-76.

Majerus, S., Collette, F., Van der Linden, M., Peigneux, P., Laureys, S., Delfiore, G., …, Salmon, E. (2002). A PET investigation of lexicality and phonotactic frequecy in oral language processing. *Cognitive Neuropsychology, 19*, 343-360.

Majerus, S., Gill-Thwaites, H., Andrews, K., & Laureys, S. (2005). Behavioural evaluation of consciousness in severe brain damage. *Progress in Brain Research, 150*, 397-413.

Martin, A., Wiggs, C. L., Ungerleider, L. G., & Haxby, J. V. (1996). Neural correlates of category-specific knowledge. *Nature, 379*, 649-652.

Maxwell, W. L., MacKinnon, M. A., Smith, D. H., McIntosh, T. K., & Graham, D. I. (2006). Thalamic nuclei after human blunt head injury. *Journal of Neuropathology and Experimental Neurology, 65*(5), 478-488.

Maxwell, W. L., Pennington, K., MacKinnon, M. A., Smith, D. H., McIntosh, T. K., Wilson, J. T., & Graham, D. I. (2004). Differential responses in three thalamic nuclei in moderately disabled, severely disabled and vegetative patients after blunt head injury. *Brain, 127*(pt 11), 2470-2478.

Merboldt, K-D., Hanicke, W., & Frahm, J. (1985). Self-diffusion NMR imaging using stimulated echoes. *Journal of Magnetic Resonance, 64*, 479-486.

Metzger, C., van der Werf, Y., & Walter, M. (2013). Functional mapping of thalamic nuclei and their integration into cortico-striatal-thalamo-cortical loops via ultra-high resolution imaging – from animal anatomy to in vivo imaging in humans. *Frontiers in Neuroscience, 7*, 1-14. doi: 10.3389/fnins.2013.00024.

Monti, M. (2012). Cognition in the vegetative state. *Annual Review of Clinical Psychology, 8*, 431-454.

Monti, M. M., Vanhaudenhuyse, A., Coleman, M. R., Boly, M., Pickard, J. D., Sci., F. M., …, Laureys, S. (2010). Disorders of consciousness. *The New England Journal of Medicine*, 579-589.

Morel, A. (2007). *Stereotactic Atlas of the Human Thalamus and Basal Ganglia*. New York London: InformaHealthcare.

Morgan, P. S., Bowtell, R. W., McIntyre, D. J. O., & Worthington, B. S. (2004). Correction of spatial distortion in EPI due to inhomogeneous static magnetic fields using the reversed gradient method. *Journal of Magnetic Resonance Imaging, 19*(4), 499-507.

Mori, S., Zhang, J. (2006). Principles of diffusion tensor imaging and its applications to basic neuroscience research. *Neuron, 51*(5), 527-539.

Mukherjee, P., Chung, S. W., Berman, J. I., Hess, C. P., & Henry, R. G. (2008). Diffusion tensor MR imaging and fiber tractography: technical considerations. *American Journal of Neuroradiology, 29*, 843-852.

The Multi-Society Task Force on PVS. (1994). Medical aspects of the persistent vegetative state (second of two parts). *The New England Journal of Medicine, 330*(22), 1572-1579.

Naci, L., & Owen, A. M. (2013). Making every word count for nonresponsive patients. *JAMA Neurology, 70*(10), 1235-1241. doi:10.1001/jamaneurol.2013.3686.

Nair, D. G., Purcott, K. L., Fuchs, A., Steinberg, F., & Kelso, J. A. S. (2003). Cortical and cerebellar activity of the human brain during imagined and executed unimanual and bimanual action sequences: a functional MRI study. *Cognitive Brain Research, 15*, 250-260.

Newcombe, V., Chatfield, D., Outtrim, J., Vowler, S., Manktelow, A., Cross, J., …, Menon, D. K. (2011). Mapping traumatic axonal injury using diffusion tensor imaging: correlations with functional outcome. *PLoS ONE, 6*(5), e19214. doi: 10.1371/journal.pone.0019214.

Newcombe, V., Williams, G. B., Scoffings, D., Cross, J., Carpenter, T. A., Pickard, J. D., …, Menon, D. K. (2010). Aetiological differences in neuroanatomy of the vegetative state: insights from diffusion tensor imaging and functional implications. *Journal of Neurology, Neurosurgery & Psychiatry, 81*, 552-561.

Ni, H., Kavcic, V., Zhu T., Ekholm, S., & Zhong, J. (2006). Effects of number of diffusion gradient directions on derived diffusion tensor imaging indices in human brain. *American Journal of Neuroradiology, 27*(8), 1776-1781.

Noirhomme, Q., Soddu A., Lehembre, R., Vanhaudenhuyse, A., Boveroux, P., Boly, M., & Laureys, S. (2010). Brain connectivity in pathological and pharmacological coma. *Frontiers in Systems Neuroscience, 4*, 1-6.

O'Donnell, L. J., & Westin, C-F. (2011). An introduction to diffusion tensor image analysis. (2011). *Neurosurgery Clinics of North America, 22*(2), 185-196. doi: 10.1016/j.nec.2010.12.004.

Owen, A. M., Coleman, M. R., Boly, M., Davis, M. J., Laureys, S., & Pickard, J. D. (2006). Detecting awareness in the vegetative state. *Science, 313*, 1402.

Parent, A., & Hazrati, L. N. (1995). Functional anatomy of the basal ganglia: i: the cortico-basal ganglia-thalamo-cortical loop. *Brain Research Reviews, 20*(1), 91-127.

Pierpaoli, C., & Basser, P. J. (1996). Toward a quantitative assessment of diffusion anisotropy. *Magnetic Resonance in Medicine, 36*(6), 893-906.

Pierpaoli, C., Jezzard, P., Basser, P. J., Barnett, A., & Di Chiro, G. (1996). Diffusion tensor MR imaging of the human brain. *Radiology, 201*, 637–648.

Polders, D. L., Hoogduin, H., Donahue, M. J., Hendrikse, J., & Luijten, P. (2009). Comparison of SNR and diffusion parameters on 1.5, 3.0, and 7.0 Tesla. *Proceedings of the Seventeenth Annual Meeting of the International Society of Magnetic Resonance in Medicine*, pp. 1406.

Polders, D. L., Leemans, A., Hoogduin, J. M., Henddrikse, J. Donahnue, M., & Luijten, P. R. (2010). Evaluating the uncertainty of DTI parameters at 1.5, 3.0 and 7.0 Tesla. *Proceedings of the Eighteenth Annual Meeting of the International Society of Magnetic Resonance in Medicine*, pp. 1641.

Polders, D. L., Leemans, A., Hendrikse, J., Donahue, M. J., Luijten, P. R., & Hoogduin, J. M. (2011). Signal to noise ratio and uncertainty in diffusion tensor imaging at 1.5, 3.0, and 7.0 Tesla. *Journal of Magnetic Resonance Imaging, 33*, 1456-1463. doi: 10.1002/jmri.22554.

Posner, J. B., Saper, C. B., Schiff, N. D., & Plum, F. (2007). *Plum and Posner's diagnosis of stupor and coma* (4th ed.). New York, NY: Oxford University Press.

Qin, W., Yu, C. S., Zhang, F., Du, X. Y., Yan, Y. X., & Li, K. C. (2009). Effects of echo time on diffusion quantification of brain white matter at 1.5 T and 3.0 T. *Magnetic Resonance in Medicine, 61*, 755-760.

Rausell, E., & Avendaño, C. (1985). Thalamocortical neurons projecting to superficial and to deep layers in parietal, frontal and prefrontal regions in the cat. *Brain Research, 347*, 159-165.

Rispal-Padel, L., Massion, J., & Grangetto. A. (1973). Relations between the ventrolateral thalamic nucleus and motor cortex and their possible role in the central organization of motor control. *Brain Research, 60*, 1-20.

Roland, P. E., Skinhøj, E., Lassen, N. A., & Larsen, B. (1980). Different cortical areas in man in organization of voluntary movements in extrapersonal space. *Journal of Neurophysiology, 43*(1), 137-150.

Sala-Llonch, R., Bosch, B., Arenaza-Urquijo, E.M., Rami, L., Bargallo, N., Junque, C., Molinuevo, J.L., Bartrés-Faz, D. (2010). Greater default-mode network abnormalities compared to high order visual processing systems in amnesic mild cognitive impairment: an integrated multi-modal MRI study. *Journal of Alzheimer's Disease: JAD, 22*(2), 523–539. doi: 10.3233/JAD-2010-101038.

Schiff, N. D. (2008). Central thalamic contributions to arousal regulation and neurological disorders of consciousness. *Annals of the New York Academy of Sciences, 1129*, 105-118.

Schiff, N. D. (2010). Recovery of consciousness after brain injury: a mesocircuit hypothesis. *TRENDS in Neuroscience, 33*(1), 1-9.

Schnakers, C., Giacino, J., & Laureys, S. (2010). Coma: Detecting signs of consciousness in severely brain injured patients recovering from coma. In J. H. Stone & M. Blouin (Eds.), *International Encyclopedia of Rehabilitation* (1-13). Buffalo: Center for International Rehabilitation Research Information and Exchange (CIRRIE).

Schnakers, C., Ledoux, D., Majerus, S., Damas, P., Damad, F., Lambermont, B., …, Laureys, S. (2008). Diagnostic and prognostic use of bispectralindex in coma, vegetative state and related disorders. *Brain Injury, 22*(12), 926-931.

Schnakers, C., Majerus, S., & Laureys, S. (2004). Diagnostic et évaluation des états de conscience altérée. *Réanimation, 13*, 368-375.

Schnakers, C., & Majerus, S. (2012). Behavioural assessment and diagnosis of disorders of consciousness. In C. Schnakers & S. Laureys (Eds.), *Coma and Disorders of Consciousness* (1-10). London: Springer-Verlag.

Schnakers, C., Vanhaudenhuyse, A., Giacino, J., Ventura, M., Boly, M., Majerus, S., …, Laureys, S. (2009). Diagnostic accuracy of the vegetative state and minimally conscious state: clinical consensus versus standardized neurobehavioural assessment. *BMC Neurology, 9*(35), 1-5. doi: 10.1186/1471-2377-9-35.

Shaw, C. B., Jensen, J. H., Deardorff, R. L., Spampinato, M. V., & Helpern, J. A. (2016). Comparison of diffusion metrics obtained at 1.5T and 3T in human brain with diffusional kurtosis imaging. *Journal of Magnetic Resonance Imaging, 45*(3), 673-680. doi: 10.1002/jmri.25380.

Shiel, A., Horn, S. A., Wilson, B. A., Watson, M. J., Campbell, M. J., & McLellan, D. L. (2000). The Wessex Head Injury Matrix (WHIM) main scale: a preliminary report on a scale to assess and monitor patient recovery after severe head injury. *Clinical Rehabilitation, 14*, 408-416.

Shinoda, Y., Futami, T., & Kano, M. (1985). Synaptic organization of the cerebello-thalamo-cerebral pathway in the cat. II. Input-output organization of single thalamocortical neurons in the ventrolateral thalamus. *Neuroscience Research, 2*, 157-180.

Smith, S. M. (2002). Fast robust automated brain extraction. *Human Brain Mapping, 17*(3), 143-155. doi: 10.1002/hbm.10062.

Soares, J. M., Marques, P., Alves, V., & Sousa, N. (2013) A hitchhiker's guide to diffusion tensor imaging. *Frontiers in Neuroscience, 7*, 1-14. https://doi.org/10.3389/fnins.2013.00031.

Song, S. K., Sun, S. W., Ramsbottom, M. J., Chang, C., Russell, J., & Cross, A. H. (2002). Dysmyelination revealed through MRI as increased radial (but unchanged axial) diffusion of water. *Neuroimage,* 17, 1429–1436.

Speck, O., & Zhong, K. (2009). Diffusion tensor imaging at 7T: Expectations vs reality check. *Proceedings of the Seventeenth Annual Meeting of the International Society of Magnetic Resonance in Medicine*, pp. 1462.

Stieltjes, B., Brunner, R. M., Fritzsche, K., & Laun, F. (2013). Introduction to diffusion imaging. In *Diffusion Tensor Imaging: Introduction and Atlas*. Retrieved from http://www.springer.com/us/book/9783642204555.

Taylor, D. G., & Bushell, M. C. (1985). The spatial mapping of translational diffusion coefficients by the NMR imaging technique. *Physics in Medicine and Biology, 30*, 345-349. doi: 10.1088/0031-9155/30/4/009.

Teasdale, G., & Jennett, B. (1974). Assessment of coma and impaired consciousness. A practical scale. *The Lancet, 2*(7872), 81-84.

Teasdale, G., Maas, A., Lecky, F., Manley, G., Stocchetti, N., & Murray, G. (2012). The Glasgow Coma Scale at 40 years: standing the test of time. *The Lancet Neurology, 13*, 844-854.

Thonnard, M., Wannez, S., Keen, S., Brédart, S., Bruno, M-A., Gosseries, O., …, Vanhaudenhuyse, A. (2014). Detection of visual pursuit in patients in minimally conscious state: A matter of stimuli and visual plane? *Brain Injury, 28*(9), 1164-1170.

Tournier, J. D., Calamante, F., & Connelly, A. (2009). How many diffusion gradient directions are required for HARDI? *Proceedings of the International Society for Magnetic Resonance in Medicine, 17*, 358.

Tseng, Y. W., Diedrichsen, J., Krakauer, J. W., Shadmehr, R., & Bastian, A. J. (2007). Sensory prediction errors drive cerebellum-dependent adaptations of reaching. *Journal of Neurophysiology, 98*, 54-62.

Vanhaudenhuyse, A., Schnakers, C., Boly, M., Perrin, F., Brédart, S., & Laureys, S. (2007). Détecter les signes de conscience chez le patient en état de conscience minimale. *Réanimation, 16*, 527-532.

Wessinger, C. M., VanMeter, J., Tian, B., Van Laren, J., Pekar, J., & Rauschecker, J. P. (2001). Hierarchical organization of the human auditory cortex revealed by functional magnetic resonance imaging. *Journal of Cognitive Neuroscience, 13*, 1-7.

Wijdicks, E. F. M., Bamlet, W. R., Maramattom, B. V., Manno, E. M., & McClelland, R. L. (2005). Validation of a new coma scale: the FOUR score. *Annals of Neurology, 58*(4), 585-593.

Wu, M., Chang, L-C., Walker, L., Lemaitre, H., Barnett, A.S., Marenco, S., Pierpaoli, C. (2008). Comparison of EPI distortion correction methods in diffusion MRI using a novel framework. *Medical Image Conputing and Computer-Assisted Intervention, 11*, 321-329.

Xiao, Y., Zitella, L., Duchin, Y., Teplitzky, B. A., Kastl, D., Adriany, G., …, Johnson, M. D. (2016). Multimodal 7T imaging of thalamic nuclei for preclinical deep brain stimulation applications. *Frontiers in Neuroscience, 10*, 1-15. doi: https://doi.org/10.3389/fnins.2016.00264.

Zatorre, R. J. & Belin, P. (2001). Spectral and temporal processing in human auditory cortex. *Cerebral Cortex, 11*, 946-953.

Zhan, L., Mueller, B., Jahanshadm, N., Jin, Y., Lenglet, C., Yacoub, E, …, Thompson, P. M. (2013). Magnetic resonance field strength effects on diffusion measures and brain connectivity networks. *Brain Connectivity, 3*(1), 72-86. doi: 10.1089/brain.2012.0114.

Zhang, Y., Brady, M., & Smith, S. M. (2001). Segmentation of brain MR images through a hidden Markov random field model and the expectation-maximization algorithm. *IEEE Transactions on Medical Imaging, 20*(1), 45-57.

Zheng, Z-H., Wu, R-P., & Xi, M-C. (1986). Thalamic projection to motor area and area 3a of the cat cerebral cortex. *Brain Research, 380*(2), 389-393.

Appendices

Appendix A: 3T diffusion tensor imaging protocols in healthy participants.

SIEMENS MAGNETOM Prisma_fit

\\USER\Fernandez-Espejo\Clara\DTI\diff_p3_b1000_65dirs
TA: 8:54 PM: FIX Voxel size: 1.5×1.5×1.5 mmPAT: 3 Rel. SNR: 1.00 : epse

Properties

Prio recon	Off
Load images to viewer	On
Inline movie	Off
Auto store images	On
Load images to stamp segments	Off
Load images to graphic segments	Off
Auto open inline display	Off
Auto close inline display	Off
Start measurement without further preparation	Off
Wait for user to start	On
Start measurements	Single measurement

Routine

Slice group	1
Slices	84
Dist. factor	0 %
Position	R0.7 A20.2 H33.9 mm
Orientation	T > C-3.5
Phase enc. dir.	A >> P
AutoAlign	---
Phase oversampling	0 %
FoV read	208 mm
FoV phase	98.6 %
Slice thickness	1.5 mm
TR	7500 ms
TE	55.0 ms
Averages	1
Concatenations	1
Filter	Raw filter, Prescan Normalize
Coil elements	HEA;HEP

Contrast - Common

TR	7500 ms
TE	55.0 ms
MTC	Off
Magn. preparation	None
Fat suppr.	None

Contrast - Dynamic

Averages	1
Averaging mode	Long term
Reconstruction	Magnitude
Measurements	1
Delay in TR	0 ms
Multiple series	Off

Resolution - Common

FoV read	208 mm
FoV phase	98.6 %
Slice thickness	1.5 mm
Base resolution	138
Phase resolution	100 %
Phase partial Fourier	6/8
Interpolation	Off

Resolution - iPAT

PAT mode	GRAPPA
Accel. factor PE	3

Resolution - iPAT

Ref. lines PE	54
Reference scan mode	EPI/separate

Resolution - Filter Image

Distortion Corr.	Off
Prescan Normalize	On
Dynamic Field Corr.	Off

Resolution - Filter Rawdata

Raw filter	On
Elliptical filter	Off

Geometry - Common

Slice group	1
Slices	84
Dist. factor	0 %
Position	R0.7 A20.2 H33.9 mm
Orientation	T > C-3.5
Phase enc. dir.	A >> P
FoV read	208 mm
FoV phase	98.6 %
Slice thickness	1.5 mm
TR	7500 ms
Multi-slice mode	Interleaved
Series	Interleaved
Concatenations	1

Geometry - AutoAlign

Slice group	1
AutoAlign	---
Position	R0.7 A20.2 H33.9 mm
Orientation	T > C-3.5
Phase enc. dir.	A >> P
Initial Position	R0.7 A20.2 H33.9
R	0.7 mm
A	20.2 mm
H	33.9 mm
Initial Rotation	0.00 deg
Initial Orientation	T > C
T > C	-3.5
> S	0.0

Geometry - Saturation

Fat suppr.	None
Special sat.	None

Geometry - Navigator

Geometry - Tim Planning Suite

Set-n-Go Protocol	Off
Table position	H
Table position	0 mm
Inline Composing	Off

System - Miscellaneous

Positioning mode	FIX
Table position	H
Table position	0 mm
MSMA	S - C - T

SIEMENS MAGNETOM Prisma_fit

System - Miscellaneous

Sagittal	R >> L
Coronal	A >> P
Transversal	F >> H
Coil Combine Mode	Adaptive Combine
Matrix Optimization	Off
AutoAlign	---
Coil Select Mode	Default

System - Adjustments

B0 Shim mode	Standard
B1 Shim mode	TrueForm
Adjust with body coil	Off
Confirm freq. adjustment	Off
Assume Dominant Fat	Off
Assume Silicone	Off
Adjustment Tolerance	Auto

System - Adjust Volume

Position	R0.7 A20.2 H33.9 mm
Orientation	T > C-3.5
Rotation	0.00 deg
A >> P	205 mm
R >> L	208 mm
F >> H	126 mm
Reset	Off

System - pTx Volumes

B1 Shim mode	TrueForm
Excitation	Standard

System - Tx/Rx

Frequency 1H	123.211178 MHz
Correction factor	1
Gain	High
Img. Scale Cor.	1.000
Reset	Off
? Ref. amplitude 1H	0.000 V

Physio - Signal1

1st Signal/Mode	None
TR	7500 ms
Concatenations	1

Physio - PACE

Resp. control	Off
Concatenations	1

Diff - Neuro

Diffusion mode	Free
Diff. directions	65
Diffusion Scheme	Monopolar
Diff. weightings	2
b-value 1	0 s/mm²
b-value 2	1000 s/mm²
b-value 1	1
b-value 2	1
Diff. weighted images	On
Trace weighted images	On
ADC maps	On
FA maps	On
Mosaic	On
Tensor	On
Noise level	40

Diff - Body

Diffusion mode	Free
Diff. directions	65
Diffusion Scheme	Monopolar
Diff. weightings	2
b-value 1	0 s/mm²
b-value 2	1000 s/mm²
b-value 1	1
b-value 2	1
Diff. weighted images	On
Trace weighted images	On
ADC maps	On
Exponential ADC Maps	Off
FA maps	On
Invert Gray Scale	Off
Calculated Image	Off
b-Value >=	0 s/mm²
Noise level	40

Diff - Composing

Inline Composing	Off
Distortion Corr.	Off

Sequence - Part 1

Introduction	On
Optimization	None
Multi-slice mode	Interleaved
Free echo spacing	Off
Echo spacing	0.93 ms
Bandwidth	1726 Hz/Px

Sequence - Part 2

EPI factor	136
RF pulse type	Low SAR
Gradient mode	Performance*
Excitation	Standard

Sequence - pTX Pulses

SIEMENS MAGNETOM Prisma_fit

\\USER\Fernandez-Espejo\Clara\DTI\diff_mb2_p2_b1000_137dirs PA
TA: 10:14 PM: FIX Voxel size: 1.5×1.5×1.5 mmPAT: 2 Rel. SNR: 1.00 : epse

Properties

Prio recon	Off
Load images to viewer	On
Inline movie	Off
Auto store images	On
Load images to stamp segments	Off
Load images to graphic segments	Off
Auto open inline display	Off
Auto close inline display	Off
Start measurement without further preparation	Off
Wait for user to start	On
Start measurements	Single measurement

Routine

Slice group	1
Slices	84
Dist. factor	0 %
Position	R0.7 A20.2 H33.9 mm
Orientation	T > C-3.5
Phase enc. dir.	P >> A
AutoAlign	---
Phase oversampling	0 %
FoV read	208 mm
FoV phase	98.6 %
Slice thickness	1.50 mm
TR	4080 ms
TE	62.40 ms
Multi-band accel. factor	2
Filter	Raw filter, Prescan Normalize
Coil elements	HEA;HEP

Contrast - Common

TR	4080 ms
TE	62.40 ms
MTC	Off
Magn. preparation	None
Flip angle	90 deg
Refocus flip angle	180 deg
Fat suppr.	None
Grad. rev. fat suppr.	Enabled

Contrast - Dynamic

Averaging mode	Long term
Reconstruction	Magnitude
Measurements	1
Delay in TR	0 ms
Multiple series	Off

Resolution - Common

FoV read	208 mm
FoV phase	98.6 %
Slice thickness	1.50 mm
Base resolution	138
Phase resolution	100 %
Phase partial Fourier	6/8
Interpolation	Off

Resolution - iPAT

PAT mode	GRAPPA

Resolution - iPAT

Accel. factor PE	2
Ref. lines PE	60
Reference scan mode	GRE

Resolution - Filter Image

Distortion Corr.	Off
Prescan Normalize	On
Dynamic Field Corr.	Off

Resolution - Filter Rawdata

Raw filter	On
Elliptical filter	Off

Geometry - Common

Slice group	1
Slices	84
Dist. factor	0 %
Position	R0.7 A20.2 H33.9 mm
Orientation	T > C-3.5
Phase enc. dir.	P >> A
FoV read	208 mm
FoV phase	98.6 %
Slice thickness	1.50 mm
TR	4080 ms
Multi-slice mode	Interleaved
Series	Interleaved
Multi-band accel. factor	2

Geometry - AutoAlign

Slice group	1
AutoAlign	---
Position	R0.7 A20.2 H33.9 mm
Orientation	T > C-3.5
Phase enc. dir.	P >> A
Initial Position	R0.7 A20.2 H33.9
R	0.7 mm
A	20.2 mm
H	33.9 mm
Initial Rotation	-180.00 deg
Initial Orientation	T > C
T > C	-3.5
> S	0.0

Geometry - Saturation

Fat suppr.	None
Grad. rev. fat suppr.	Enabled
Special sat.	None

Geometry - Navigator

Geometry - Tim Planning Suite

Set-n-Go Protocol	Off
Table position	H
Table position	0 mm
Inline Composing	Off

System - Miscellaneous

Positioning mode	FIX
Table position	H

SIEMENS MAGNETOM Prisma_fit

System - Miscellaneous

Table position	0 mm
MSMA	S - C - T
Sagittal	R >> L
Coronal	A >> P
Transversal	F >> H
Coil Combine Mode	Sum of Squares
Matrix Optimization	Off
AutoAlign	---
Coil Select Mode	Default

System - Adjustments

B0 Shim mode	Standard
B1 Shim mode	TrueForm
Adjust with body coil	Off
Confirm freq. adjustment	Off
Assume Dominant Fat	Off
Assume Silicone	Off
Adjustment Tolerance	Auto

System - Adjust Volume

Position	R0.7 A20.2 H33.9 mm
Orientation	T > C-3.5
Rotation	180.00 deg
A >> P	205 mm
R >> L	208 mm
F >> H	126 mm
Reset	Off

System - pTx Volumes

B1 Shim mode	TrueForm

System - Tx/Rx

Frequency 1H	123.211178 MHz
Correction factor	1
Gain	High
Img. Scale Cor.	1.000
Reset	Off
? Ref. amplitude 1H	0.000 V

Physio - Signal1

1st Signal/Mode	None
TR	4080 ms
Multi-band accel. factor	2

Physio - PACE

Resp. control	Off
Multi-band accel. factor	2

Diff - Neuro

Diffusion mode	Free
Diff. directions	137
Diffusion Scheme	Monopolar
Diff. weightings	2
b-value 1	0 s/mm^2
b-value 2	1000 s/mm^2
b-value 1	1
b-value 2	1
Diff. weighted images	On
Trace weighted images	Off
ADC maps	Off
FA maps	On
Mosaic	On
Tensor	On

Diff - Neuro

Noise level	50

Diff - Body

Diffusion mode	Free
Diff. directions	137
Diffusion Scheme	Monopolar
Diff. weightings	2
b-value 1	0 s/mm^2
b-value 2	1000 s/mm^2
b-value 1	1
b-value 2	1
Diff. weighted images	On
Trace weighted images	Off
ADC maps	Off
Exponential ADC Maps	Off
FA maps	On
Invert Gray Scale	Off
Calculated Image	Off
b-Value >=	0 s/mm^2
Noise level	50

Diff - Composing

Inline Composing	Off
Distortion Corr.	Off

Sequence - Part 1

Introduction	Off
Multi-slice mode	Interleaved
Free echo spacing	Off
Echo spacing	0.93 ms
Bandwidth	1812 Hz/Px

Sequence - Part 2

EPI factor	136
Gradient mode	Performance*
RF spoiling	Off

Sequence - Special

Excite pulse duration	3840 us
Refocus pulse duration	6400 us
Single-band images	On
MB LeakBlock kernel	Off
MB RF phase scramble	On
Time-shifted MB RF	Off
SENSE1 coil combine	Off
Invert RO/PE polarity	Off
Online multi-band recon.	Online
FFT scale factor	1.00
GRE iPAT ref. FA	12.0 deg
Physio recording	Off

SIEMENS MAGNETOM Prisma_fit

\\USER\Fernandez-Espejo\Clara\DTI\diff_mb2_p2_b2000_139dirs_2shells PA
TA: 11:04 PM: FIX Voxel size: 1.5×1.5×1.5 mmPAT: 2 Rel. SNR: 1.00 : epse

Properties

Prio recon	Off
Load images to viewer	On
Inline movie	Off
Auto store images	On
Load images to stamp segments	Off
Load images to graphic segments	Off
Auto open inline display	Off
Auto close inline display	Off
Start measurement without further preparation	Off
Wait for user to start	On
Start measurements	Single measurement

Routine

Slice group	1
Slices	84
Dist. factor	0 %
Position	R0.7 A20.2 H33.9 mm
Orientation	T > C-3.5
Phase enc. dir.	P >> A
AutoAlign	---
Phase oversampling	0 %
FoV read	208 mm
FoV phase	98.6 %
Slice thickness	1.50 mm
TR	4370 ms
TE	69.40 ms
Multi-band accel. factor	2
Filter	Raw filter, Prescan Normalize
Coil elements	HEA;HEP

Contrast - Common

TR	4370 ms
TE	69.40 ms
MTC	Off
Magn. preparation	None
Flip angle	90 deg
Refocus flip angle	180 deg
Fat suppr.	None
Grad. rev. fat suppr.	Enabled

Contrast - Dynamic

Averaging mode	Long term
Reconstruction	Magnitude
Measurements	1
Delay in TR	0 ms
Multiple series	Off

Resolution - Common

FoV read	208 mm
FoV phase	98.6 %
Slice thickness	1.50 mm
Base resolution	138
Phase resolution	100 %
Phase partial Fourier	6/8
Interpolation	Off

Resolution - iPAT

PAT mode	GRAPPA

Resolution - iPAT

Accel. factor PE	2
Ref. lines PE	60
Reference scan mode	GRE

Resolution - Filter Image

Distortion Corr.	Off
Prescan Normalize	On
Dynamic Field Corr.	Off

Resolution - Filter Rawdata

Raw filter	On
Elliptical filter	Off

Geometry - Common

Slice group	1
Slices	84
Dist. factor	0 %
Position	R0.7 A20.2 H33.9 mm
Orientation	T > C-3.5
Phase enc. dir.	P >> A
FoV read	208 mm
FoV phase	98.6 %
Slice thickness	1.50 mm
TR	4370 ms
Multi-slice mode	Interleaved
Series	Interleaved
Multi-band accel. factor	2

Geometry - AutoAlign

Slice group	1
AutoAlign	---
Position	R0.7 A20.2 H33.9 mm
Orientation	T > C-3.5
Phase enc. dir.	P >> A
Initial Position	R0.7 A20.2 H33.9
R	0.7 mm
A	20.2 mm
H	33.9 mm
Initial Rotation	180.00 deg
Initial Orientation	T > C
T > C	-3.5
> S	0.0

Geometry - Saturation

Fat suppr.	None
Grad. rev. fat suppr.	Enabled
Special sat.	None

Geometry - Navigator

Geometry - Tim Planning Suite

Set-n-Go Protocol	Off
Table position	H
Table position	0 mm
Inline Composing	Off

System - Miscellaneous

Positioning mode	FIX
Table position	H

SIEMENS MAGNETOM Prisma_fit

System - Miscellaneous

Table position	0 mm
MSMA	S - C - T
Sagittal	R >> L
Coronal	A >> P
Transversal	F >> H
Coil Combine Mode	Sum of Squares
Matrix Optimization	Off
AutoAlign	---
Coil Select Mode	Default

System - Adjustments

B0 Shim mode	Standard
B1 Shim mode	TrueForm
Adjust with body coil	Off
Confirm freq. adjustment	Off
Assume Dominant Fat	Off
Assume Silicone	Off
Adjustment Tolerance	Auto

System - Adjust Volume

Position	R0.7 A20.2 H33.9 mm
Orientation	T > C-3.5
Rotation	180.00 deg
A >> P	205 mm
R >> L	208 mm
F >> H	126 mm
Reset	Off

System - pTx Volumes

B1 Shim mode	TrueForm

System - Tx/Rx

Frequency 1H	123.211178 MHz
Correction factor	1
Gain	High
Img. Scale Cor.	1.000
Reset	Off
? Ref. amplitude 1H	0.000 V

Physio - Signal1

1st Signal/Mode	None
TR	4370 ms
Multi-band accel. factor	2

Physio - PACE

Resp. control	Off
Multi-band accel. factor	2

Diff - Neuro

Diffusion mode	Free
Diff. directions	139
Diffusion Scheme	Monopolar
Diff. weightings	2
b-value 1	0 s/mm²
b-value 2	2000 s/mm²
b-value 1	1
b-value 2	1
Diff. weighted images	On
Trace weighted images	Off
ADC maps	Off
FA maps	On
Mosaic	On
Tensor	On

Diff - Neuro

Noise level	50

Diff - Body

Diffusion mode	Free
Diff. directions	139
Diffusion Scheme	Monopolar
Diff. weightings	2
b-value 1	0 s/mm²
b-value 2	2000 s/mm²
b-value 1	1
b-value 2	1
Diff. weighted images	On
Trace weighted images	Off
ADC maps	Off
Exponential ADC Maps	Off
FA maps	On
Invert Gray Scale	Off
Calculated Image	Off
b-Value >=	0 s/mm²
Noise level	50

Diff - Composing

Inline Composing	Off
Distortion Corr.	Off

Sequence - Part 1

Introduction	Off
Multi-slice mode	Interleaved
Free echo spacing	Off
Echo spacing	0.93 ms
Bandwidth	1812 Hz/Px

Sequence - Part 2

EPI factor	136
Gradient mode	Performance*
RF spoiling	Off

Sequence - Special

Excite pulse duration	3840 us
Refocus pulse duration	6400 us
Single-band images	On
MB LeakBlock kernel	Off
MB RF phase scramble	On
Time-shifted MB RF	Off
SENSE1 coil combine	Off
Invert RO/PE polarity	Off
Online multi-band recon.	Online
FFT scale factor	1.00
GRE iPAT ref. FA	12.0 deg
Physio recording	Off

Appendix B: 7T diffusion tensor imaging protocols in healthy participants.

SIEMENS MAGNETOM Investigational_Device_7T syngo MR B17

\\USER\Fernandez-Espejo\Davinia\Clara_DTI_Comp\ep2d_advdiff_p3_b1000_65dirs
TA: 7:00   PAT: 3   Voxel size: 1.5×1.5×1.5 mm   Rel. SNR: 1.00   USER: ep2d_advdiff_940

Properties

Prio Recon	Off
Before measurement	
After measurement	
Load to viewer	On
Inline movie	Off
Auto store images	On
Load to stamp segments	Off
Load images to graphic segments	Off
Auto open inline display	Off
Start measurement without further preparation	On
Wait for user to start	Off
Start measurements	single

Routine

Slice group 1	
Slices	84
Dist. factor	0 %
Position	L0.0 P7.3 F10.2
Orientation	Transversal
Phase enc. dir.	A >> P
Rotation	0.00 deg
Phase oversampling	0 %
FoV read	208 mm
FoV phase	87.0 %
Slice thickness	1.5 mm
TR	6000 ms
TE	49.2 ms
Averages	1
Concatenations	1
Filter	Raw filter
Coil elements	E1,2

Contrast

MTC	Off
Magn. preparation	None
Fat suppr.	None
Extra Fat Suppr.	off
Saturation Mode	standard
Averaging mode	Long term
Reconstruction	Magnitude
Delay in TR	0 ms
Multiple series	Off

Resolution

Base resolution	138
Phase resolution	100 %
Phase partial Fourier	6/8
Interpolation	Off
PAT mode	GRAPPA
Accel. factor PE	3
Ref. lines PE	54
Reference Scan Mode	multi-shot EPI
Distortion Corr.	Off
Prescan Normalize	Off
Raw filter	On
Intensity	Weak
Slope	25
Elliptical filter	Off
Hamming	Off

Geometry

Multi-slice mode	Interleaved
Series	Interleaved
Special sat.	None
Table position	H
Table position	0 mm
Inline Composing	Off

System

E1	On
E2	On
Positioning mode	REF
MSMA	S - C - T
Sagittal	R >> L
Coronal	A >> P
Transversal	F >> H
Coil Combine Mode	Adaptive Combine
AutoAlign	---
Auto Coil Select	Default
Shim mode	Standard
Adjust with body coil	Off
Confirm freq. adjustment	Off
Assume Silicone	Off
? Ref. amplitude 1H	0.000 V
Adjustment Tolerance	Auto
Adjust volume	
Position	L0.0 P7.3 F10.2
Orientation	Transversal
Rotation	0.00 deg
R >> L	208 mm
A >> P	181 mm
F >> H	126 mm

Physio

1st Signal/Mode	None
PMU Recording	off
Resp. control	Off

Diff

Diffusion mode	Free
Diff. weightings	1
b-value	1000 s/mm²
Diff. weighted images	On
Trace weighted images	On
Average ADC maps	On
Individual ADC maps	On
FA maps	On
Mosaic	On
Tensor	On
Noise level	40
Diff. directions	65

Sequence

Introduction	Off
Bandwidth	1510 Hz/Px
Optimization	None
Free echo spacing	Off
Echo spacing	0.75 ms
EPI factor	120
RF pulse type	Low SAR
Gradient mode	Fast
Add. FFT Scale Factor	1.0

1/+

SIEMENS MAGNETOM Investigational_Device_7T syngo MR B17

\\USER\Fernandez-Espejo\Davinia\Clara_DTI_Comp\mbep2d_diff_b1000_137dirs_AP
TA: 10:03   PAT: 3   Voxel size: 1.5×1.5×1.5 mm   Rel. SNR: 1.00   USER: cmrr_mbep2d_diff

Properties

Prio Recon	Off
Before measurement	
After measurement	
Load to viewer	On
Inline movie	Off
Auto store images	On
Load to stamp segments	Off
Load images to graphic segments	Off
Auto open inline display	Off
Start measurement without further preparation	On
Wait for user to start	Off
Start measurements	single

Routine

Slice group 1	
Slices	84
Dist. factor	0 %
Position	L0.1 P1.1 H2.6
Orientation	T > C-12.6
Phase enc. dir.	A >> P
Rotation	0.00 deg
Phase oversampling	0 %
FoV read	208 mm
FoV phase	100.0 %
Slice thickness	1.50 mm
TR	4000 ms
TE	53.4 ms
Multi-band accel. factor	2
Filter	None
Coil elements	E1,2

Contrast

MTC	Off
Magn. preparation	None
Flip angle	90 deg
Refocus flip angle	180 deg
Fat suppr.	None
Grad. rev. fat suppr.	Disabled
Averaging mode	Long term
Reconstruction	Magnitude
Measurements	1
Delay in TR	0 ms
Multiple series	Off

Resolution

Base resolution	138
Phase resolution	100 %
Phase partial Fourier	6/8
Interpolation	Off
PAT mode	GRAPPA
Accel. factor PE	3
Ref. lines PE	60
Reference scan mode	GRE
Distortion Corr.	Off
Prescan Normalize	Off
Raw filter	On
Elliptical filter	Off
Hamming	Off

Geometry

Multi-slice mode	Interleaved
Series	Interleaved
Special sat.	None
Table position	H
Table position	0 mm
Inline Composing	Off

System

E1	On
E2	On
Positioning mode	FIX
MSMA	S - C - T
Sagittal	R >> L
Coronal	A >> P
Transversal	F >> H
Coil Combine Mode	Sum of Squares
AutoAlign	---
Auto Coil Select	Default
Shim mode	Standard
Adjust with body coil	Off
Confirm freq. adjustment	Off
Assume Silicone	Off
? Ref. amplitude 1H	0.000 V
Adjustment Tolerance	Auto
Adjust volume	
Position	L0.1 P1.1 H2.6
Orientation	T > C-12.6
Rotation	0.00 deg
R >> L	208 mm
A >> P	208 mm
F >> H	126 mm

Physio

1st Signal/Mode	None

Diff

Diffusion mode	Free
Diff. weightings	2
b-value 1	0 s/mm²
b-value 2	1000 s/mm²
Diff. weighted images	On
Trace weighted images	On
Average ADC maps	On
Individual ADC maps	On
FA maps	On
Mosaic	On
Tensor	On
Noise level	100
Diff. directions	137

Sequence

Introduction	On
Bandwidth	1576 Hz/Px
Free echo spacing	Off
Echo spacing	0.72 ms
EPI factor	138
Gradient mode	Fast
RF spoiling	Off
Excite pulse duration	5120 us
Refocus pulse duration	40960 us
Diffusion Scheme	Monopolar
Single-band images	On
MB LeakBlock kernel	Off

2/+

SIEMENS MAGNETOM Investigational_Device_7T syngo MR B17

\\USER\Fernandez-Espejo\Davinia\Clara_DTI_Comp\mbep2d_diff_b2000_139dirs_2sh_AP

TA: 10:11   PAT: 3   Voxel size: 1.5×1.5×1.5 mm   Rel. SNR: 1.00   USER: cmrr_mbep2d_diff

Properties

Prio Recon	Off
Before measurement	
After measurement	
Load to viewer	On
Inline movie	Off
Auto store images	On
Load to stamp segments	Off
Load images to graphic segments	Off
Auto open inline display	Off
Start measurement without further preparation	On
Wait for user to start	Off
Start measurements	single

Routine

Slice group 1	
Slices	84
Dist. factor	0 %
Position	L0.1 P1.1 H2.6
Orientation	T > C-12.6
Phase enc. dir.	A >> P
Rotation	0.00 deg
Phase oversampling	0 %
FoV read	208 mm
FoV phase	100.0 %
Slice thickness	1.50 mm
TR	4000 ms
TE	60.2 ms
Multi-band accel. factor	2
Filter	None
Coil elements	E1,2

Contrast

MTC	Off
Magn. preparation	None
Flip angle	90 deg
Refocus flip angle	180 deg
Fat suppr.	None
Grad. rev. fat suppr.	Disabled
Averaging mode	Long term
Reconstruction	Magnitude
Measurements	1
Delay in TR	0 ms
Multiple series	Off

Resolution

Base resolution	138
Phase resolution	100 %
Phase partial Fourier	6/8
Interpolation	Off
PAT mode	GRAPPA
Accel. factor PE	3
Ref. lines PE	60
Reference scan mode	GRE
Distortion Corr.	Off
Prescan Normalize	Off
Raw filter	On
Elliptical filter	Off
Hamming	Off

Geometry

Multi-slice mode	Interleaved

Series	Interleaved
Special sat.	None
Table position	H
Table position	0 mm
Inline Composing	Off

System

E1	On
E2	On
Positioning mode	FIX
MSMA	S - C - T
Sagittal	R >> L
Coronal	A >> P
Transversal	F >> H
Coil Combine Mode	Sum of Squares
AutoAlign	---
Auto Coil Select	Default
Shim mode	Standard
Adjust with body coil	Off
Confirm freq. adjustment	Off
Assume Silicone	Off
? Ref. amplitude 1H	0.000 V
Adjustment Tolerance	Auto
Adjust volume	
Position	L0.1 P1.1 H2.6
Orientation	T > C-12.6
Rotation	0.00 deg
R >> L	208 mm
A >> P	208 mm
F >> H	126 mm

Physio

1st Signal/Mode	None

Diff

Diffusion mode	Free
Diff. weightings	2
b-value 1	0 s/mm²
b-value 2	2000 s/mm²
Diff. weighted images	On
Trace weighted images	On
Average ADC maps	On
Individual ADC maps	On
FA maps	On
Mosaic	On
Tensor	On
Noise level	100
Diff. directions	139

Sequence

Introduction	On
Bandwidth	1576 Hz/Px
Free echo spacing	Off
Echo spacing	0.72 ms
EPI factor	138
Gradient mode	Fast
RF spoiling	Off
Excite pulse duration	5120 us
Refocus pulse duration	40960 us
Diffusion Scheme	Monopolar
Single-band images	On
MB LeakBlock kernel	Off

6/+

Appendix C: Ethics approval notice for data collection in patients with disorders of consciousness.

Western Research

Research Ethics

Western University Health Science Research Ethics Board
HSREB Annual Continuing Ethics Approval Notice

Date: June 22, 2017
Principal Investigator: Dr. Adrian Owen
Department & Institution: Social Science\Psychology, Western University

Review Type: Full Board
HSREB File Number: 100963
Study Title: Assessing residual cognitive function in patients with disorders of consciousness (REB #18124)
Sponsor: Canadian Excellence Research Chair

HSREB Renewal Due Date & HSREB Expiry Date:
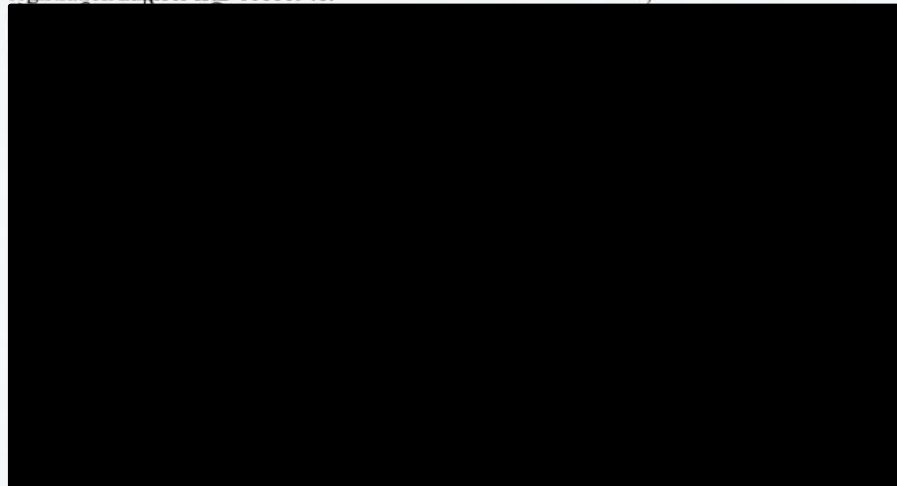Renewal Due -2018/06/30
Expiry Date -2018/07/05

The Western University Health Science Research Ethics Board (HSREB) has reviewed the Continuing Ethics Review (CER) Form and is re-issuing approval for the above noted study.

The Western University HSREB operates in compliance with the Tri-Council Policy Statement Ethical Conduct for Research Involving Humans (TCPS2), the International Conference on Harmonization of Technical Requirements for Registration of Pharmaceuticals for Human Use Guideline for Good Clinical Practice (ICH E6 R1), the Ontario Freedom of Information and Protection of Privacy Act (FIPPA, 1990), the Ontario Personal Health Information Protection Act (PHIPA, 2004), Part 4 of the Natural Health Product Regulations, Health Canada Medical Device Regulations and Part C, Division 5, of the Food and Drug Regulations of Health Canada.

Members of the HSREB who are named as Investigators in research studies do not participate in discussions related to, nor vote on such studies when they are presented to the REB.

The HSREB is registered with the U.S. Department of Health & Human Services under the IRB registration number IRB 00000940.

Appendix D: Ethics approval notice for 3T data collection in healthy participants.

Western Research   Research Ethics

Western University Health Science Research Ethics Board
HSREB Annual Continuing Ethics Approval Notice

Date: March 22, 2017
Principal Investigator: Dr. Adrian Owen
Department & Institution: Social Science\Psychology, Western University

Review Type: Full Board
HSREB File Number: 106215
Study Title: Investigating movement-related brain activity: Implications for patients with Disorders of Consciousness
Sponsor: Canadian Excellence Research Chair

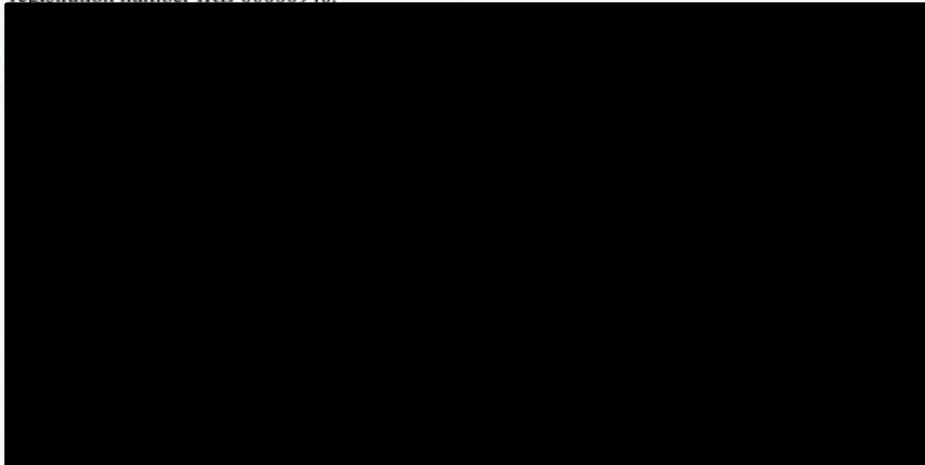**HSREB Renewal Due Date & HSREB Expiry Date**:
Renewal Due -2018/03/31
Expiry Date -2018/04/02

The Western University Health Science Research Ethics Board (HSREB) has reviewed the Continuing Ethics Review (CER) Form and is re-issuing approval for the above noted study.

The Western University HSREB operates in compliance with the Tri-Council Policy Statement Ethical Conduct for Research Involving Humans (TCPS2), the International Conference on Harmonization of Technical Requirements for Registration of Pharmaceuticals for Human Use Guideline for Good Clinical Practice (ICH E6 R1), the Ontario Freedom of Information and Protection of Privacy Act (FIPPA, 1990), the Ontario Personal Health Information Protection Act (PHIPA, 2004), Part 4 of the Natural Health Product Regulations, Health Canada Medical Device Regulations and Part C, Division 5, of the Food and Drug Regulations of Health Canada.

Members of the HSREB who are named as Investigators in research studies do not participate in discussions related to, nor vote on such studies when they are presented to the REB.

The HSREB is registered with the U.S. Department of Health & Human Services under the IRB registration number IRB 00000940.

Appendix E: Ethics approval notice for 7T data collection in healthy participants.

Western Research

Research Ethics

Western University Health Science Research Ethics Board
HSREB Annual Continuing Ethics Approval Notice

Date: January 13, 2017
Principal Investigator: Prof. Adrian Owen
Department & Institution: Social Science\Psychology, Western University

Review Type: Full Board
HSREB File Number: 104836
Study Title: Establishing healthy baselines for structural measures of consciousness
Sponsor: Canadian Institutes of Health Research

HSREB Renewal Due Date & HSREB Expiry Date:
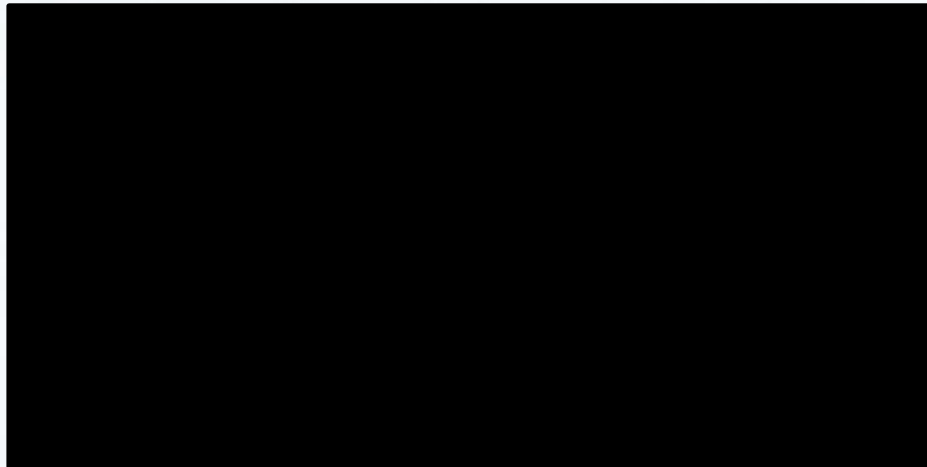Renewal Due -2018/01/31
Expiry Date -2018/02/11

The Western University Health Science Research Ethics Board (HSREB) has reviewed the Continuing Ethics Review (CER) Form and is re-issuing approval for the above noted study.

The Western University HSREB operates in compliance with the Tri-Council Policy Statement Ethical Conduct for Research Involving Humans (TCPS2), the International Conference on Harmonization of Technical Requirements for Registration of Pharmaceuticals for Human Use Guideline for Good Clinical Practice (ICH E6 R1), the Ontario Freedom of Information and Protection of Privacy Act (FIPPA, 1990), the Ontario Personal Health Information Protection Act (PHIPA, 2004), Part 4 of the Natural Health Product Regulations, Health Canada Medical Device Regulations and Part C, Division 5, of the Food and Drug Regulations of Health Canada.

Members of the HSREB who are named as Investigators in research studies do not participate in discussions related to, nor vote on such studies when they are presented to the REB.

The HSREB is registered with the U.S. Department of Health & Human Services under the IRB registration number IRB 00000940.

Appendix F: Letter of information for 3T data collection in healthy participants.

Western
The Brain and
Mind Institute

Letter of Information & Consent

Version: 3   Date: 17/03/2016

Investigating Movement Related Brain Activity: Implications for patients with Disorders
of Consciousness

You are being invited to participate in a research study. You have been invited for this study because you fulfil the criteria for MRI scanning as well as the age and health requirements for our study, which collects data on healthy brains to serve as a normal baseline for brain-injured patients. This sheet provides preliminary information regarding the study.

Purpose of the Study
The purpose of this study is to collect data on the structure and function of brain areas involved with movement and the sensations associated with it (eg. the sensation of your arm moving), also known as "sensorimotor" functions. We will measure brain activity in response to tasks involving sensorimotor abilities in healthy participants, such as you, using a magnetic resonance imaging (MRI) scanner. The overall aim of this study is to investigate preserved sensorimotor brain activity in disorders of consciousness (DOCs). DOCs result from severe brain injuries, and include a spectrum of disorders where a person's wakefulness and/or awareness of themselves and their environment are impaired. We can then use the in-depth examination of healthy brains as a base to compare and assess brain responses to movement in brain-damaged patients. This will help us to determine if they have preserved sensorimotor abilities, which may not be detected using traditional behavioural assessments of consciousness.

What is MRI scanning?
We can learn a great deal about how the brain works by looking at the blood flow to different parts of the brain whilst the brain performs different tasks. We need to obtain this information in both healthy individuals and individuals who have a disease.

We measure brain function using images taken with a magnetic resonance imaging scanner. This scanner uses a strong magnetic field to create detailed images of brain structure and function. By taking a series of images whilst you perform a task we can build up a picture of the brain areas activated by this type of function. The scan does not involve any injections or X-rays and MRI is thought to be a safe, non-invasive imaging technique. Each experiment within the project will involve approximately 15 participants. The entire research project will involve approximately 30 people.

Initials of Participant____   1

Like faces, brains come in all shapes and sizes, so that there are many normal variations of what the scan shows. There is a chance of less than 1:100 that your MR scan may show a significant abnormality of which you are unaware. It should be emphasised that the scan is not for medical purposes. However, if one of the technical or research staff finds an abnormality, your scans will be forwarded to a consultant neurologist who will contact you should counselling be appropriate. Such early detection has the benefit of starting treatment early but, in a small number of cases, may have implications for future employment and insurance.

What does the study involve?
Scanning will be undertaken in the 3 Tesla Siemens MRI scanner at the Robarts scan facility. It is a standard machine that is used widely for both medical and research purposes. Before your scan, a member of staff will ask you some questions to ensure that you have no metal within you before you enter the strong magnetic field. You will then be asked to lie in the scanner and the scanning will start. The scanning can be noisy and so we shall give you ear plugs as well as headphones to reduce this noise. It may not be appropriate for you to be scanned if you are very claustrophobic. We do not scan women who are pregnant. During some of the scans we will ask you to perform simple tasks, described below. The scanning sessions will take about 30 minutes to 1.5 hours each, although you will not actually be scanned for more than 60 minutes of this time. To monitor the movements, we will use MR-compatible electromyography equipment. This consists of three electrodes placed on your arm to measure your muscle activity.

What will you be doing during the study?
In this study, we are investigating the brain activity associated with different types of movement. You will come for one scanning session in the 3T MRI scanner at the Robarts scan facility. Your scanning task will involve one or a combination of imagined, executed and passive movements (where the experimenter will passively move your hand, arm, or foot). Task instructions and movement cues will be played via headphones.

If you decide to take part in this study, you will be asked to sign a consent form.

Risks
Part of your participation in this study will involve a research test with Magnetic Resonance Imaging (MRI) system, a common medical diagnostic tool that uses a strong magnetic field, a low frequency magnetic field, and a radio frequency field. No X-rays are used. As with any technology there is a risk of death or injury. For MRI the risk of death is less than 1 in 10 million and the risk of injury is less than 1 in 100,000. These risks do not arise from the MRI process itself, but from a failure to disclose or detect MRI incompatible objects in or around the body of the subject or the scanner room. It is therefore very important that you answer all the questions honestly and fully on the MRI screening questionnaire. Almost all the deaths and injuries related to MRI scans have occurred

Initials of Participant _____   2

because the MRI operator did not know that surgically implanted metal hardware (such as a cardiac pacemaker) was present inside the subject during the MRI scan. Other remote risks involve temporary hearing loss from the loud noise inside the magnet. This can be avoided with ear headphone protection that also allows continuous communication between the subject and staff during the scan. For comparison, the risk of death in an MRI is similar to travelling 10 miles by car, while the risk of injury during an MRI is much less than the risks associated with normal daily activities for 1 hour.

You may not be allowed to continue in this research study if you are unable to have a MRI scan because, for example, you have some MRI incompatible metal in your body, you may be pregnant or attempting to become pregnant, or you may have a drug patch on your skin that contains a metal foil. Should you require a medically necessary MRI scan in the future, the final decision as to whether you can be scanned will be made by a qualified physician considering all the risks and benefits.

MRI exclusion criteria

If you have any history of head or eye injury involving metal fragments, if you have some type of implanted electrical device (such as a cardiac pacemaker), if you have severe heart disease (including susceptibility to heart rhythm abnormalities), you should not have an MRI scan unless supervised by a physician. Additionally you should not have a MRI scan if you have conductive implants or devices such as skin patches, non-removable body piercing or tattoos containing metallic inks because there is a risk of heating or induction of electrical currents within the metal element causing burns to adjacent tissue.

Participation

Participation in this study is voluntary. You may refuse to participate, refuse to answer any questions or withdraw from the study at anytime with no effect on your academic status. You may withdraw from the study at any time without explaining why, and if you choose to do, so your data will also be withdrawn from the study. You do not waive any of your legal rights by signing the consent form.

Compensation

You will be compensated $25 per hour for your time, parking, and the inconveniences associated with participating in the study.

Confidentiality

All the information we collect is kept confidential and is only seen by members of the research team at the Centre for Brain and Mind. The results will be kept securely for a minimum of 5 years and possibly indefinitely in the Centre for Brain and Minds data archive in accordance with good research practice. Representatives of the University of Western Ontario Health Sciences Research Ethics Board may contact you or may require access to your study related records to monitor the conduct of the research. Representatives of the Lawson Quality Assurance (QA) Education Program may look at data from this

study for quality assurance purposes. Any report published about this study will not identify you by name.

Benefits

You will not receive any direct benefit by participating in this study. By looking at healthy participants, this study will help establish a "normal" baseline for brain function and anatomy associated with movement and sensation of movement. We can use this in-depth examination of a healthy brain as a base to then compare and assess brain-damaged patients. Improving our understanding of normal conscious cognitive processes will help us determine exactly how and why DOC patients are impaired, and could contribute to the development of therapeutic interventions or treatments.

If you would like further information or would like to discuss any aspect of volunteering, then please contact either of the following:

Dr. Adrian M. Owen   Clara Stafford   Dr. Davinia Fernandez-Espejo
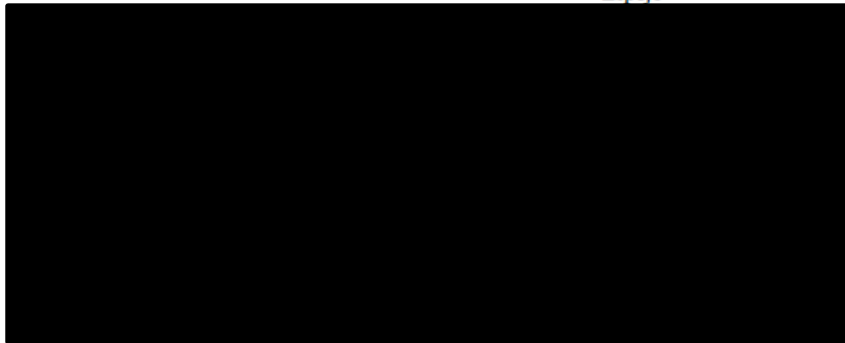
You will receive a copy of this letter of information and the signed consent form.

Consent

Investigating Movement Related Brain Activity: Implications for patients with Disorders of Consciousness

1. I have read the letter of information, have had the nature of the study explained to me and I agree to participate. All questions have been answered to my satisfaction.

Initials of Participant _____   4

Version: 3   Date: 17/03/2016

2. I give permission to be contacted about other possible future
   research studies

Printed Name of Participant

Signature of Participant   Date

Printed Name of the Person Obtaining Consent

Signature of the Person Obtaining Consent   Date

Appendix G: Letter of information for 7T data collection in healthy participants

Version: 2	12/02/2015

<div align="center">

_____
Letter of Information

Establishing Healthy Baselines for Structural Measures of Consciousness

</div>

You are being invited to participate in a research study. This sheet provides information regarding the study.

Purpose of the Study

We can learn a great deal about consciousness by examining the brain regions associated with creating and maintaining it. In this study, we want to explore the role that a specific brain structure, called the thalamus, plays in consciousness. Before we can examine this structure in patients with disorders of consciousness, we first need to study healthy volunteers to establish what a normal, functioning thalamus looks like. You have been recruited for this study to help us collect data from healthy participants to create a "normal baseline". We can then use this baseline to compare with individuals who have a disease. To study the thalamus in both healthy individuals and patients, we use a technique called Magnetic Resonance Imaging (MRI), which gives us high-resolution, detailed images of the brain structures we're interested in.

What is MRI scanning?

We study brain structure using images taken with a magnetic resonance imaging scanner. This scanner uses a strong magnetic field to create detailed images of brain structure and function. By taking a series of images whilst you lie resting or performing certain tasks in the scanner, we can build up a picture of the structure and function of the brain areas we're interested in. The scan does not involve any injections or X-rays and MRI is thought to be a safe, non-invasive imaging technique. The standard magnet strength (measured in units called "Tesla", abbreviated to "T",) for MRI scanners commonly used in diagnostic tests ranges from 1.5 to 3T. More powerful MRI scanners with higher strength magnets (eg. 7, 8 and 9.4 T) are less common and primarily used in research. The scanner used in this study is a 7 Tesla MRI scanner. The 7T scanner is considered along with 3T and 1.5T scanners to present no serious or permanent adverse health effects. The United States Food and Drug Administration (FDA) states the 7T MRI scanner system is "without significant risk" for humans of at least one month of age, and current Canadian guidelines follow this recommendation. The entire research project will involve approximately 50 people.

What does the study involve?

Scanning will be undertaken in the 7 Tesla Varian/Siemens MRI scanner at the Robarts Research Institute. This is a standard machine that is used for research purposes. Before your scan, a member of staff will ask you some questions to ensure that you have no metal within you before you enter the strong magnetic field. You will then be asked to lie in the scanner and the scanning will start. The scanning can be noisy and so we shall give you ear plugs as well as headphones to reduce this noise. It may not be appropriate for you to be scanned if you are very claustrophobic. We do not scan women who are pregnant. During some of the scans we will ask you to perform simple tasks, and we'll measure the blood flow to different parts of the brain—this is called functional MRI (fMRI). The scanning sessions will take about two hours each although you will not actually be scanned for more than 90 minutes of this time. While measuring brain function we will use several different imaging sequences.

If you would like further information or would like to discuss any aspect of volunteering, then please contact either of the following:

Dr Adrian M. Owen (Principal Investigator)   Dr Davinia Fernandez-Espejo   Clara Stafford
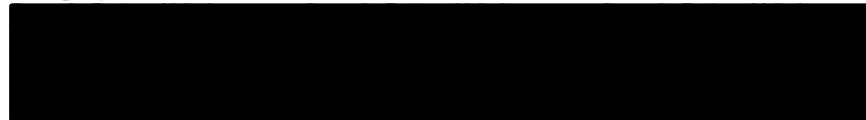
Initials of Participant _____

Version: 2	12/02/2015

What will you be doing during the study?

In this study, we are investigating the structure and function of certain brain systems associated with creating and maintaining consciousness and awareness. Your task will involve lying still in the scanner while we take highly detailed images of these structures. If you decide to take part in this study, you will be asked to sign a consent form.

Risks

Your participation in this study will involve a research test with Magnetic Resonance Imaging (MRI) system, a common medical diagnostic tool that uses a strong magnetic field, a low frequency magnetic field, and a radio frequency field. No X-rays are used. As with any technology there is a risk of death or injury. For MRI the risk of death is less than 1 in 10 million and the risk of injury is less than 1 in 100,000. These risks do not arise from the MRI process itself, but from a failure to disclose or detect MRI incompatible objects in or around the body of the subject or the scanner room. It is therefore very important that you answer all the questions honestly and fully on the MRI screening questionnaire. Almost all the deaths and injuries related to MRI scans have occurred because the MRI operator did not know that surgically implanted metal hardware (such as a cardiac pacemaker) was present inside the subject during the MRI scan. Other remote risks involve temporary hearing loss from the loud noise inside the magnet. This can be avoided with ear headphone protection that also allows continuous communication between the subject and staff during the scan. For comparison, the risk of death in an MRI is similar to travelling 10 miles by car, while the risk of injury during an MRI is much less than the risks associated with normal daily activities for 1 hour.

You may not be allowed to continue in this research study if you are unable to have a MRI scan because, for example, you have some MRI incompatible metal in your body, you may be pregnant or attempting to become pregnant, or you may have a drug patch on your skin that contains a metal foil. Should you require a medically necessary MRI scan in the future, the final decision as to whether you can be scanned will be made by a qualified physician considering all the risks and benefits.

MRI exclusion criteria

If you have any history of head or eye injury involving metal fragments, if you have some type of implanted electrical device (such as a cardiac pacemaker), if you have severe heart disease (including susceptibility to heart rhythm abnormalities), you should not have an MRI scan unless supervised by a physician. Additionally you should not have a MRI scan if you have conductive implants or devices such as skin patches, body piercing or tattoos containing metallic inks because there is a risk of heating or induction of electrical currents within the metal element causing burns to adjacent tissue.

Participation

Participation in this study is voluntary. You may refuse to participate, refuse to answer any questions or withdraw from the study at anytime with no effect on your future care/academic status or employment. You may withdraw from the study at any time without explaining why. You do not waive any of your legal rights by signing the consent form. If you choose to withdraw from the study, your data will also be withdrawn.

Compensation

You will be compensated $25 per hour for your time.

Confidentiality

All the information we collect is kept confidential and is only seen by members of the research team at the Centre for Brain and Mind. The results will be kept securely for a minimum of 5 years and possibly indefinitely in the Centre for Brain and Minds data archive in accordance with good research practice. Representatives of the University of Western Ontario Health Sciences Research Ethics Board may contact you or may require access to your study related records to monitor the conduct of the research. Any report published about this study will not identify you by name.

Incidental Findings

The MRI facility staff are not qualified to detect pathologies, and radiologists do not regularly review MRI scans. However, in the rare case that the images acquired in this study reveal a previously undiagnosed brain pathology, the Facility Manager/MRI Technologist and Principal Investigator will be notified. If an incidental finding is confirmed, the Principal Investigator will notify the participant, advise them of their follow up options and may provide them with a copy of their images (as outlined in the Robarts Standard Operating Procedures 305.)

Initials of Participant _____

Version: 2	12/02/2015

Benefits
You will not receive any direct benefit by participating in this study. However, participating provides a valuable learning experience that exposes you to current research in cognitive neuroscience using state-of-the-art imaging technology. Participating in this study will benefit society because examining healthy participants will help establish a normative baseline for brain anatomy in neural substrates associated with consciousness and key regions that are often damaged in patients with disorders of consciousness. We can use this in-depth examination of a healthy brain as a base to then compare and assess brain-damaged patients. Improving our understanding of normal consciousness will help us determine exactly how and why DOC patients are impaired, and could contribute to the development of therapeutic interventions or treatments. Once our methods have been shown to produce robust and informative results, they can also be used to improve diagnosis and prediction of clinical outcome, so that any potential intervention can be started as early as possible.

If you have any questions about your rights as a research participant you may contact ██████████████████ ██████████████████████████ You will receive a copy of this letter of information and the signed consent form.

Initials of Participant _____

| Version: 2 | 12/02/2015 |

Consent Form

Brain Structures Associated with Consciousness

I have read the letter of information, have had the nature of the study explained to me and I agree to participate. All questions have been answered to my satisfaction.

_____
Printed Name of Participant

_____   _____
Signature of Participant   Date

_____
Printed Name of the Person Obtaining Consent

_____   _____
Signature of the Person Obtaining Consent   Date

Initials of Participant _____

Curriculum Vitae

Name: Clara Alexandra Stafford

Post-secondary   Champlain Regional College
Education and   Saint-Lambert, Quebec, Canada
Degrees: 2010-2012 D.E.C. (Psychology)

                      McGill University
                      Montreal, Quebec, Canada
                      2012-2015 B.A. (Psychology)

                      The University of Western Ontario
                      London, Ontario, Canada
                      2015-present MSc. (Psychology)

Honours and   Reva Gerstein Fellowship for Masters Study in Psychology
Awards: Donor Award
                      2016

                      George Hannah Global Opportunities Award
                      Travel Award
                      2016

Related Work   Post-Graduate Visiting Research Student
Experience   University of Birmingham, UK
                      June 2016-August 2016

                      Teaching Assistant
                      The University of Western Ontario
                      2015-2017

                      Research Assistant
                      The University of Western Ontario
                      May 2015-August 2015

Publications:

Presentations:

Stafford, C. A., Owen, A. M., & Fernández-Espejo, D. (2016, November). The relationship between overt responsiveness and white matter abnormalities in patients with

disorders of consciousness. Poster present at the annual conference of the Society for Neuroscience, San Diego, California, USA.

Stafford, C. A., Owen, A. M., & Fernández-Espejo, D. (2016, June). The role of thalamo-motor fiber damage in overt motor responses in disorders of consciousness. Poster presented at the annual conference of the Canadian Association for Neuroscience, Toronto, Ontario, Canada.

Stafford, C. A., Gati, J., Owen, A. M., & Fernández-Espejo, D. (2016, February). Mapping structural connectivity of thalamic nuclei at ultra-high fields. Poster presented at the annual conference of the Lake Ontario Visionary Establishment, Niagara Falls, Ontario, Canada.